University of South Bohemia in České Budějovice

Faculty of Science

Detection of intracellular H_2O_2 molecules using the genetically encoded fluorescent marker HyPer7

Master thesis

Bc. Miroslava Bromová

Supervisor: doc. RNDr. Alena Panicucci Zíková, Ph.D.

Co-supervisor: BSc. Brian Panicucci

České Budějovice 2024

Bromová, M., 2024: Detection of intracellular H_2O_2 molecules using the genetically encoded fluorescent marker HyPer7. Mgr. Thesis, in English. – 80 p., Faculty of Science, University of South Bohemia, České Budějovice, Czech Republic.

Annotation:

In order to discern the role that mitochondrial reactive oxygen species (ROS) play during procyclic *Trypanosoma brucei* differentiation, we implemented the next-generation hydrogen peroxide biosensor Hyper7 to detect when and where ROS is being generated. Hyper7 fluorescence assays were optimized to determine the efficacy of this probe in an evolutionary divergent organism. In addition, we initiated studies to examine if a mitochondrial outer membrane thioredoxin participates in a redox-mediated intracellular signaling pathway.

I hereby declare that I am the author of this thesis and that while writing it I used only the sources listed in references.

České Budějovice, 11.4.2024 ……..

Bc. Miroslava Bromová

Acknowledgement

I would like to thank doc. Alena Panicucci Zíková who trusted me and gave me the chance to spend another two years under her friendly supervision. I will always be grateful for this experience to work in a laboratory of such a strong and inspiring role model. Furthermore, I would like to thank Brian Panicucci who invested a lot of time, energy and patience to teach me all the new methods and also showed me how to think about scientific problems differently than I was used to which I also consider to be a valuable life experience. Huge thanks go to Míša Kunzová and Míša Husová who made my stay in the lab the best I could possibly imagine and always had my back when I needed it. I cannot forget to thank my other wonderful colleagues with which I had a chance to work alongside - Evča, Ondra, Martina, Prashant, Wong, Israa, Ayyüce, Markét, Minal, Julie, Niky and Vojta, there is no better team that I could wish for. Additionaly, I would like to thank dr. Radek Litvín for sharing with me his expertise which helped me a lot when I needed to understand the physics behind HyPer7 in *T. brucei* system. Last but not least, I would like to thank my family and boyfriend for their unlimited love, support and patience.

List of abbreviations

AAC	ATP/ADP carrier
ADP	adenosine diphosphate
ANT	adenine nucleotide translocase medium
AOX	alternative oxidase
APRT	adenine phosphoribosyltransferase
ATP	adenosine triphosphate
BARP	bloodstream alanine-rich proteins
BSA	bovine serum albumin
CCD	charge-coupled device
cMM	complete minimal media
cpYFP	circularly permutated yellow fluorescent protein
DAAO	D-amino acid oxidase
DAPI	4',6-diamidino-2-phenylindole
DIC	differential interference contrast
dKO	double knock out
DMSO	dimethyl sulfoxide
DTT	dithiotreitol
EDTA	ethylendiamine tetraacetic acid
EGTA	ethylene glycol-bis(β-aminoethyl ether)-N,N,N',N'-tetraacetic acid
EP	procyclins with glutamic acid (E) and proline (P) repeats
ETC	electron transport chain
ETFQOR	electron transferring flavoprotein ubiquinone oxidoreductase
FACS	Fluorescence-activated cell sorting
$FADH_2$	dihydroflavin adenine dinucleotide
FBS	fetal bovine serum
FITC	fluorescein isothiocyanate
F_oF_1 ATPase	F_oF_1 ATP synthase
gDNA	genomic DNA
GPEET	procyclins with Glu-Pro-Glu-Glu-repeats

GPI	glycosylphosphatidylinositol
HAT	Human African trypanosomiasis
HRP	horseradish peroxidase
HSP70	mitochondrial heat shock protein 70
IC_{50}	half-maximal inhibitory concentration
IFA	immunofluorescence assay
IR	intergenic region
KO1	knock out of the first allele
KO2	knock out of the second allele
LB	lysogeny broth
MiR05	mitochondrial respiration medium
mVSG	metacyclic variable surface glycoprotein
NADH	reduced nicotinamide adenine dinucleotide
OXPHOS	oxidative phosphorylation
PBS	phosphate buffer saline
PBS-G	phosphate buffer saline with glucose
PBS-T	phosphate buffer saline with Tween
PCR	polymerase chain reaction
PE	phycoerythrin
PF	procyclic form
PVDF	polyvinylidene fluoride
RBP	RNA binding protein
rDNA	recombinant DNA
roGFP	reduction-oxidation green fluorescent protein
ROS	reactive oxygen species
RRM	RNA recognition motif
RT	room temperature
SDS	sodium dodecyl sulfate
SDS PAGE	sodium dodecyl sulfate polyacrylamide gel
sKO	single knock out

SOD	superoxide dismutase
SSC	saline-sodium citrate buffer
Tb	trypanosomal
TbIscU	trypanosomal iron-sulfur clusters assembly
TCA	tricarboxylic acid cycle
TetO2	tetracycline promoter
TetR	tetracycline repressor
Thx	thioredoxin
TMRE	tetramethylrhodamine ethyl ester
UTR	untranslated region
VSG	variable surface glycoprotein
WCL	whole cell lysate
wt	wild type
YFP	yellow fluorescent protein

Table of content

1 Introduction

1.1 *Trypanosoma brucei*

Trypanosoma brucei is a protozoan parasite whose subspecies *Trypanosoma brucei gambiense* and *Trypanosoma brucei rhodesiense* cause Human African trypanosomiasis (HAT) also known as sleeping sickness. The parasite is transmitted by the tsetse fly (*Glossina* spp.) which is native to sub-Saharan Africa where the rural population in particular is exposed to the infection (https://www.who.int). In the past, *T. brucei* was mainly studied for its negative impact to the human population, but nowadays this parasite also represents an excellent model organism for molecular and genetic research.

During its digenetic life cycle, the parasite alternates between two hosts– the tsetse fly and a mammal. As these two hosts represent very different environments, *T. brucei* undergoes significant changes in morphology, metabolism and gene expression.

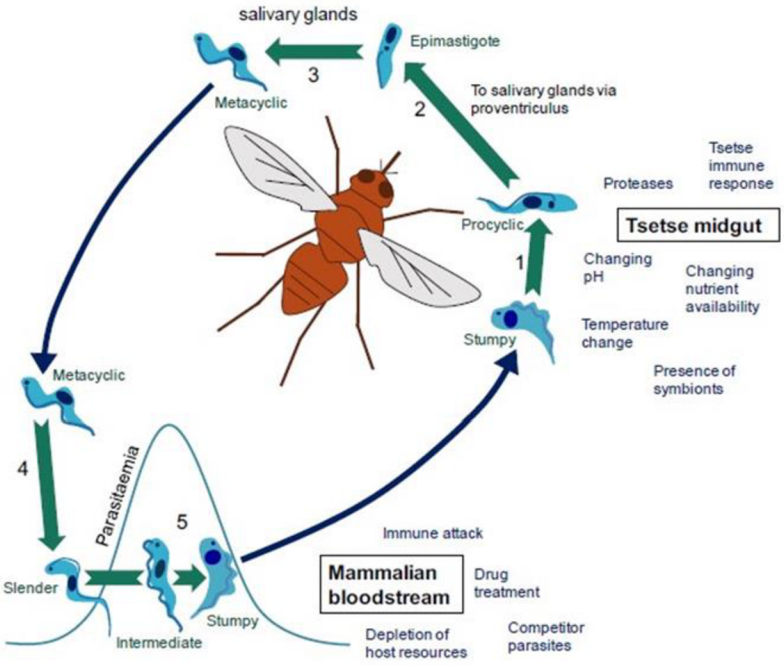

Figure 1: *Trypanosoma brucei* life cycle (Sivester *et al*., 2017).

T. brucei enters a tsetse fly as a bloodstream form trypomastigote with a short stumpy subpopulation that can differentiate to the procyclic form and a long slender subpopulation that is not able to transform and dies (Vickerman, 1985), (Ooi & Bastin, 2013).

Ingested blood containing trypanosomes flows from labrum via the crop to enter the midgut lumen where the bloodstream form differentiates to procyclic trypomastigotes (Vickerman *et al*., 1988). A typical hallmark for differentiated procyclics is a new protein coat that consists of EP and GPEET procyclins. The kinetoplast, a mitochondrial genome, is in sub- terminal position at the posterior side of the nucleus (Matthews, 2005). In the low- glucose tsetse midgut, the parasite relies on the breakdown of amino acids. Amino acids as proline, threonine and leucine are the main source of energy and carbon (Dyer *et al*., 2013), (Smith *et al*., 2017). The procyclic mitochondrion is branched with discoidal cristae, contains cytochromes and an active tricarboxylic acid (TCA) cycle and produces ATP through substrate and oxidative phosphorylation (OXPHOS) (Vickerman *et al*., 1988), (Dyer *et al*., 2013). The electron transport chain is part of OXPHOS and consists of protein complexes I, II, III and IV localized to the inner mitochondrial membrane and generates proton gradient that is used by the F_oF_1 ATP synthase to form ATP molecules.

From the tsetse midgut, the trypanosomes migrate further into the salivary glands where they develop into proliferating epimastigotes which are anchored to the epithelium with their flagella. The hallmarks of this form are the kinetoplast at the anterior side of the nucleus and a glycosylphosphatidylinositol (GPI) anchored alanine-rich protein (BARP) on the cell surface (Urwyler *et al*., 2006). The epimastigotes in the salivary glands go through two cycles of proliferation. The first cycle ensures a rapid replication, since two equivalent cells are formed on the epithelium. The second cycle occurs predominantly later and produces a cell which develops into infectious form for the the mammalian host (Rotureau *et al*., 2012), (Rotureau & Van Den Abbeele, 2013). This form is called metacyclic and is characterized by the kinetoplast back at the posterior end of the nucleus, tubular mitochondria and a new surface protein coat of metacyclic variable surface glycoprotein (mVSG). (Vickerman *et al*., 1988) (Sharma *et al*., 2009). The metacyclic form is a non-proliferative, quiescent stage that awaits infection.

The metacyclic form enters the mammalian host with the tsetse saliva during a blood meal. In the mammalian bloodstream *T. brucei* differentiates into the long slender bloodstream form, which is proliferative. The surface coat consists of tightly packed VSG molecules attached to the surface membrane by GPI anchors. The VSG coat is a crucial protection of the parasite to evade the mammalian immune response as it is regularly changed (Matthews,

2005). When the parasite number in the mammalian bloodstream increases, the slender form irreversibly differentiates into the other type of the bloodstream form called stumpy. This short, non-proliferative type is a parasite pre-adapted to the tsetse host environment and ready for transmission (Smith *et al*., 2017).

The bloodstream form mitochondrion is tubular with highly reduced cristae and it is overall less developed than the procyclic one. In mammalian bloodstream glucose is the main source of energy and carbon. Glucose is catabolized to pyruvate in the aerobic glycolysis providing majority of the cellular ATP. Intriguingly, the bloodstream form lacks the canonical ETC containing cytochromes and respiration is maintained solely by alternative oxidase (AOX) (Chaudhuri *et al*., 2006). Consequently, F_oF_1 ATP synthase does not generate ATP, because it works in a reverse mode to maintain the mitochondrial proton gradient by hydrolyzing ATP to ADP (Smith *et al*., 2017).

Due to the alternation between two different hosts, *T. brucei* must rapidly remodel its own metabolism to adapt to the new environmental conditions. This adaptation requires changes in gene expression regulation which are usually regulated at the post-transcriptional level. One of the most important ways in which *T. brucei* controls gene expression is through RNA binding proteins (RBP) (Kolev *et al*. 2014). *T. brucei* possesses about 70 different proteins that contain at least one RNA recognition motif (RRM). Approximately half of these proteins is essential for growth in the different life stages. Here, I would like to mention two RRM-domain proteins that are involved in regulating gene expression during the parasite life cycle – RBP6 drives the differentiation of insect forms while RBP10 is essential for the development of the bloodstream form (Clayton, 2013).

The induced overexpression of RBP6 triggers the differentiation of procyclic trypomastigotes into epimastigotes and then into infectious metacyclics in culture. These *in vitro* generated metacyclics have typical metacyclic features like kinetoplast on the posterior end of the nucleus, undulating membrane, mVSG (Kolev *et al*., 2012). Similarly, the presence of RBP10 promotes the differentiation of the parasite into the bloodstream form. If the protein is removed from the bloodstream form, the cells can only survive in the procyclic form. When the protein is overexpressed in the procyclic form, the cells transform into bloodstream forms and skip the epimastigote and metacyclic life cycle stages (Mugo & Clayton, 2017).

The overexpression of RBP6 is a useful tool to induce procyclic differentiation *in vitro* while the availability of large numbers of differentiating cells enables us to study in detail the molecular mechanisms of *T. brucei* differentiation.

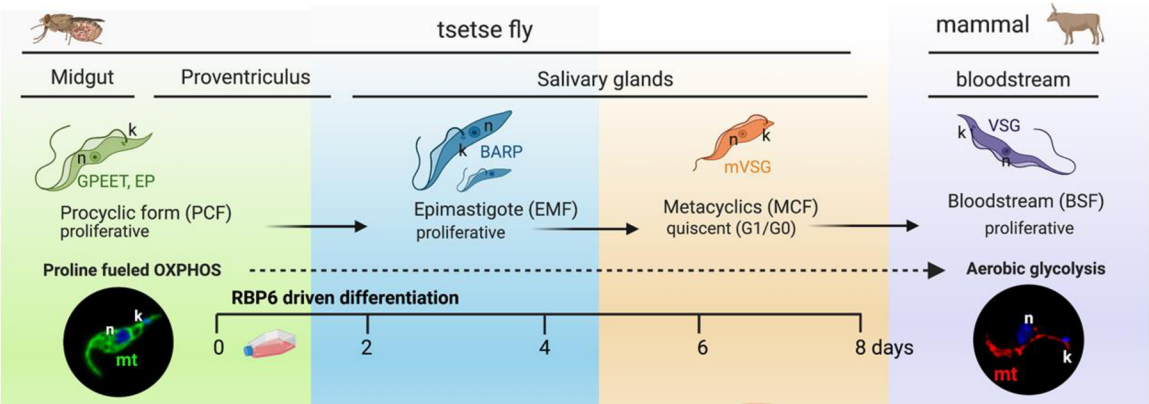

Figure 2: *T. brucei in vitro* differentiation enhaced by the overexpression of RBP6 (created by A. Zíková via BioRender).

One of the most striking features of the insect forms development is the remodeling of the parasite's mitochondrion. Using cell-based and multi-omics analyses, our laboratory detected a redirection of electrons from the canonical cytochrome-containing pathway to AOX, increased activity in complex II, elevated utilization of proline and higher expression of enzymes involved in the TCA cycle. These changes were also accompanied by increased levels of reactive oxygen species (ROS) molecules which appeared to act as signaling molecules (Doleželová *et al.*, 2020). When catalase, a ROS scavenger naturally missing in *T. brucei*, was overexpressed in the cytosol, the differentiation from epimastigotes to metacyclics was blocked. Additionally, the observed epimastigotes did not express the BARP containing coat, their typical surface glycoproteins (Doleželová *et al.*, 2020). This indicates that ROS molecules may have an important role in the parasite differentiation

1.2 ROS scavenger system in *T. brucei*

ROS is a group of molecules that are all derived from oxygen and possesses some extra electrons. These molecules are highly reactive because of the electron excess and they can oxidize other molecules in their immediate vicinity. A single electron reduction of oxygen forms radical superoxide. Radical superoxide molecules are converted into the hydrogen peroxide (H_2O_2) by superoxide dismutases (SODs). H_2O_2 has several ways how to influence cellular processes in a cell. Through the Fenton reaction it can accept an electron from Fe^{2+}

and turn into a dangerous hydroxyl radical, or it can oxidize redox-sensitive cysteine residues in proteins which can lead to the cellular signal transduction. In the mammalian cells, physiological levels of H_2O_2 are maintained by catalase, peroxiredoxins or glutathione peroxidases (Sullivan & Chandel, 2014).

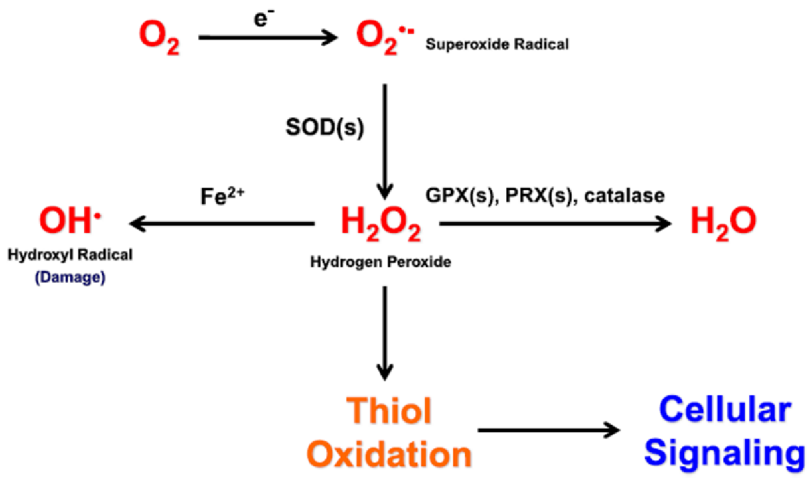

Figure 3: The creation and pathways of main ROS molecules (Sullivan & Chandel, 2014).

Mitochondria are considered to be the main source of ROS molecules due to the presence of ETC coupled to OXPHOS. During the process, electrons from NADH + H^+ are taken up by complex I and electrons from $FADH_2$ by complex II. These two complexes pass the electrons ubiquinone forming reduced ubiquinol. Ubiquinol is then oxidized by complex III, electrons are passed to cytochrome c and finally to complex IV, where they reduce oxygen molecules and form water molecules. The energy released during this process in invested to generation of a proton gradient by complexes I, III and IV that powers the F_oF_1- ATP synthase to produce ATP molecules. ETC components leak some small percentage of transporting electrons which can then react with the oxygen present in the matrix to form superoxide radicals and/or hydrogen peroxide (Muller, 2000).

In a typical mammalian mitochondrion, there are at least eleven different sites that generate superoxide radicals. These include ubiquinone-binding sites of complex I and complex III, glycerol 3-phosphate dehydrogenase, the flavin in complex I, ETFQOR (electron transferring flavoprotein ubiquinone oxidase), pyruvate dehydrogenase and 2-oxoglutarate dehydrogenase (Brand, 2010). However, the main sites that generate superoxide radicals in the mitochondria are complex I and complex III (Brand, 2016). All mentioned sites release the superoxide radicals into the mitochondrial matrix, although glycerol 3-phosphate

dehydrogenase and complex III release superoxide radicals also into the intermembrane space (Muller *et al*., 2004).

The concentration of ROS molecules is of decisive importance for the further fate of the cell, because if the levels are too high, this can lead to pathological effect and cell death. The cell is therefore able to regulate the ROS content through efficient scavenging systems. In the mammalian cells, major scavenging systems involves catalase, glutathione-based system and thioredoxin system (Sena & Chandel, 2012). However, *T. brucei* differs considerably, the parasite lacks catalase, glutathione reductase and thioredoxin reductase (Penketh & Klein, 1986). Instead of the glutathione system *T. brucei* uses trypanothione, a molecule consisted of two glutathione molecules and one spermidine molecule. Since it is a dithiol molecule, it is much more reactive than glutathione (Schmidt & Krauth-Siegel, 2003), (Manta *et al*., 2013). Therefore, the traditional role of the thioredoxin and glutathione system is replaced in this case by the trypanothione system. In mammals, H_2O_2 is reduced by thioredoxin peroxidase which oxidizes thioredoxin which is then reduced back to its reduced state by thioredoxin reductase. On the other hand, in *T. brucei* trypanothione reduces tryparedoxin, which reduces tryparedoxin peroxidase which finally reduces H_2O_2 to water (Figure 4). Thioredoxin and thioredoxin peroxidase are equivalents to trypanoredoxin-I and trypanoredoxin peroxidase (Alphey *et al*., 1999).

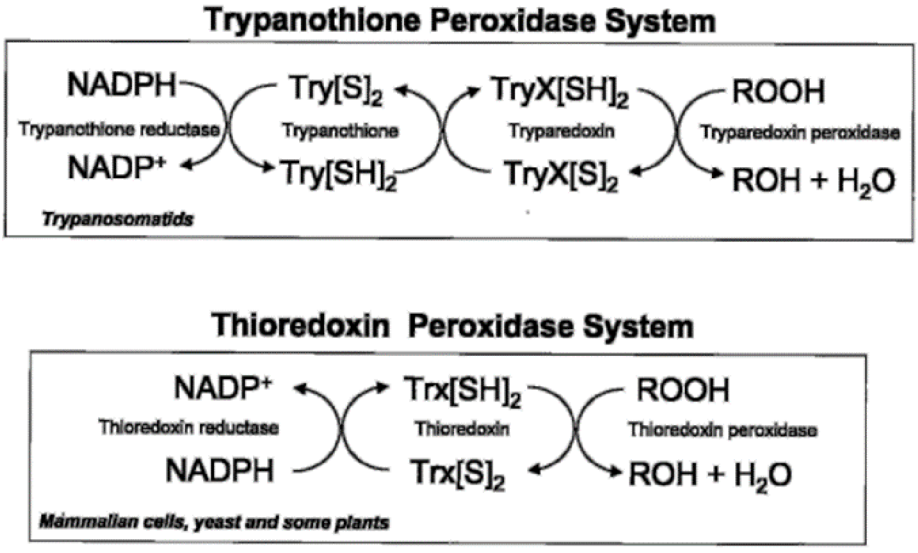

Figure 4: The differences between mammalian thioredoxin system and trypanosomatid trypanothione system (Alphey at al., 1999).

Interestingly, *T. brucei* also possesses thioredoxins, which play a role in H_2O_2 scavenging, although they are not recycled by thioredoxin reductases but most likely by trypanothione directly (Schmidt & Krauth-Siegel, 2003).

T. brucei genome contains six thioredoxins. We noticed that one of the thioredoxins, thioredoxin Tb927.7.5780, is strongly regulated during the *in vitro* differentiation of RBP6 *T. brucei* cell line as its expression is highly elevated already in the epimastigote form (Doleželová *et al.*, 2020). Considering that no other redox-relevant enzymes were changed we hypothesize that this protein may have an important role for *T. brucei* differentiation. Therefore, in the frame of my project I also generated double knock out of this protein.

1.3 H_2O_2 detecting fluorescent probes

To gain insight in the role of H_2O_2 molecules in intracellular signaling, it is important to be able to monitor their spatio-temporal dynamics. Therefore, H_2O_2 sensitive probes are still under development. They are usually based on fluorescent probes that are able to bind hydrogen peroxide and simultaneously generate a fluorescence response whose intensity corresponds to the intracellular H_2O_2 concentration. The most commonly used probes are roGFP (reduction-oxidation sensitive green fluorescent protein) and HyPer (hydrogen peroxide fluorescent probe) (Hanson *et al.*, 2004), (Belousov *et al.*, 2006). In this thesis I used the seventh generation of HyPer probes called HyPer7.

1.3.1 H_2O_2 sensitive fluorescent probe HyPer7

HyPer7 is a fluorescent probe that specifically detects H_2O_2 in the cell. The seventh generation of these probes contains an OxyR domain from *Neisseria meningitis* into which a circularly permuted yellow fluorescent protein (cpYFP) with several mutations to enhance the brightness of the signal is incorporated (Figure 5a). One of the mutations, G298S, changes the amino acids sequence in a way that corresponds to the wtGFP in *Aequorea victoria* (Pak *et al.*, 2020).

Another important advantage of HyPer7 is its high sensitivity which was achieved by selecting the most suitable OxyR domain. A total of eleven OxyR domains from different, evolutionary distant organisms were tested. The OxyR regulatory domain from *Neisseria meningitis* was selected as the final one, where the developers inserted cpYFP between position 126 and 127. Another advantage of this probe is pH stability, and recyclability and ratiometric property. This fluorescent probe has two excitation maxima at 400 nm and 499 nm

and an emission peak at 516 nm. As soon as the probe is oxidized, the absorption spectrum changes ratiometrically. There is a decrease at 400 nm and an increase at 499 nm (Figure 5b) (Pak *et al*., 2020).

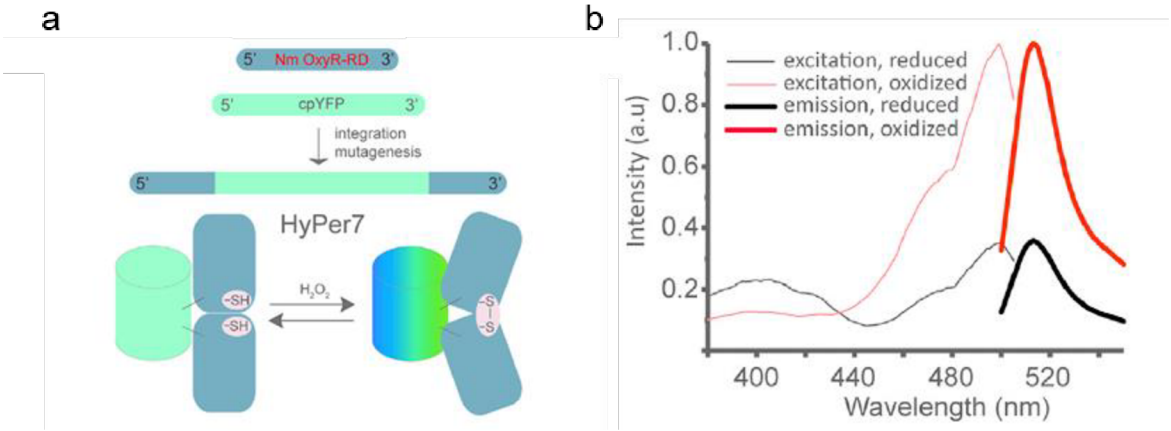

Figure 5: Fluorescent probe HyPer7 a) the schema of creation, b) the absorption and emission spectra of oxidized and reduced state (modified from Pak *et al*., 2020).

An alternative probe for detection of H_2O_2 is roGFP2 and its variants fused to peroxiredoxins, thioredoxins, glutaredoxins or other H_2O_2 scavengers. Although both probes work on similar principles, there are some important differences. HyPer7 is mainly reduced by thioredoxin system (Kritsiligkou *et al*., 2021). In contrast, roGFP2 is reduced by the glutathione system and the thioredoxin system does not efficiently reduce this probe (Gutscher *et al*., 2008). HyPer7 was also shown to be reduced faster than highly sensitive roGFP-Tsa2ΔC_R variant (Kritsiligkou *et al*., 2021).

We chose to use the HyPer7 probe to investigate the role of H_2O_2 in signaling during *T. brucei* differentiation. In order to monitor the production of H_2O_2 molecules in the cytosol or mitochondria, we targeted this probe to these two cellular compartments. Subsequently, we optimized the detection of the reduced and oxidized form of HyPer7 by several independent methods. The overall goal of this approach is to map spatio-temporal dynamics of H_2O_2 and to determine the primary source(s) of ROS that drive *T. brucei* differentiation.

2 Aims

- Create constitutive and inducible *Trypanosoma brucei* expression plasmids that target Hyper7 to the cytosol or mitochondrion
- Verify correct Hyper7 localization of genetically modified *T. brucei* cell lines
- Optimize Hyper7 fluorescence assays
- Generate a *T. brucei* thioredoxin (Tb.927.7.5780) double knock out cell line

3 Methods

3.1 *Trypanosoma brucei* cell lines

In all our experiments we used the wild type of the *T. brucei* 427 Lister strain or its derivative called 29.13 which contains a dual promoter system of T7 and PARP promoters for the expression of a selective marker and gene of interest. The parental 29.13 procyclic *T. brucei* strain has been genetically engineered to constitutively express the T7 RNA polymerase, which specifically transcribes only the DNA downstream of the T7 promoter (Wirtz *et al.*, 1999). Furthermore, this transcription can be turned on and off due to the constitutive expression of the bacterial tetracycline repressor that binds the tetracycline operator placed immediately downstream of the T7 promoter in the plasmid. When the repressor is bound to the operator, it sterically blocks T7 RNA transcription. Once the antibiotic tetracycline is added to the cell medium, it binds the repressor and causes a conformational change that releases the tetracycline repressor from the plasmid DNA that has been integrated into the parasite genome. This then allows for the T7 RNA transcription to proceed in a regulated manner. For the induced *T. brucei in vitro* differentiation we used a RBP6 cell line in which the expression of RNA binding protein 6 can be induced by tetracycline (Kolev *et al.*, 2012, Doleželová *et al.*, 2020).

3.1.1 Cell culturing

Procyclic cells were routinely grown at 27 °C in SDM-79 media containing glucose and 10% fetal bovine serum (FBS). Cultures were usually grown in 25 cm^2 in 10 ml of medium with appropriate selectable antibiotics in 1:1000 dilution and pH 7.3. The densities of all cultures were maintained between $1x10^6$ to $2x10^7$ cells/ml. Culture density was measured with a Z2 Coulter Counter (Beckman Coulter Inc.) in a 10ml plastic cuvette with 5 ml of Hemasol solution and 50 µl of a 1:1 mixture of cell culture and Cell Fix Solution (1x SSC; 3,6% Formaldehyde) with cells subsequently counted by the integrated computer with a pre-set dilution factor. For differentiation, the RBP6 cells were grown in SDM-80 media without glucose with 10% FBS and 50 mM N-acetyl glucosamine (Sigma Aldrich).

The *in vitro* differentiation of the RBP6 cell line was triggered by addition of 10 µg/ml of tetracycline to the SDM-80 culture medium with the corresponding antibiotics. Each day of differentiation when the cells were split, the tetracycline was added accordingly to the fresh media to keep its concentration constant during the 6-day process.

Table 1: Cell lines with appropriate final concentration of selective antibiotics in medium. cytoH7 – cytoHyPer7, mitoH7 – mitoHyPer7

	29.13	29.13 cyto H7	29.13 mito H7	RBP6	RBP6 cyto H7	RBP6 mito H7	29.13 Thx sKO	RBP 6 Thx sKO	29.13 Thx dKO	RBP6 Thx dKO
Geneticin 418 (15 µg/ml)	✓	✓	✓	✓	✓	✓	✓	✓	✓	✓
Hygromycin (25 µg/ml)	✓	✓	✓	✓	✓	✓	✓	✓	✓	✓
Puromycin (2,5 µg/ml)		✓	✓		✓	✓	✓	✓	✓	✓
Phleomycin (1 µg/ml)				✓	✓	✓		✓		✓
Blasticidin (10 µg/ml)									✓	✓

3.2 Molecular cloning

3.2.1 Cloning of the HyPer7 gene into pHD1344-t plasmid

The pHD1344-t plasmid contains C-terminal β-tubulin coding sequence that can be digested by the restriction enzyme NotI yielding a linearized plasmid with homologous ends for the tubulin locus. By choosing this plasmid we were able to target our gene of interest into the β-tubulin locus in the *T. brucei* genome and to constitutively express our gene using endogenous promoters. This plasmid also contains the *Escherichia coli* replication origin pBR322, the β-lactamase coding sequence which is responsible for ampicillin resistance in bacterial cells, the puromycin acetyltransferase coding sequence for resistance to puromycin as a selectable marker in *T. brucei* and 3x V5 tag at the C-terminus. The V5 tag is a short peptide that facilitates the detection and purification of the tagged proteins of interest.

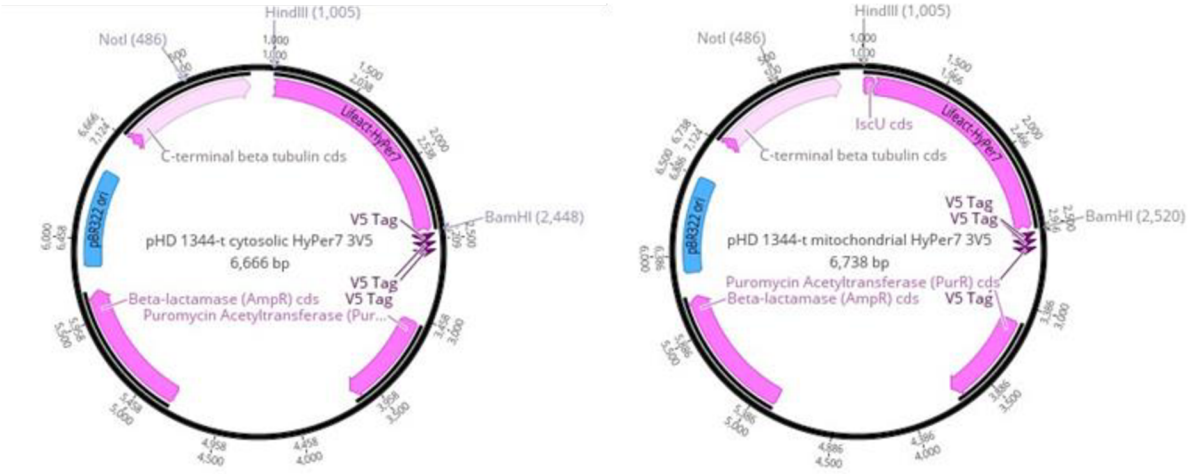

Figure 6: The plasmid map of pHD 1344-t with cytosolic HyPer7 (left) and pHD 1344-t with mitochondrial HyPer7 (right) with highlighted restriction sites. Created by Geneious software. AmpR – ampicilin resistence, PurR – puromycin resistence, cds – coding sequence, IscU – iron-sulfur cluster assembly.

The HyPer7 inserts of interest were produced in two variants, one targeted to the cytosol (cytoHyPer7) and the other one targeted to the mitochondrial matrix (mitoHyPer7). The mitoHyPer7 was created by fusing the N-terminal mitochondrial targeting sequence of the trypanosome iron-sulfur clusters assembly protein (TbIscU) (Mach *et al*., 2013) to HyPer7.

A polymerase chain reaction (PCR) was performed to generate and amplify the genes of interest (cytoHyPer7 and mitoHyper7). KOD polymerase (Merck), which is a hot-start proofreading polymerase, was used for this PCR. Oligonucleotides were designed with 5'end restriction sites HindIII for the forward primers (AZ1503; AZ1505) and BamHI for reverse the primer (AZ1504). The forward primer for mitoHyPer7 (AZ1505) also contained the IscU mitochondrial localization signal sequence to target HyPer7 into the mitochondrial matrix. All primers ale listed in Table 2.

Table 2: Oligonucleotide sequences used for creation of targeted HyPer7. All sequences are displayed in 5' → 3' direction.

Primer name and orientation	Code	Sequence
Forward (cytoHyPer7)	AZ1503	GTACAAGCTTATGCACCTGGCTAATGAGGAG
Forward (mitoHyPer7)	AZ1505	TACTAAGCTTATGCGGCGACTGATATCATCACACAT TGTACTGCCGACGCTGGCAGCCTCACTTCGGTCACTGT ACAGCCCACTACACCTGGCTAATGAGGAGCAAAAC
Reverse (both)	AZ1504	GTCAGGATCCATCGCAGATGAAGCTAACAC

The PCR was designed for the final volume of 50 µl. Reagents needed for the reaction are listed in Table 3 and the PCR program is described in Table 4.

Table 3: The reagents used in the PCR mix

Solution	Volume [µl]
10x Buffer for KOD Hot Start polymerase	5
25 mM $MgSO_4$	3
dNTPs (2mM each)	5
PCR grade water	31
Forward primer (10 µM)	1.5
Reverse primer (10 µM)	1.5
Template DNA (10 ng)	2
KOD Hot Start DNA polymerase	1

Table 4: The PCR program for targeted HyPer7 creation

Step	Number of cycles	Temperature [°C]	Time
Polymerase activation	1	95	2 min
Denature	30	95	20 sec
Annealing		52	10 sec
Extension		70	30 sec
Finish	1	70	5 min
		12	∞

To ensure that the PCR reaction was successful and the genes of interest were generated, both PCR reactions were resolved by DNA electrophoresis on a 1% agarose gel with 1 µl of ethidium bromide. To each reaction, 6 µl of 10x DNA loading dye (39% glycerol; 0,5% SDS; 10 mM EDTA; 0,1% xylene cyanol) was added before loading onto the gel. Afterwards, the amplicon was purified from the gel by using GelElute Gel Extraction Kit

(Sigma Aldrich) and the final concentrations were measured on Nanodrop 1000 (M.G.P. spol. s.r.o.). Both amplicons were then digested with the restriction enzymes HindIII and BamHI by incubating the DNA with the enzymes at 37 °C for 1 hour. Afterwards the mixtures were purified using the GenElute PCR Clean-up Kit (Sigma Aldrich).

Using the same restriction enzymes and under the same conditions, our plasmid pHD1344-t was digested, resolved on a 0.8% agarose gel with 1 µl of ethidium bromide and gel purified using the GelElute Gel Extraction Kit (Sigma Aldrich).

The amplified and digested DNA Hyper7 fragments were ligated into digested plasmid pHD1344-t. A 10 µl ligation reaction was prepared with an insert (cytoHyPer7 or mitoHyper7) and a vector (plasmid) at a µM ratio of 3:1, 1 µl 10x ligase buffer and 1 µl T4 DNA ligase (Invitrogen) and the reaction was incubated overnight at 4 °C.

The next day, ligation mixture was transformed into *E. coli* XL-1 blue chemically competent bacterial cells. These cells were freshly thawed on ice for 20 minutes and afterwards 3 µl of ligation reaction were added to 50 µl of cells. Cells and DNA were incubated on ice for 20 minutes followed by the heat shock at 42 °C for 45 seconds in a water bath. Immediately after the heat shock, the cells were placed on ice for 2 minutes. 250 µl of SOC media (0.5% yeast extract; 2% Tryptone; 10 mM NaCl; 2.5 mM KCl; 10 mM $MgSO_4.7H_2O$; 10 mM $MgCl_2.6H_2O$; 20 mM glucose; pH 7.3) were added to the cooled competent cells and the whole mixture was placed into the shaker at 37 °C, 200 rpm for 45 minutes. Finally, 250 µl of transformed cells were spread onto an LB agar plate with ampicillin (100 µg/ml) and incubated upside down in 37 °C for 16 hours. The next day some of the colonies were selected and each of them was transferred in the 5 ml LB medium (1% Trypton; 0.5% NaCl; 0.5% yeast extract; pH 7.25) with 5 µl of ampicillin (100 µg/ml) to grow overnight.

The plasmid DNA was isolated from bacterial cells using the GenElute HP Plasmid Miniprep Kit (Sigma Aldrich). The extracted plasmids were digested with HindIII and BamHI and resolved on the 0.8% agarose gel with 1 µl of ethidium bromide. For each of the Hyper7 variants one clone was selected and sequenced to verify the cloning.

For transfection with *T. brucei* cells, the verified clones were grown overnight in 50 ml LB medium with 50 µl ampicillin (100 µg/ml). The next day, the plasmids were isolated using the GenElute HP Plasmid Midiprep Kit (Sigma Aldrich). The plasmids were linearized overnight at 37 °C using the restriction enzyme NotI. DNA from the reaction was precipitated

with 2.5 volumes of 97% EtOH and 1/10 volumes of 3M sodium acetate, incubated at -80 °C for 30 minutes and spun at 4 °C for 30 minutes at maximum speed (15 000xg). The DNA pellet was washed with 200 µl of 70% EtOH, centrifuged and air dried under sterile conditions. The dried DNA pellet was resuspended in 30 µl pre-warmed sterile distilled H_2O and the final concentration was measured with the Nanodrop.

3.2.2 Subcloning HyPer7 gene into pT7 3V5 PAC plasmid

For the purposes of the project, the Hyper7 genes were also subcloned into the pT7 3V5 PAC plasmid. This plasmid after digestion by restriction enzyme Not I targets the gene of interest into rDNA intergenic spacer region in the *T. brucei* genome. The plasmid also contains the *E. coli* replication origin pBR322, the β-lactamase gene for ampicillin resistance (AmpR), the puromycin acetyltrasferase (PAC) gene for puromycin resistance and also 3x V5 tag. Another important feature of this plasmid is that it possesses strong T7 promotor which is recognized by T7 RNA polymerase and drives independent transcription of the inserted gene. The plasmid also possesses TetO2 operator allowing for inducible expression after tetracycline addition.

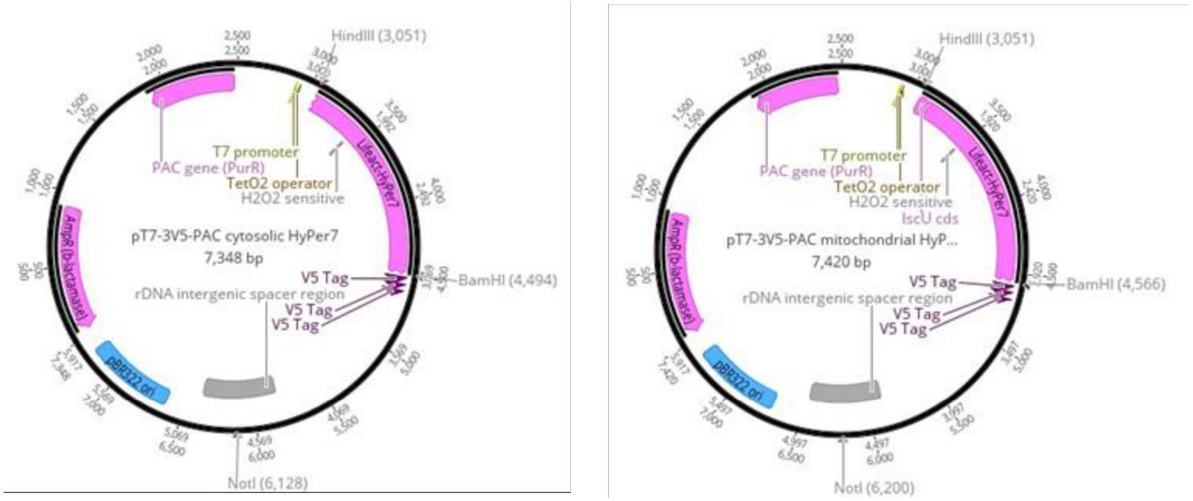

Figure 7: The plasmid map of pT7-3V5-PAC with cytosolic HyPer7 (left) and pT7-3V5-PAC with mitochondrial HyPer7 (right) with highlighted restriction sites. Created by Geneious software. AmpR – ampicilin resistence, PurR – puromycin resistence, cds – coding sequence, IscU – iron-sulfur cluster assembly.

Previously created pHD1344-t plasmids containing cytoHyPer7 or mitoHyPer7 sequences and the original plasmid pT7 3V5 PAC were digested with HindIII and BamHI as previously described and resolved on 1% agarose gel containing 1 µl of ethidium bromide.

Individual pieces were gel purified by GelElute Gel Extraction Kit (Sigma Aldrich). The DNA inserts (cytoHyper7 and mitoHyPer7) were ligated into the plasmid pT7 3V5 PAC by a ligation reaction with 10x ligase buffer and T4 DNA ligase at 4 °C overnight. The ligation mixture was transformed into *E. coli* XL-1 blue competent bacterial cells the next day and the pT7 plasmids containing cytoHyper7 or mitoHyPer7 were isolated and verified the same way as previously described in the chapter 3.2.1. Final selected clones of each of the HyPer7 genes were sequenced by SEQme confirming successful subcloning. The verified clones were linearized with NotI and ethanol precipitated.

3.2.3 Generation of thioredoxin 5780 amplicons for double knock out

To completely remove thioredoxin 5780 from the genome of *T. brucei*, a double knock out procedure was performed. Fusion PCR was used to generate DNA cassettes to replace both thioredoxin 5780 allelles. The first allele was replaced with a DNA cassette (KO1) containing a gene ensuring resistance to puromycin. The second allele was replaced with a DNA cassette containing a gene ensuring the resistance blasticidin.

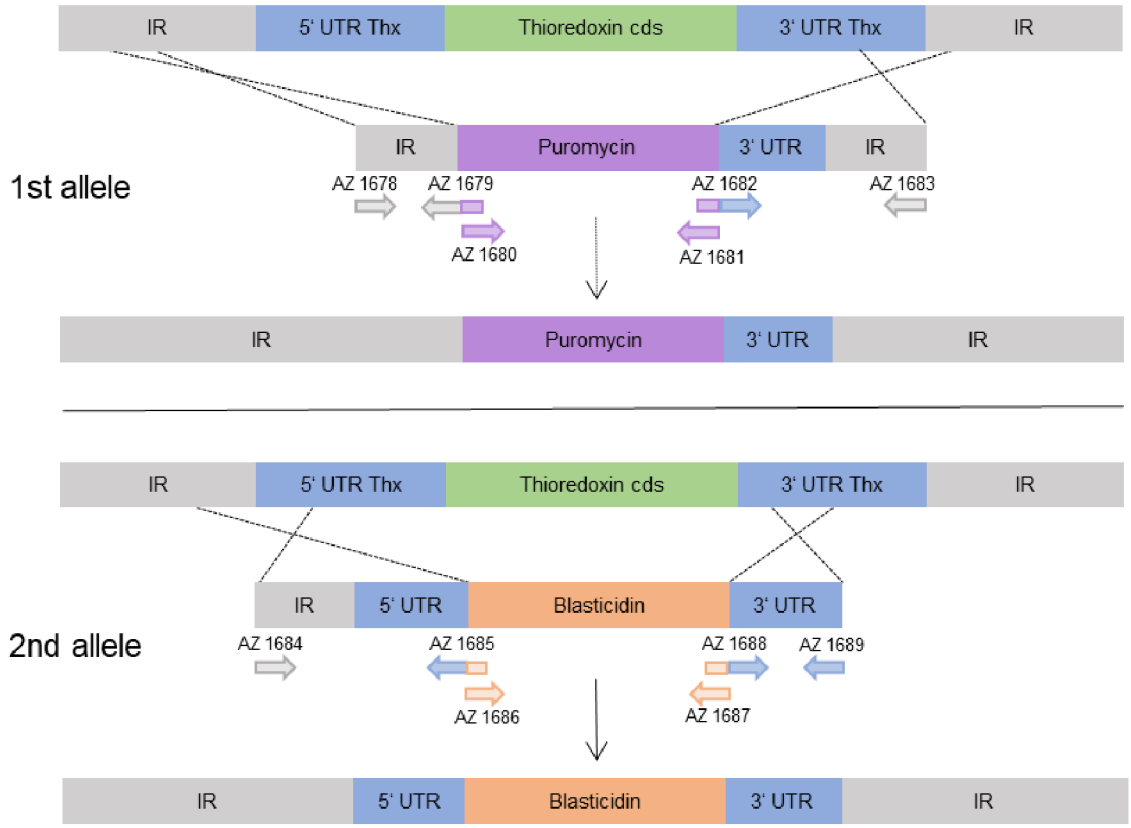

Figure 8: Scheme of thioredoxin Tb927.7.5780 dKO with primers and their annealing positions. IR - intergenic region; UTR – untranslated region.

To generate the DNA cassettes for allelic exchange, three individual pieces of DNA were fused together in two fusion PCR reactions in two runs. The first and second DNA pieces were amplified from genomic DNA of the Lister cell line 427 and represented the 5' IR end or 3' IR of thioredoxin 5780, respectively. The third DNA piece contained genes for resistance to puromycin or blasticidin. In total, it was performed 6 PCR reactions with 12 different primers in one PCR program. The 5' IR reverse primers and the 3' IR forward primers contained overlapping regions with the genes for puromycin and blasticidin resistance, respectively, to allow the fusion of all three parts. All primers and the appropriate matching template DNAs are listed in Table 5.

Table 5: List of primers for KO1 and KO2 individual pieces and appropriate template DNA for each primer pair used in PCR reactions

Primer name and orientation	Code	Sequence	Template DNA
5' IR KO1 Forward	AZ1678	GTTTGGTTTTAGCGCGTGTG	genomic DNA PF 427 wt
5780 5' IR KO1 Reverse	AZ1679	CTAAATAAGAGCGGAGACTGCGAAA TAGACGCCGATGAGAATCCC	
Puromycin cds Forward	AZ1680	GCAGTCTCCGCTCTTATTTAG	plasmid PT7 3V5 PAC
Puromycin cds Reverse	AZ1681	CAATCATGTCGACACACCAAG	
5780 3' IR KO1 Forward	AZ1682	CTTGGTGTGTCGACATGATTGCAAGT GGGGAAGCGTCTATTG	genomic DNA PF 427 wt
5780 3' IR KO1 Reverse	AZ1683	CCGCAAAAGGAAAGGAAAGG	
5780 5' IR KO2 Forward	AZ1684	CTCCCTCTTTTACTGATAGGCG	genomic DNA PF 427 wt
5780 5' IR KO2 Reverse	AZ1685	GAATTTCAGAAGACCTTGCTGTGCCC GCTTCTTCTCGCCAAGTGTTG	
Blasticidine Forward	AZ1686	GGGCACAGCAAGGTCTTCTGAAATTC	plasmid pHD1344 with blasticidin
Blasticidine Reverse	AZ1687	CGAATCCCCCCATTTTCTTC	
5780 3' IR KO2 Forward	AZ1688	GAAGAAAATGGGGGGATTCGGGAGG AGGAAAAGAGTTACC	genomic DNA PF 427 wt
5780 3' IR KO2 Reverse	AZ1689	GGAAGAAGTGTTGAATGCCG	

KOD polymerase was used for these PCR reactions. Concentration of the template DNA differed between the reactions (gDNA: 137.7 ng/reaction, plasmid DNA: 10 ng/reaction). Reagents needed for the reaction are listed in Table 6 and the PCR program is described in Table 7.

Table 6: The reagents used in the PCR reaction with the KOD polymerase

Solution	Volume [µl]
10x Buffer for KOD Hot Start polymerase	5
25 mM $MgSO_4$	3
dNTPs (2mM each)	5
PCR grade water	31
Forward primer (10 µM)	1.5
Reverse primer (10 µM)	1.5
Template DNA	individual
KOD Hot Start DNA polymerase	1

Table 7: The PCR program for the creation KO1 and KO2 individual pieces

Step	Number of cycles	Temperature [°C]	Time
Polymerase activation	1	95	2 min
Denature	35	95	20 sec
Annealing		52	10 sec
Extension		70	17 sec
Finish	1	70	5 min
Finish	1	70	5 min
		12	∞

To ensure that the PCR reactions were successful, all were resolved on the 1.2% agarose gel with 1 µl ethidium bromide. Verified bands were then extracted from the gel using the commercial kit GelElute Gel Extraction Kit (Sigma Aldrich).

The fusion PCR to generate KO1 cassette (Figure 9) required a lot of optimizations until it was finally optimized with a significant yield. The template DNA included the three individual DNA pieces – 5' IR KO1, puromycin cds, 3' IR KO1 in equimolar amount of approximately 160 ng of each. Nested primers (Table 8) were used to increase the DNA yield. The optimal melting temperature was chosen based on gradient PCR which was performed before the optimization process.

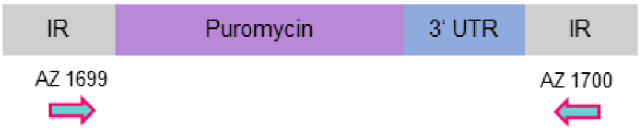

Figure 9: The Scheme of fusion PCR KO1 amplicon with nested primers and their annealing positions. IR - intergenic region; UTR – untranslated region.

Table 8: Nested primers for KO1 amplicon

Primer name and orientation	Code	Sequence
5780 KO1 nested Forward	AZ1699	GTGCTGATTAGCTGTTGCTG
5780 KO1 nested Reverse	AZ1700	GTTTAAGTGAAGACTCAACG

For this purpose, KOD polymerase was also used in a 50-µl reaction, and the reagents were the same as in Table 6. The fusion PCR was performed in two separate runs. The first run was performed without primers to allow the overlapping parts of each piece to anneal. The second run started immediately after the first run, only the nested primers and an additional 0.5 µl of KOD polymerase were added to the reaction. Both runs are described in Tables 9 and 10.

Table 9: The first PCR run for KO1 amplicon

Step	Number of cycles	Temperature [°C]	Time
Polymerase activation	1	95	2 min
Denature	15	95	20 sec
Annealing		48	10 sec
Extension		70	60 sec
Finish	1	70	5 min
		12	∞

Table 10: The second PCR run for KO1 amplicon

Step	Number of cycles	Temperature [°C]	Time
Polymerase activation	1	95	2 min
Denature	35	95	20 sec
Annealing		48	10 sec
Extension		70	60 sec
Finish	1	70	5 min
		12	∞

The fusion PCR for the KO2 cassette (Figure 10) was performed similarly to the KO1 fusion PCR just with different amount of template DNA – 5' IR KO2, blasticidin cds, 3' IR

KO2. This PCR did not required the usage of nested primers. Equimolar concentrations were used again for the three individual starting pieces of DNA but this time 50 ng of each was enough for significant yield. The runs are described in Tables 11 and 12.

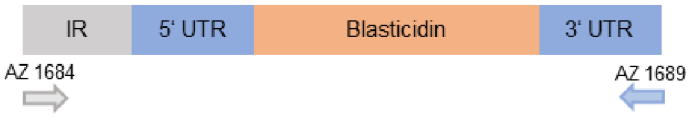

Figure 10: The scheme of complete fusion PCR KO2 amplicon with primers and their annealing positions. IR - intergenic region; UTR – untranslated region

Table 11: The first PCR run for KO2 amplicon

Step	Number of cycles	Temperature [°C]	Time
Polymerase activation	1	95	2 min
Denature	15	95	20 sec
Annealing		48 - 62	10 sec
Extension		70	60 sec
Finish	1	70	5 min
		12	∞

Table 12: The second PCR run for KO1 amplicon

Step	Number of cycles	Temperature [°C]	Time
Polymerase activation	1	95	2 min
Denature	35	95	20 sec
Annealing		48 - 62	10 sec
Extension		70	60 sec
Finish	1	70	5 min
		12	∞

Three things seemed to be crucial for the optimization of these fusion PCR reactions: the equimolar amount of template DNA, the construction of the PCR in two runs and the fact that we could only ever generate a complete amplicon if we started the PCRs with the three original single pieces. Amplification of the extracted complete amplicons was never successful. Both KO1 and KO2 amplicons were sterilized by ethanol precipitation.

3.2.4 PCR verification of thioredoxin 5780 sKO and dKO cell lines

Thioredoxin 5780 single knock out and double knock out cell lines in the background of 29.13 and RBP6 were verified by PCR reaction. The used primers are listed in Table 13 and 16. The PCR reaction conditions are shown in Table 14 and 15.

Table 13: Primers used for thioredoxin 5780 sKO cell lines verification. All primers are listed in 5' → 3' direction

Primer name and orientation	Code	Sequence
KO1 Thx 5' forward	AZ1710	TCCTTTCAGAGATTCTCCCC
KO1 Thx 5' reverse	AZ1711	GGCTTGTACTCGGTAACCAT
KO1 Thx 3' forward	AZ1712	CAACCTCCCCTTCTACGAG
KO1 Thx 3' reverse	AZ1713	CGGGCTCTTGTGGATGTTAT
Thx cds forward	AZ1714	CACTACATTTGTCCTCGCAC
Thx cds reverse	AZ1715	CTGTCCAGTAATGGAAGGAG

Table 14: The reagents used in the PCR reaction with the OneTaq polymerase

Solution	Volume [µl]
5x OneTaq Standard Reaction Buffer	10
10 mM dNTPs	1
10 µM Forward primer	1
10 µM Reverse primer	1
OneTaq polymerase	0,25
110 ng Template DNA	individual

Table 15: The PCR program for thioredoxin 5780 sKO and dKO cell lines verification

Step	Number of cycles	Temperature [°C]	Time
Initial denaturation	1	94	30 sec
Denature	35	94	20 sec
Annealing		52	10 sec
Extension		68	1 min 10 sec
Final extension	1	68	5 min
Infinite hold		4	∞

Table 16: Primers used for thioredoxin 5780 KO2 verification. All primers are listed in 5'→3' direction.

Primer name and orientation	Code	Sequence
KO2 Thx 5' forward	AZ1716	GCTCTACTCTCAGAATGTCC
KO2 Thx 5' reverse	AZ1717	GGGTGGATTCTTCTTGAGAC
KO2 Thx 3' forward	AZ1718	TCGTGAATTGCTGCCCTCTG
KO2 Thx 5' reverse	AZ1719	TTGTCCCTCCTTCCACTTCC

After the PCRs, to an aliquot of PCR reaction were added 6 µl of 10x DNA loading dye and samples were resolved on the 1% agarose gel with 1 µl of ethidium bromide and visualized at the Chemidoc Imaging system.

3.3 Cell transfections

For the transfection of 29.13 and RBP6 cells with a plasmid containing a cytosolic or mitochondrial HyPer7 gene to create 29.13 cytoHyPer7, 29.13 mitoHyPer7, RBP6 cytoHyPer7 and RBP6 mitoHyPer7 cell lines, $5x10^7$ cells were harvested at mid-log phase and spun down at 1300xg for 10 minutes at 4 °C. The pellet was washed once with 10 ml of ice- cold CytoMix buffer (25 mM HEPES, pH 7.6; 120 mM KCl; 0.15 mM $CaCl_2$; 10 mM potassium phosphate buffer, pH 7.6; 2 mM EDTA, 5 mM $MgCl_2$; 6 mM glucose), spun down and resuspended in 1 ml ice-cold CytoMix. The cuvettes (0.2 cm gap) were then loaded with

10 µg of sterile DNA (linearized pHD 1344-t with cyto or mitoHyPer7) and 0.5 ml of cell suspension. The BTX ECM electroporator with preset values of 1600 V, 25 Ω and 50 µF was used for electroporation. The electroporated cells were resuspended in 6 ml SDM-79 medium with 10% FBS, but without the selection antibiotic, and incubated overnight at 27 °C for 16 hours. The next day, 6 ml of SDM-79 medium with 10% FBS and twice the concentration of a suitable selective antibiotic were added. Semiclonal cell lines were obtained by dilution in 24- well plates. 2 ml of the prepared culture were added to the first row of wells, 1.5 ml of fresh SDM-79 medium (10% FBS, 1x concentration of a selective antibiotic) to the second and third row and 1 ml of the same fresh SDM-79 medium to the fourth row. From the first column, 0.5 ml was transferred to the second and so on until each well contained 1.5 ml of the cell culture.

The cell lines 29.13 Thx sKO and RBP6 Thx sKO were generated by transfection of 4 µg of the KO1 cassette (Figure 9). The 29.13 Thx dKO and RBP6 Thx dKO cell lines were generated by transfection of 4 µg of the KO2 cassette (Figure 10) into the respective Thx sKO cell lines. From each sKO cell line, $5x10^7$ cells were harvested and after spinning, the pellet was washed once in 10 ml sterile 1x PBS-G (7 mM Na_2HPO_4; 3 mM NaH_2PO_4; 0.13 M NaCl; 6 mM glucose; pH 7.4) and finally resuspended in 100 µl AMAXA Human T- cell solution at 4 °C and loaded into the provided cuvette (2 mm distance). Electroporation was performed using the AMAXA Nucleofor II (Lonza) electroporator with the preset program X- 014. The rest of the process was the same as described above.

It is very difficult to generate true clones that originate from a single cell in PF *T. brucei*. Therefore, we perform a serial dilution and select the transfectants that arise from the highest diluted plate. Thus, we will refer to these cell lines as clonal.

3.4 Preparation of the whole cell lysate

Whole cell lysates were prepared by spinning $1x10^8$ cells in the Centrifuge 5810 (Eppendorf) at 1300xg for 10 min at 4 °C. The cells were then washed once with 1x PBS (7 mM Na_2HPO_4; 3 mM NaH_2PO_4; 0.13 M NaCl; pH 7.4) and finally resuspended in 200 µl of 1x PBS and 100 µl of 3x SDS PAGE loading dye (6% SDS; 300 mM DTT, 150 mM Tris pH 6.8; 30% glycerol; 0,02% bromophenol blue). SDS gives the proteins a negative charge so that they can migrate towards the positively charged electrode (the anode) during electrophoresis. The samples were incubated on the heat block at 97 °C for 10 minutes and stored at -20 °C.

3.5 SDS PAGE and western blot analysis

Whole cell lysates ($1x10^7$ cells/well) or protein samples from the subcellular fractionation (equivalent to $6.7x10^5$ cells/well, $2.7x10^6$ cells/well or $2x10^6$ cells/well depending on the primary antibody) were again heated to 97 °C for 3 minutes and loaded on the commercial Invitrogen Novex WedgeWell 4 to 20 %, Tris – Glycine gel (Thermo Fisher Scientific) which was placed in the apparatus filled with 1x SDS running buffer (25 mM Tris; 192 mM glycine; 0.1% SDS). Electrophoresis was performed for 2.5 hours at 110 V until the bromophenol blue dye ran out of the gel. After the electrophoresis, proteins were transferred on the activated PVDF membrane (Thermo Fisher Scientific) through electroblotting. Activation of the membrane included the immersion in the methanol for 40 seconds, then in milliQ water for 2 minutes and finally in the 1x transfer buffer (39 mM glycine; 37 mM Tris) for at least 5 minutes. All other components of the sandwich were also soaked up with the 1x transfer buffer. The sandwich was assembled in this order: black plastic cassette, sponge, filter paper, gel, membrane, filter paper, sponge, red plastic cassette, placed in the apparatus at 4 °C and the transfer ran at 90 V for 90 minutes. The membranes were placed in a 50 ml Falcon tube with 5 % milk and rotated for 1 hour at RT. The membranes were then stored overnight at 4 °C. The next day, the membranes were probed with appropriate primary antibodies – mouse α-V5 antibody (1:1000), rabbit α-AAC antibody (1:1000), rabbit α-GFP antibody (1:1000), rabbit α-APRT (adenosine phosphoribosyl transferase, 1:500), monoclonal α-HSP70 (1:5000) in 5 ml of 5% milk. The tubes containing the membranes and antibodies were rotated for 1 hour and then washed three times with 25 ml 1x PBS-T (7 mM Na_2HPO_4; 3 mM NaH_2PO_4; 0.13 M NaCl; pH 7.4; 0.05% Tween 20). The first wash lasted 15 minutes and the other two 5 minutes each. The membranes were then probed with secondary antibodies – goat anti-mouse HRP or goat anti-rabbit HRP, both at a dilution of 1:2000 in 5 ml of 5% milk. The membranes were again incubated in the rotator for 1 hour and then washed as before. Then they were placed on the plastic foil and the probed proteins were visualized using the Clarity Western ECL substrate (BioRad) containing two reagents: – Clarity Western Peroxide Reagent and Clarity Western Luminol/Enhancer Reagent.

These reagents were mixed in a ratio of 1:1 in a total volume of 500 µl and applied to the membrane. The mixture generates a chemiluminescence signal when it comes into contact with the HRP bound to the secondary antibody and this signal was detected using the Chemidoc Imaging System (BioRad).

3.6 Subcellular fractionation

For subcellular fractionation $1x10^8$ cells were harvested, washed once in 1x PBS. The pelleted cells were resuspended in 500 µl of SoTE (20 mM Tris-HCl, pH 7.5; 0.6 M sorbitol; 2mM EDTA) and then 500 µl of warm SoTE/0.03% digitonin (20 mM Tris-HCl, pH 7.5; 0.6 M sorbitol; 2 mM EDTA; 0.03% digitonin) was added. The tube was inverted once and the mixture was incubated on ice for 5 minutes. Then the samples were spun at 7000 rpm for 3 minutes at 4 °C. The supernatant represents a cytosolic fraction while the pellet contains organelles including mitochondria. 500 µl of the cytosolic fraction were mixed with 250 µl of 3x SDS PAGE loading dye. Pellet was washed once with 950 µl of 1x PBS and resuspended in 950 µl of 1x PBS. 500 µl of this mixture was mixed with 250 µl of 3x SDS PAGE loading dye. All the samples were then boiled at 97 °C for 10 minutes in the heat block and stored at -20°C. Later, the samples were resolved by SDS PAGE and the proteins were visualized by western blot.

3.7 Immunofluorescence assay

$5x10^7$ cells in their mid-log phase (density 0,6-0,8$x10^7$ cells/ml) were spun at 1300xg for 10 minutes at room temperature. In the TC hood the pellet was resuspended in 1 ml of SDM-79 media and cells were transferred to the original flask with extra 4 ml of SDM-79. The cells were incubated with 2 µl of 500 µM MitoTracker (Thermo Fisher Scientific) on a shaker at dark, 27 °C for 30 minutes. The cells were then spun down at 1300xg for 10 minutes at RT. The pellet was resuspended in 1 ml of fresh SDM-79 medium and transferred to a new 25 cm^2 culture flask. A further 4 ml of fresh medium were added and the cells were shaken for 5 minutes in the 27 °C incubator. Then $2x10^7$ cells were harvested by centrifugation as before in 2ml Eppendorf tubes. During the whole process the cells were kept in the dark. The cell pellet was washed with 1.8 ml of 1x PBS, resuspended in 200 µl 1x PBS and fixed by adding another 200 µl of 7.4% formaldehyde (pH 7.4). 40 µl of fixed cells were applied to the cover slip and incubated for 15 minutes at RT with the cover placed on top to protect them from light. After incubation, the buffer was aspirated and the cells were washed 3x with 100 µl of 1x PBS. The cells were permeabilized by 100 µl of 0.1% Triton X- 100 in 1x PBS for 10 minutes and washed 3x with 1x PBS. After permeabilization, the cells were incubated with 100 µl of 5.5% fetal bovine serum (FBS)/PBS for 1 hour to block unspecific interaction. The buffer was then removed, cells were washed 2x with 1x PBS and probed with primary antibody mouse α-V5 (40 µl α-V5 at 1:200 dilution in 3% BSA/PBS)

for 1 hour in the dark at RT. Then they were washed 3x with 100 µl of 1x PBS-T and 2x with 100 µl of 1x PBS. Finally, the cells were then probed with the goat anti-mouse Alexa fluor 488 (Invitrogen) secondary antibody at a ratio of 1:400 (40 µl of secondary antibody in the 3% BSA/PBS) for 1 hour in the dark at RT.

In addition, the ProLong Glass Antifade mounting medium with Nunc Blue (Invitrogen) was appliaed to stain the nucleus and kinetoplast DNA. The mountant was warmed up to the room temperature and 2 drops were applied directly onto the prepared samples. The slide was pressed onto the coverslip to avoid bubbles and also to bring the cells into the same layer. The excess liquid was removed with soft napkin.

To visualize only the nucleus and the kinetoplast, $5x10^7$ cells were harvested, washed with 1x PBS and fixed with 7.4% formaldehyde as described above. $2x10^6$ cells were placed on the cover slip and mounted with the ProLong Glass Antifade Mountant with Nunc Blue. The slides were pressed onto the coverslip and the prepared samples were stored in 4 °C.

The slides were viewed under the imaging fluorescence microscope Axioplan 2 (Zeiss) using FITC filter to detect HyPer7 (α-V5), Texas Red filter to detect MitoTracker and DAPI filter to detect DNA (nucleus and kinetoplast). The shape and overall morphology of cells was visualized by polarized light. The images were taken by CCD camera DP73 (Olympus) and processed by using the Photoshop (Adobe).

3.8 HyPer7 fluorescence measurements

3.8.1 HyPer7 fluorescence measurement on the Spark microplate reader

To scan for changes in fluorescence of HyPer7, we used the Spark multimode microplate reader (Tecan). This device for fluorescence measurements possesses, apart other features, the Xenon flash lamp, double monochromators and the photomultiplier as detector. It enables to read fluorescence from top or bottom of the microplate and also contains an automatic injector. The excitation and emission lights are directed to the fiber by rotating the mirror and fiber end and the wavelength selection is done either by filter or double monochromators. After reflecting at the mirror the fluorescent signal is detected by photomultiplier (Tecan Spark manual, 2022). For our HyPer7 measurements we used two excitation wavelengths – 390 nm (with 10 nm bandwidth) and 469 nm (with 20 nm bandwidth) and one emission wavelength – 525 nm (with 20 nm bandwidth).

All our samples (100 µl) were measured in black NUN96fb FluoroNunc™ plate (ThemoFisher Scientific) reading the fluorescence from the top. The harvested cells were washed once in non-fluorescent medium to remove all traces of the SDM-79 medium which contains fluorescent phenol red. The final cell concentration was either $1x10^6$ cells/100 µl or $1x10^7$ cells/100. We tested three types of non-fluorescent media – cMM media (140 mM NaCl; 5 mM KCl; 1 mM $MgCl_2$; 2 mM $CaCl_2$; 20 mM HEPES; 10 mM glucose; 10% FBC; pH 7.4) (Poburko *et al.* 2011), MiR05 media (0,5 mM EGTA; 3 mM $MgCl_2$; 60 mM lactobionic acid; 20 mM taurine; 10 mM KH_2PO_4; 20 mM HEPES; 110 mM D-sucrose; 1g/l BSA; pH 7.1) (Gnaiger *et al*., 2000) and ANT media (8 mM KCl; 110 mM K – gluconate; 10 mM NaCl; 10 mM HEPES; 10 mM K_2HPO_4; 0,015 mM EGTA; 0.5 mg/ml BSA; 10 mM mannitol; pH 7.25) (Chinopoulos *et al.* 2009).

We performed a series of experiments with $1x10^7$ cells/ml and $1x10^8$ cells/ml to measure HyPer7 response to external 1 mM H_2O_2, 50 mM DTT, 1 mM KCN (complex IV inhibitor) and 10 µg/ml oligomycin (F_oF_1 ATP synthase inhibitor).

3.8.2 HyPer7 fluorescence measurement using spectrofluorometer

The fluorometer measurements were done with cytoHyPer7 and mitoHyPer7 29.13 cell lines compared to the 29.13 parental cell line. $1x10^7$ cells were harvested by centrifugation (1300xg, 10 minutes, RT), washed and resuspended in total of 10 ml of the Mir05 media. The fluorescence measurement was done on the Fluorolog 3 machine (HORIBA Jobin Yvon) with double monochromators, a Xenon flash lamp and a photomultiplier tube as a detector. Samples were measured in 1ml volume in a cuvette with 1cm path length at the RT. Within the experiment the cells were also treated with 294 mM H_2O_2 to see whether the probe reacts to the externally added hydrogen peroxide.

3.8.3 HyPer7 fluorescence measurement using the fluorescence activated cell sorting method (FACS)

Flow cytometry is a method that uses light to measure some properties of cells such as size and granulosity. The light source is a laser and cells are moved past the light source through a fluidic system. As the cells travel through the system they scatter the light and fluorescent particles, for example HyPer7, emit fluorescence. This fluorescence is later filtered and transformed into an electrical signal by a set of detectors, in this case a photodiode and several photomultipliers (BD FACS Canto II Reference manual, 2019). The instrument is able

to measure the fluorescence signal coming from individual cells so that we can learn which cells from our cell population express the fluorescent protein the most.

This method was used to perform a series of experiments in which we examined the forward scatter (size) and the side scatter (granulosity) as well as the fluorescence response using the FITC filter for HyPer7 probe or the PE filter for TMRE. We always measured 10 000 events (cells). Samples were measured in a BD tube in 1 ml 1x PBS to which we added 200 µl of each prepared sample.

In the first experiment, the $1x10^7$ cells were washed and resuspended in the MiR05 medium. Samples were treated with either 1 mM H_2O_2 (5 minutes of incubation) or 30 mM DTT (10 minutes of incubation) and analyzed by FACS as described above.

In the second experiment, we used two OXPHOS inhibitors. $5x10^6$ cells were harvested (1300xg, 5 minutes), washed once and resuspended in the MiR05 medium. Then the cells were treated with the 60 nM TMRE (27 °C for 30 minutes) to measure mitochondrial membrane potential. After the incubation, the cells were analyzed by FACS (time 0 min). Then they were treated with 10 µg/ml oligomycin and analyzed at different time intervals (10, 30 and 50 minutes).

In the last experiment, we examined the Hyper7 fluorescence in the cells undergoing differentiation (i.e. RBP6 induced cells). This time only the intracellular H_2O_2 concentrations were measured during the entire 6 days of differentiation and also on day 0, i.e. on cells without induction (not treated with tetracycline). $1x10^7$ cells were harvested on each day of differentiation. Again, we stained the cells with TMRE, washed them once and resuspended them in MiR05 medium. The TMRE allowed us to measure the membrane potential, which enabled us to check whether differentiation had taken place.

4 Results

4.1 CytoHyPer7 and mitoHyPer7 cell line creation

Since it was previously determined that H_2O_2 production plays a role in PF Tb differentiation, we implemented the genetically encoded biosensor Hyper7 into the RBP6 inducible cell line. Initially, we wanted to determine when and where in the cell H_2O_2 was generated during PF differentiation, so we targeted the Hyper7 to either the cytosol or the mitochondrial matrix. We also generated Hyper7 parasites in the parental cell line 29.13 to first verify the efficacy of the biosensor in various conditions.

4.1.1 Generation of pHD 1344-t plasmid with HyPer7 gene

Hyper7 does not contain any targeting sequence, so it will be localized in the cytosol. In order to target Hyper7 to the mitochondrial matrix, it was fused with the well-defined mitochondrial targeting sequence of the iron sulfur cluster assembly protein, IscU. The codons for the first 25 amino acids of the N-terminus of IscU were included in the forward primer used to amplify the Hyper7 coding sequence. This same approach has been used previously to target other ectopic proteins to the mitochondrion of *T. brucei* (Taleva *et al.*, 2023). HyPer7 was amplified from the pLifeAct-Hyper7 (Pak *et al.*, 2020) plasmid (purchased from Addgene, plasmid #136464) using the proof-reading polymerase KOD. The PCR amplicons were resolved on a 1% agarose gel and visualized with ethidium bromide to reveal a prominent band of the expected sizes (1457 bp cyto, 1529 bp mito) (Figure 11).

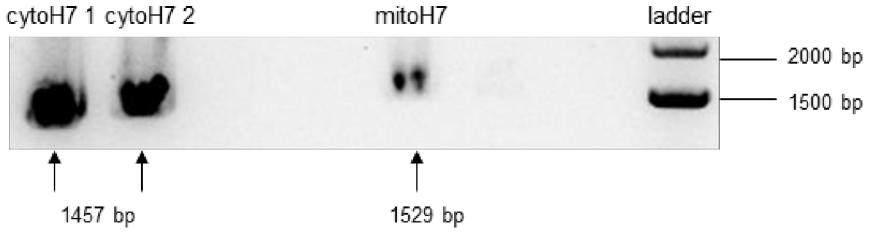

Figure 11: Representative PCR fragments of cytosolicHyPer7 and mitochondrial HyPer7. CytoH7 – cytosolic HyPer7, mitoH7 – mitochondrial HyPer7. Ladder: GeneRuler 1kb Plus DNA ladder (Thermo Fisher Scientific).

The PCR fragments (cytoH7 1 and mitoH7) were digested with the restriction enzymes BamHI and HindIII before being ligated into the similarly digested pHD1344-t plasmid. To verify the successful cloning, we isolated plasmid DNA from transformed bacterial colonies and analyzed the clones by restriction digest (Figure 12).

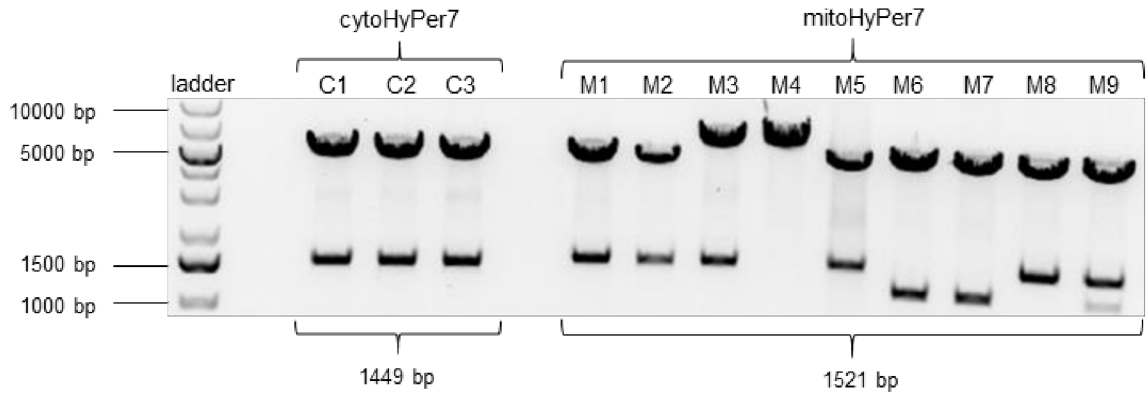

Figure 12: Representative digest analysis of plasmids pHD1344-t with cytosolic or mitochondrial HyPer7. C1-C3 – clones of cytosolic HyPer7, M1-M9 – clones of mitochondrial HyPer7. Ladder: GeneRuler 1kb Plus DNA ladder (Thermo Fisher Scientific).

The majority of the clones contained DNA fragments of the expected sizes. To verify that no errors were introduced into the Hyper7 coding sequence, clone cytoHyPer7 C2 and mitoHyPer7 M1 were sent for sequencing at SEQme (Prague). Sequencing alignments comparing the generated plasmids with predicted *in silico* molecules did not reveal any mutations that would affect the primary amino acid sequence. Therefore, these two clones were linearized and electroporated with the 29.13 and RBP6 cell lines to generate four new Hyper7 cell lines – 29.13 cytoHyPer7, 29.13 mitoHyPer7, RBP6 cytoHyPer7 and RBP6 mitoHyPer7.

4.2 Verification of HyPer7 expression

4.2.1 CytoHyPer7 and mitoHyper7 29.13 and RBP6 cell line verification

To determine if different clonal cell lines contained varying levels of Hyper7 expression, whole cell lysates were generated and analyzed by western blots probed with an antibody specific for the V5 epitope tag (Figure 13). As a loading control, the membranes were also probed with an antibody raised against the ADP/ATP carrier.

While all tested clones from the 29.13 and RBP6 cell lines expressed HyPer7, there were some significant differences in protein levels between clones. Based on this preliminary screening of Hyper7 expression, the following clones were selected for further analyses: 29.13 cytoHyPer7 D2 and D4 clones, 29.13 mitoHyPer7 C3 and C4, RBP6 cytoHyPer7 D2 and D5 and RBP6 mitoHyper7 C2 and C4.

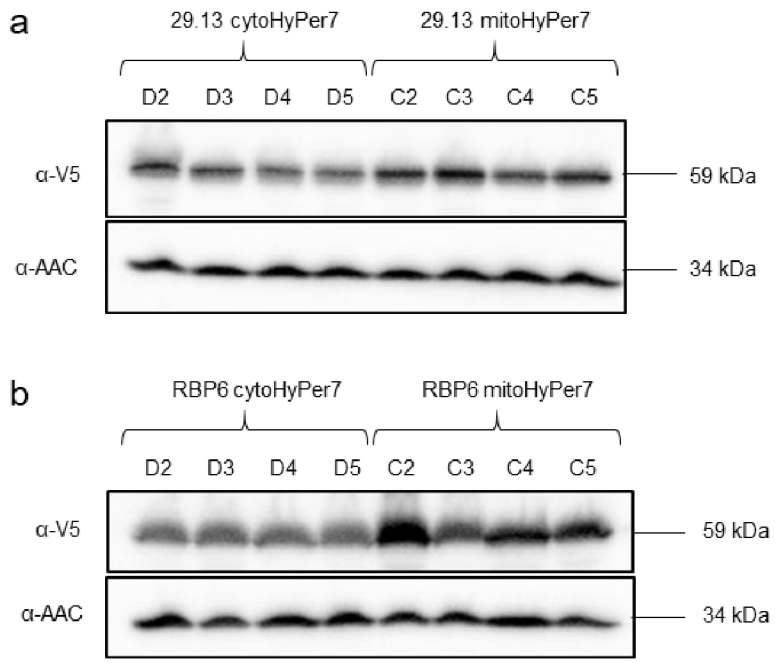

Figure 13: Western blots illustrating the expression of cytosolic or mitochondrial HyPer7 detected by α-V5 antibody in clones of a) 29.13 cell line and **b)** RBP6 cell line. AAC antibody as a loading control. Loaded $1x10^7$ cells per well.

Further, another western blot was performed to determine whether it is possible to detect the HyPer7 by α-GFP (green fluorescent protein) antibody. While it is common to fuse HyPer7 to proteins for subcellular localization or increased functionality, future experiments might be improved if we could avoid tagging HyPer7. Therefore, we compared Hyper7 expression levels on western blots probed with either an α-V5 antibody or an α-GFP antibody (Figure 14). The western blots confirmed that HyPer7 can be detected by the α-GFP antibody, as it produced sharp bands of similar intensity as observed with the α-V5 antibody.

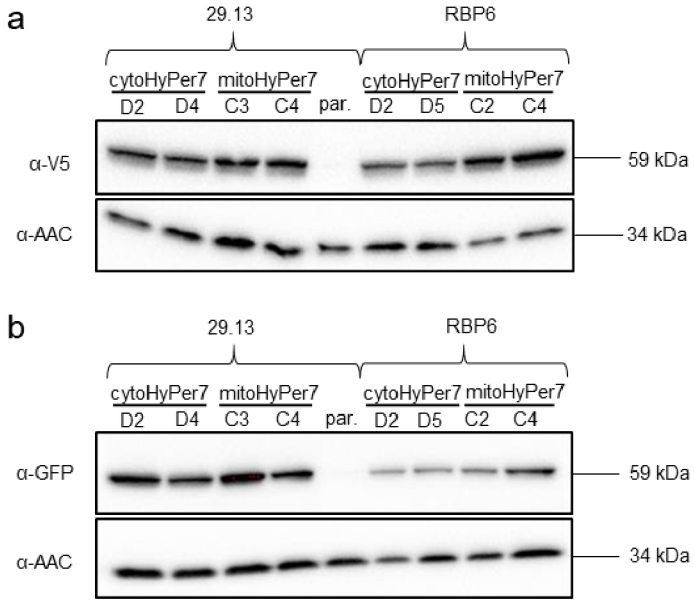

Figure 14: Western blots illustrating the expression of cytosolic or mitochondrial HyPer7 in clones of 29.13 cell line and RBP6 cell line detected by a) α-V5 and **b)** α-GFP antibody. α-AAC antibody as loading control. par. – 29.13 parental cell line. Loaded $6.66x10^6$ cells per well.

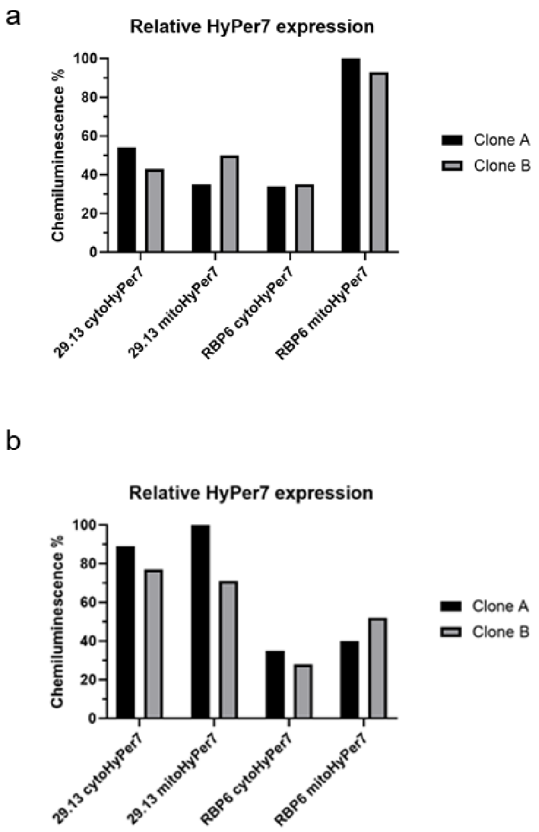

Figure 15: Scanning densitometry analysis for western blots probed by a) α-V5 **and b)** α-GFP **antibodies.** 29.13 cytoHyPer7 Clone A = D2, Clone B = D4; 29.13 mitoHyPer7 Clone A = C3, Clone B = C4; RBP6 cytoHyPer7 Clone A = D2, Clone B = D5; RBP6 mitoHyPer7 Clone A = C2, Clone B = C4.

In order to more carefully analyze the Hyper7 expression levels between clones and cell lines, the results were quantified using scanning densitometry with the ADP/ATP carrier signal acting as a loading control (Figure 15). The quantification of the Hyper7 protein levels analyzed with the α-V5 antibody did not reveal any big discrepancies between pairs of clones of any of the cell lines. The most striking observation is that the RBP6 mitoHyper7 expression levels are almost twice that of the other cell lines. However, this difference is not observed in the western blots probed with the α-GFP antibody. In fact, the quantification from this analysis indicates that Hyper7 is expressed significantly more in the 29.13 cell lines, irrespective of the subcellular localization. While this quantification needs to repeated with biological triplicates to validate the outcome, we preferred the slightly more consistent AAC signals on the membrane probed with α-GFP. Therefore, additional experiments were performed using the following clones that exhibited slightly higher Hyper7 expression levels according to the α- GFP data set: 29.13 cytoHyPer7 D2 and mitoHyPer7 C3; RBP6 cytoHyPer7 D2 and mitoHyPer7 C4 cell lines.

4.2.2 HyPer7 subcellular localization

The subcellular fractionation was performed to confirm the intended localization of cytoHyPer7 or mitoHyPer7 in the 29.13 and RBP6 cell lines. Applying the proper ratio of digitonin to cellular protein amount will result in the disruption of the cellular membrane but leave the mitochondria intact. This occurs because digitonin preferentially binds sterol lipids, which are the most prominent in the cytoplasmic membrane. After this controlled lysis, it is possible to separate the cytosolic and organellar fraction by differential centrifugation.

Equal amounts of both the cytosolic and organellar fractions were analyzed by immunoblotting. An equivalent amount of whole cell lysates was included to indicate the maximum amount of protein expression possible in either subcellular fraction. To verify the purity of the subcellular fractions, the membranes were probed with either the cytosolic marker adenine phosphoribosyl transferase (APRT) or with the mitochondrial heat shock protein 70 (HSP70). The results from these controls demonstrated successful fractionation between the cytosol and organellar fractions as neither marker was detected as a contaminate in the other fraction (Figure 16). As expected, all of the cytoHyper7 was completely restricted to the cytosolic fraction in the RBP6 clone. However, a trace amount was still detected in the organellar fraction of the 29.13 cell line. This slight contamination observed in the mitochondrial fraction is unusual, as the previous heterologous expression of other

proteins in *T. brucei* has not detected this mislocalization. Perhaps this is a sensitivity issue or simply the result of high levels of overexpression overwhelming the *T. brucei* protein trafficking machinery. While the subcellular fractionation data indicates that the mitoHyper7 is predominantly localized in the organellar fraction, there is a small amount detected in the cytosolic fraction for both the 29.13 and RBP6 clones. While the IscU mitochondrial targeting system is the most efficient out of many we have tested in the lab, it is not completely surprising that a very small proportion of the Hyper7 is not fully incorporated into the *T. brucei* mitochondrion. However, this result will need to be considered as we interpret data from future experiments involving these cell lines.

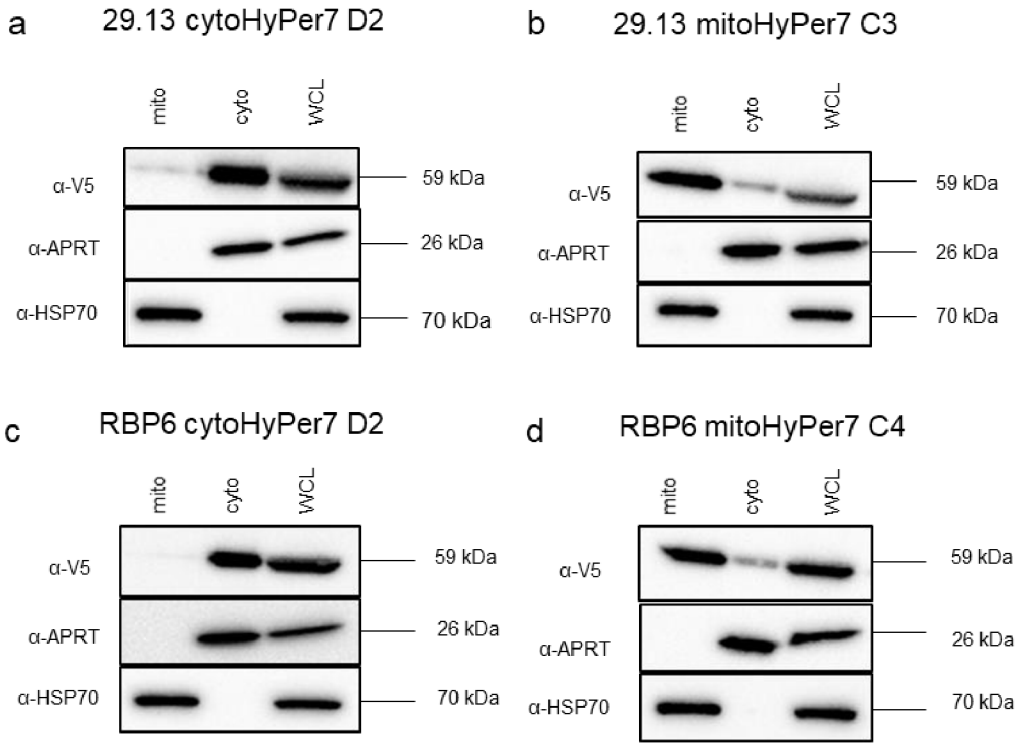

Figure 16: Western blots showing the verification of cytosolic or organellar localization of adequately localized HyPer7 in a) 29.13 cytoHyPer7 D2, **b)** 29.13 mitoHyPer7 C3, **c)** RBP6 cytoHyPer7 D2 and **d)** RBP6 mitoHyPer7 C4. Cytosolic APRT and mtHSP70 are used as controls. WCL – whole cell lysate. Number of cells loaded per well: for α-V5 – $2x10^6$; for α-APRT – $2.67x10^6$; for α-HSP70 – $6.67x10^5$. The antibodies dilutions were 1:2000 for α-V5, 1:500 for the α-APRT and 1:5000 for the α-HSP70

4.3 HyPer7 fluorescence responses detected by the Spark microplate reader

As described in the introduction, the fluorescent probe Hyper7 has two excitation maximas at 400 nm and 499 nm and one emission peak centered at 516 nm. The excitation and absorption spectra of HyPer7 change in a ratiometric way upon oxidation, resulting in

a decrease in 400 nm and an increase of the 499 fluorescence (Pak *et al*. 2020). This oxidized state of the probe is reversible by different reducing systems, allowing us to measure the fluorescence repeatedly.

4.3.1 Cytosolic HyPer7 characteristics in the procyclic 29.13 *T. brucei* cell line

Currently, there are very few references for HyPer7 measurements performed with a plate reader. Most experiments in the literature were performed either using microscopy with single cells or a flow cytometer to analyze a population of cells. While the single cell microscopy experiments are powerful, at the moment this is very technically difficult for us to achieve with our motile parasites. We began our Hyper7 fluorescence measurements with the plate reader because of the ability to quickly screen many conditions in a single experiment, the flexibility provided by injecting up to two different activators of ROS to a cell population and the precision of the measurements due to its ability to excite the cells with a monochromator. To determine how well the HyPer7 probe works in *T. brucei*, we first analyzed the cytoHyPer7 cell line when it was treated with 1 mM H_2O_2. While this was in large excess of the physiological levels of H_2O_2 that we hope to eventually measure in our *T. brucei* system, this was the most direct experiment to analyze how HyPer7 responds to peroxide within the parasite's system. Fluorescence emissions at 525 nm were measured every 2 minutes. Each well on a plate was first excited at 390 nm and then at 469 m (Hoehne *et al*. 2022). From here on forward, we will refer to the fluorescence emmissions detected at 525 nm with reference to the excitation wavelengths of either 390 or 469 nm with the following nomenclature: fluorescence (exc. 390 or exc. 469).

Our first experiment was to compare the H_2O_2 induced Hyper7 responses from two different cytoHyPer7 clonal cell lines. These parasites were seeded at $1x10^7$ cells/100 µl for a high density of $1x10^8$ cells/ml in the low fluorescence media ANT (Figure 17). After allowing time to reach a baseline fluorescence reading, H_2O_2 was injected after 14 minutes.

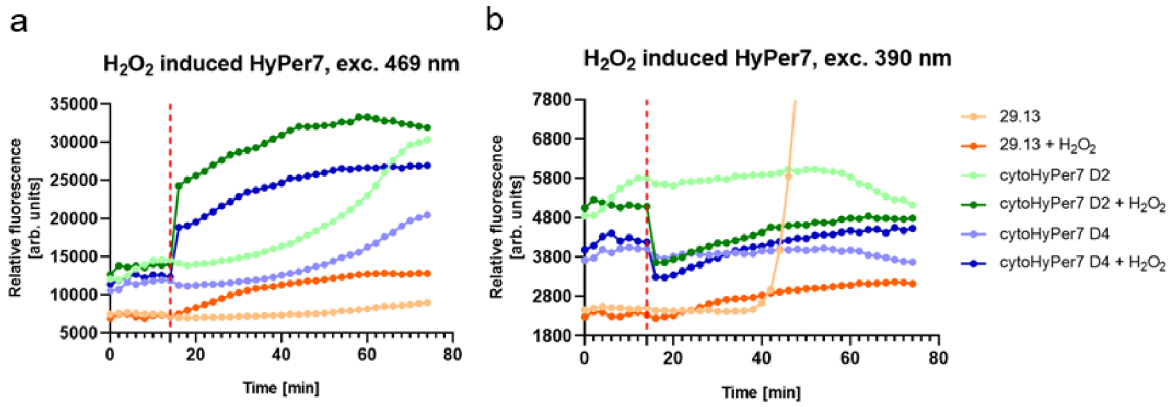

Figure 17: The fluorescence responses of HyPer7 cell lines when induced by H_2O_2 a) cell lines seeded at $1x10^8$ cells/ml, exc. 469 nm and **b)** cell lines seeded at $1x10^8$ cells/ml, exc. 390 nm. The fluorescence was also measured for each H_2O_2 untreated clone as well as the 29.13 parental cell line without Hyper7**.** All cell lines were resuspended in ANT medium. H_2O_2 injected after 14 minutes (red line).

An immediate jump in fluorescence (exc. 469 nm) (Figure 17a) was detected when H_2O_2 was added to both cytoHyPer7 clones compared to the parental 29.13 cell line that does not contain the fluorescence probe HyPer7. This indicates that the kinetics of the cytosolic HyPer7 is very quick, occurring within 4-5 minutes of the H_2O_2 challenge. Most importantly, this spike in fluorescence was not detected in the same clones that were not treated with H_2O_2. Interestingly, the fluorescence responses gradually increased slightly over time in the 29.13 parental cell line treated with H_2O_2. This phenomenon was also observed on a similar level after the initial spike in fluorescence of the cytoHyPer7 cell lines. Therefore, this trailing increase is not representative of the H_2O_2 induced HyPer7 fluorescence.

Another beneficial characteristic of the HyPer7 is that it should be fully reversible and the fluorescence levels should eventually return towards the baseline levels observed before the H_2O_2 challenge. However, this did not occur over the 80 minutes that we monitored the fluorescence. This can be the result of an overwhelming H_2O_2 challenge that saturates not only the Hyper7, but also the endogenous *T. brucei* ROS detoxification components. Future experiments can be performed with decreasing amounts of H_2O_2 to determine if the Hyper7 can be recycled on a shorter time frame to report successive H_2O_2 production events.

As expected, the cytoHyPer7 cell lines exposed to H_2O_2 had significant decreases in fluorescence (exc. 390 nm) compared to the H_2O_2 treated 29.13 parental cell line (Figure 17b). This effect was also observed over a very short time frame of about 2-4 minutes from

the injection with H_2O_2. Importantly, this effect was not observed in the cytoHyPer7 cell lines not challenged with H_2O_2. Once again, the fluorescence levels (exc. 390 nm) in the cell lines treated with H_2O_2 gradually increased over the 80-minute time frame of the experiment. Since a similar rate of fluorescence change was measured even in the 29.13 parental cell line without Hyper7, this phenomenon probably does not represent the recycling of the Hyper7.

These increases in fluorescence are plotted as the fold difference compared to the changes measured in the 29.13 parental cell line during the same time period (Figure 18). This analysis correlates to the slightly higher levels of cytoHyPer7 expression we measured in clone D2, whether analyzed with the α-V5 or α-GFP antibodies (Figure 15).

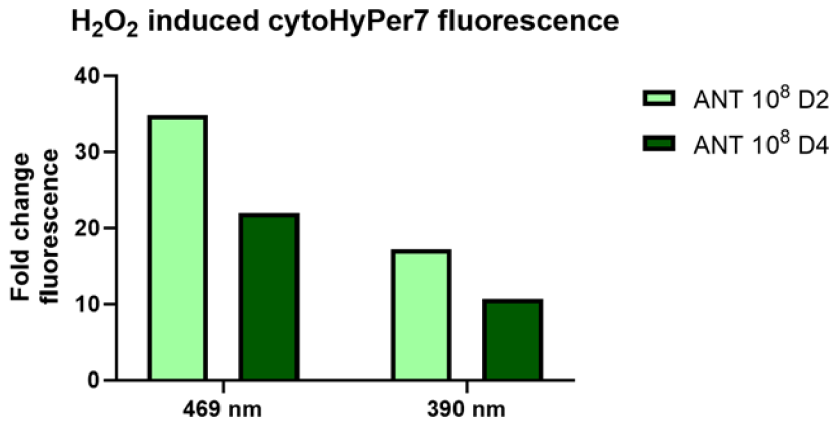

Figure 18: Fold change fluorescence analysis for 29.13 cytoHyPer7 clones D2 and D4 treated with 1 mM H_2O_2 ANT media seeded at $1x10^8$ cells/ml.

4.3.1.1 Optimization of low fluorescence media

The standard culturing medium for *T. brucei* SDM-79 contains many potential molecules that can cause fluorescence (i.e. phenol red, FBS, aromatic amino acids, etc.). Thus, the challenge is to find a medium that minimizes fluorescence background but also provides enough essential nutrients to limit any unintentional stress on the parasites throughout the course of the more than 80-minute experiment. Therefore, we performed the Hyper7 measurements with cell resuspended in various media previously used in similar assays. The first experiment used the ANT buffer, which is used to measure the kinetic rates of the mitochondrial ADP-ATP carrier of intact cells (Chinopoulos *et al.*, 2009). We also compared this to the fluorescence levels measured in Hyper7 cell lines resuspended in MiR05 medium, which was previously optimized to measure the rate of respiration of intact cells (Gnaiger *et al.*, 2000). Finally, we also tried the complete minimal medium (cMM) previously

used to measure fluorescence from HEK293 cells expressing Hyper7 (Jacobs *et al*. 2022), (Poburko *et al*., 2011). The fluorescence assay was performed as previously described with $1x10^8$ cells/ ml of each of the cytoHyper7 clonal cell lines resuspended in the cMM and Mir05 buffers (Figure 19).

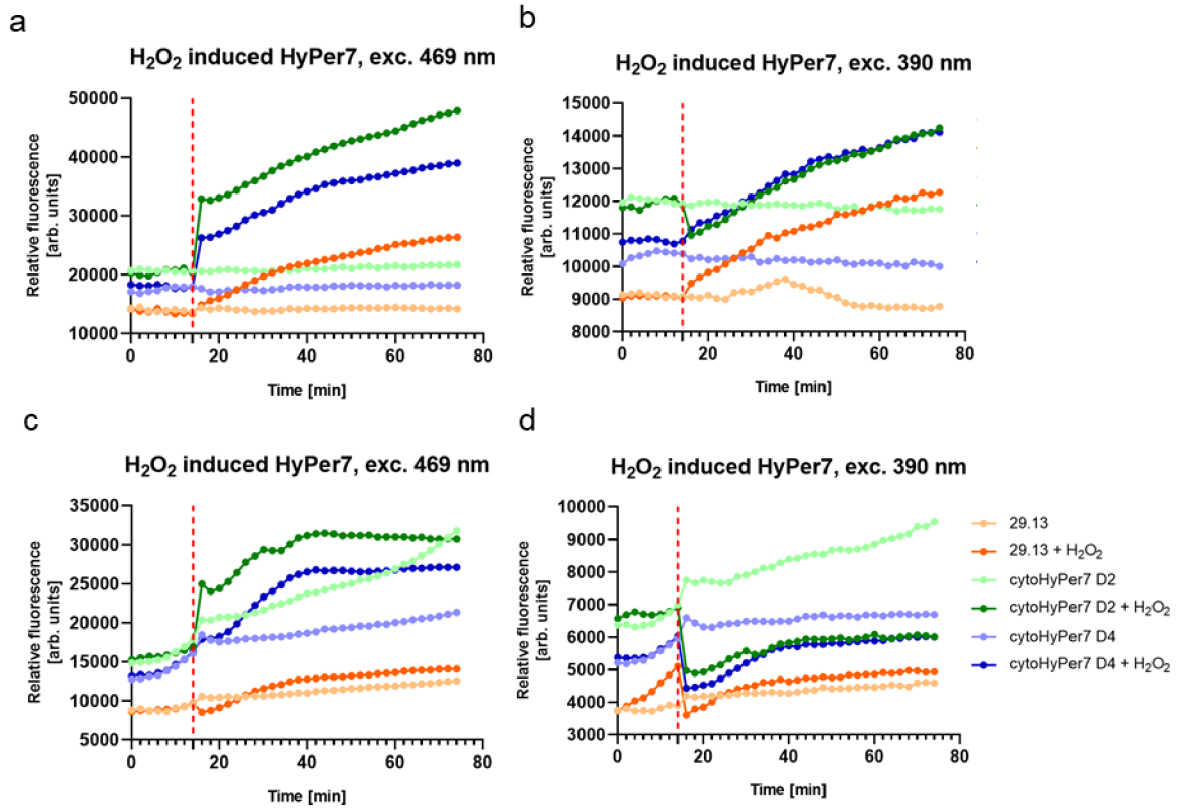

Figure 19: The fluorescence responses of HyPer7 cell lines when induced by H_2O_2 in comparison with noninduced cell lines a) cMM medium, excited at 469 nm **b)** cMM medium, excited at 390 nm **c)** MiR05 medium, excited at 469 nm **d)** MiR05 medium, excited at 390 nm. All cell lines seeded at $1x10^8$ cells/ml. H_2O_2 injected in 14 minutes (red line). 29.13 – parental cell line without HyPer7.

We observed sharp increases in the fluorescence (exc. 469 nm) of both cytoHyPer7 clones resuspended in cMM medium compared to the 29.13 parental cell line, however this increase was not as large as cytoHyPer7 cells in the ANT medium (Figure 17a, Figure 20).

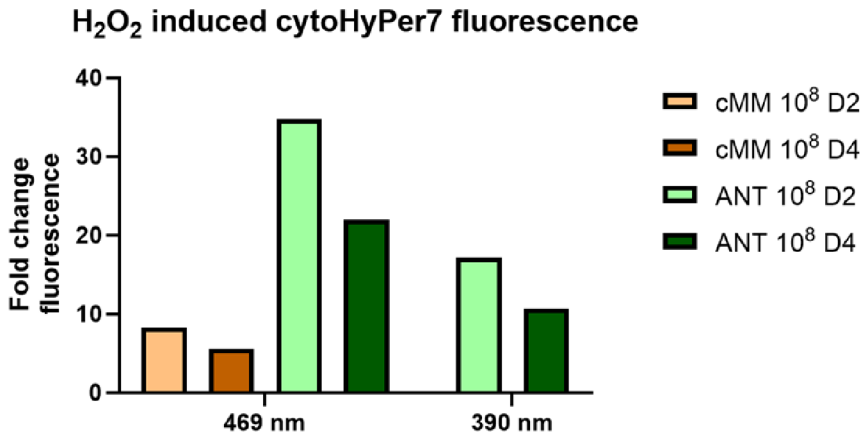

Figure 20: Fold change fluorescence analysis for 29.13 cytoHyPer7 clones D2 and D4 treated with 1 mM H_2O_2 in cMM and ANT media seeded at $1x10^8$ cells/ml.

The fluorescence (exc. 390 nm) data for the cell lines resuspended in cMM was however difficult to interpret as both the 29.13 parental and 29.13 cytoHyPer7 D4 increased significantly upon H_2O_2 stimulation. Only the 29.13 cytoHyPer7 D2 cell line had the predicted decrease in fluorescence (exc. 390 nm) upon H_2O_2 treatment. The data for cell lines resuspended in MiR05 was also difficult to interpret. The fluorescence (exc. 469 nm) coming from the cytoHyPer7 D2 had a sharp increase compared to the parental cell line, however the other cytoHyPer7 D4 clone had no significant increase. Furthermore, while the fluorescence (exc. 390 nm) decreased for both of the cytoHyPer7 cell lines resuspended in MiR05, the decrease was not significantly larger than what was measured in the parental cell line.

The largest changes were observed in the fluorescence responses (both exc. 469 nm and exc. 390 nm) coming from the cells resuspended in the ANT medium. These fluorescence responses at both excitations were also the most consistent with outcomes previously characterized in other HyPer7 literature.

4.3.1.2 Optimizing the density of *T. brucei* parasites

In our experiments we first seeded the cells at $1x10^8$ cells/ml which is quite dense compared to the densities in which the cultures routinely grow in our culturing flasks. Therefore, we also tried the experiments with cells seeded at $1x10^7$ cells/ml (Figure 21).

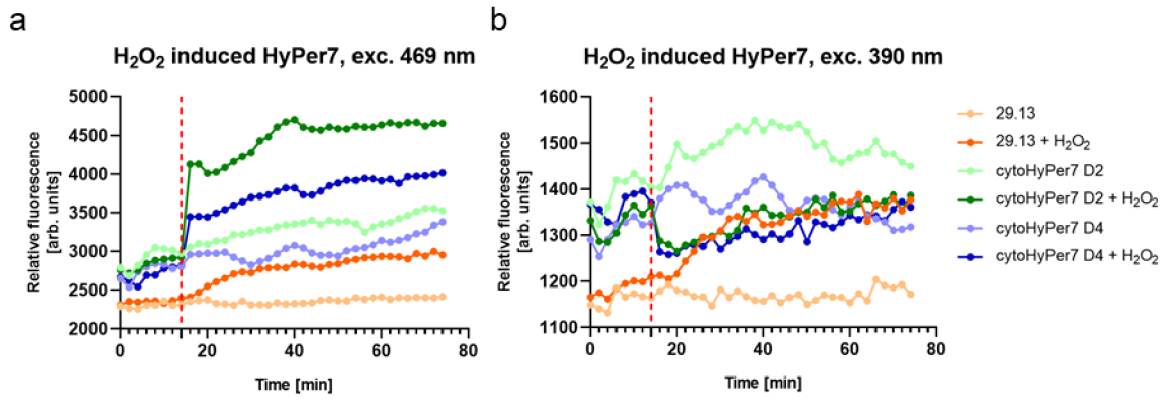

Figure 21: The fluorescence responses of HyPer7 cell lines when induced by H_2O_2 when excited at a. 469 nm and **b.** 390 nm **in comparison with noninduced cell lines.** All cell lines in ANT medium and seeded at $1x10^7$ cells/ml. 29.13 – parental cell line without HyPer7. H_2O_2 injected in 14 minutes (red line). 29.13 – parental cell line without HyPer7.

Again we observed increases in the fluorescence (exc. 469 nm) of the cytoHyPer7 cell lines treated with H_2O_2 compared to the 29.13 parental. While we also observed decreased fluorescence (exc. 390 nm) in the cytoHyPer7 cell lines treated with H_2O_2, there was a lot of fluctuations in the fluorescence of the treated 29.13 parental cell line and untreated cell lines. This was presumably due to the lower dynamic fluorescence range of the assay. The maximum fluorescence (exc. 469 nm) changes occur around 1000 arbitrary units or less and at fluorescence (exc. 390 nm) the difference is around 100 units. Whereas, when more cells were used in the assay ($1x10^8$ cells/ml) the changes in fluorescence (exc. 469 nm) were around 6500 – 10000 units and for fluorescence (exc. 390 nm) around 900 – 1500 units. This suggests that the decreased total amount of Hyper7 in the $1x10^7$ cells/ml was near the limit of the assay's sensitivity. Interestingly, the fold change of both of the fluorescence values (exc. 469 nm and exc. 390 nm) compared to treated parental 29.13 cells was even greater than in the $1x10^8$ cells/ml assay performed with the same cell line resuspended in the ANT medium (Figure 22).

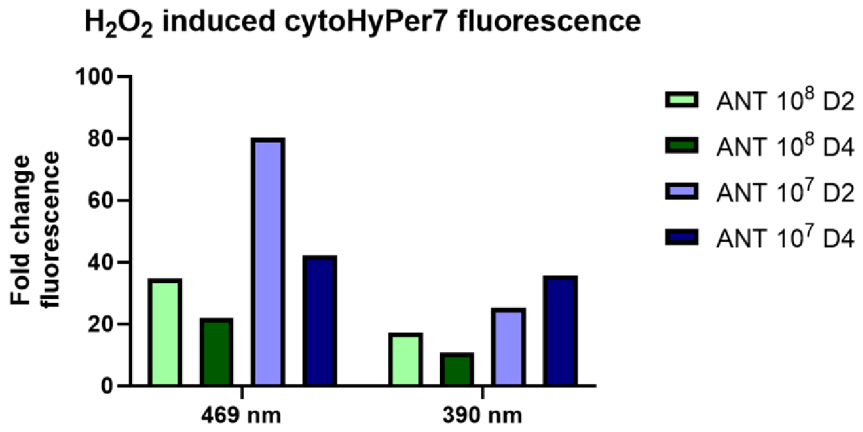

Figure 22: Fold change fluorescence analysis for a) 29.13 cytoHyPer7 cells treated with 1 mM H_2O_2 ANT media seeded at $1x10^8$ cells/ ml or $1x10^7$ cells/ml.

The worry is that we eventually need to measure much smaller changes in H_2O_2 that more closely represent physiological level of H_2O_2. Therefore, we would suggest to use the larger number of cells under these conditions.

4.3.1.3 The ability of *T. brucei* to recycle oxidized HyPer7

HyPer7 has been reported to be recycled by the thioredoxin system – cytosolic thioredoxin and thioredoxin reductase (de Cubas *et al*. 2021). As mentioned earlier, we did not observe a decrease in the H_2O_2 induced HyPer7 fluorescence (exc. 469 nm) even after 80 minutes of 1 mM H_2O_2. While this might simply represent a saturation of the Hyper7 by an overwhelming amount of H_2O_2, it could also indicate that the oxidized Hyper7 enzyme is incapable of being reduced by the *T. brucei* thioredoxins.

Therefore, to determine if our *T. brucei* C-terminal V5 tagged HyPer7 probe is indeed a reversible enzyme, we treated the cytoHyPer7 cell lines with 1 mM H_2O_2 for 4 minutes, before adding 50 mM DTT (Figure 23).

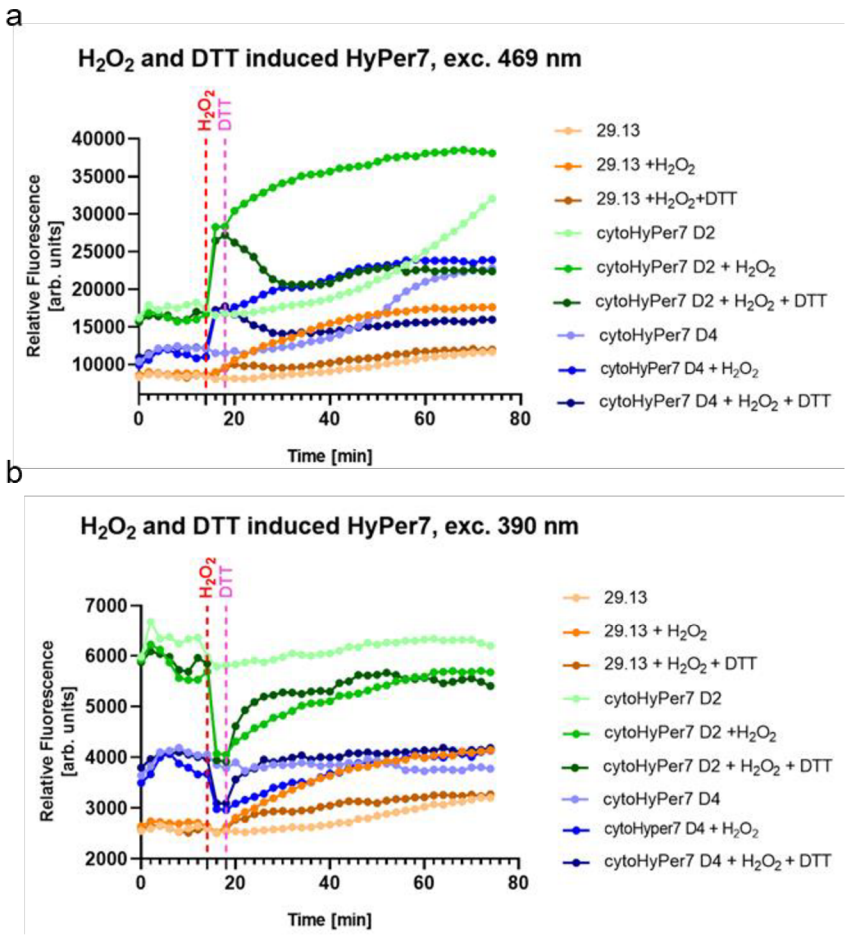

Figure 23: The fluorescence responses of HyPer7 cell lines when induced by H_2O_2 and DTT and excited at a) 469 nm and **b)** 390 nm **in comparison with just H_2O_2 induced cell lines and noninduced cell lines.** All cell lines in ANT medium and seeded at $1x10^8$ cells/ml. 29.13 – parental cell line without HyPer7.

As observed previously, there was an increase in fluorescence (exc. 469 nm) in the cytoHyPer7 cell lines treated with H_2O_2. Then upon addition of DTT, we observed significant reductions in fluorescence (exc. 469 nm) in the cytoHyPer7 cell lines almost immediately. This reduction in fluorescence did not quite reach the basal level of fluorescence (exc. 469 nm) observed before the cells were treated with H_2O_2, but it remained at a steady level that was significantly less than the same cytoHyPer7 cell lines with just the H_2O_2 treatment.

Since the reduced HyPer7 biosensor has a more intense fluorescence emission when excited at 390 nm compared to 469 nm, the fluorescence (exc. 390 nm) curve reacts in the opposite manner. Upon H_2O_2 treatment, we observed a sharp decrease in fluorescence (exc. 390 nm) in the cytoHyPer7 cell lines. This trend reversed upon the addition of DTT as the fluorescence (exc. 390 nm) increased much more rapidly than in the cytoHyPer7 cell

lines with only H_2O_2. Around the 40-minute mark of the assay, the fluorescence (exc. 390 nm) levels of the cytoHyPer7 cell lines treated with only H_2O_2 and those treated with H_2O_2 + DTT reached and maintain similar levels. Once again, more significant changes in fluorescence were observed with the cytoHyPer7 clone D2 than D4.

This experiment reveals that the V5 tagged HyPer7 probe can be reduced *in vivo* when enough of a reducing agent is presented to the parasites. However, this seems to suggest that under these conditions, the *T. brucei* thioredoxin system is unable to reduce oxidized Hyper7 localized in the cytosol.

4.3.2 Mitochondrial HyPer7 characteristics in procyclic 29.13 *T. brucei* cell line

Next, we wanted to test if HyPer7 localized to the *T. brucei* mitochondrion can detect increased production of H_2O_2 when we treat the parasites with oxidative phosphorylation inhibitors. We tried two OXPHOS interrupters: 1) KCN, which is a cytochrome bc1 complex (respiratory chain complex III) inhibitor and 2) oligomycin, which is an inhibitor of ATP synthase. First, we tested the effect of 1 mM KCN on 29.13 mitoHyPer7 and 29.13 cytoHyPer7 cell lines at two different densities – $1x10^8$ cells/ml and $1x10^7$ cells/ml (Figure 24).

Both the mitoHyPer7 (Figure 24a) and cytoHyper7 (Figure 24c) cell lines resuspended at $1x10^8$ cells/ml were much less responsive to KCN treatment that the cytoHyPer7 cell lines treated with H_2O_2 and DTT. The most consistent responses were observed in the cell lines resuspended in cMM medium; however, even these were erratic. While a modest increase in the fluorescence (exc. 469 nm) was detected in the mitoHyPer7 cell lines treated with KCN, we also detected a similar rise in fluorescence (exc. 469 nm) in the 29.13 parental cell line (without HyPer7) treated with KCN (Figure 24a).

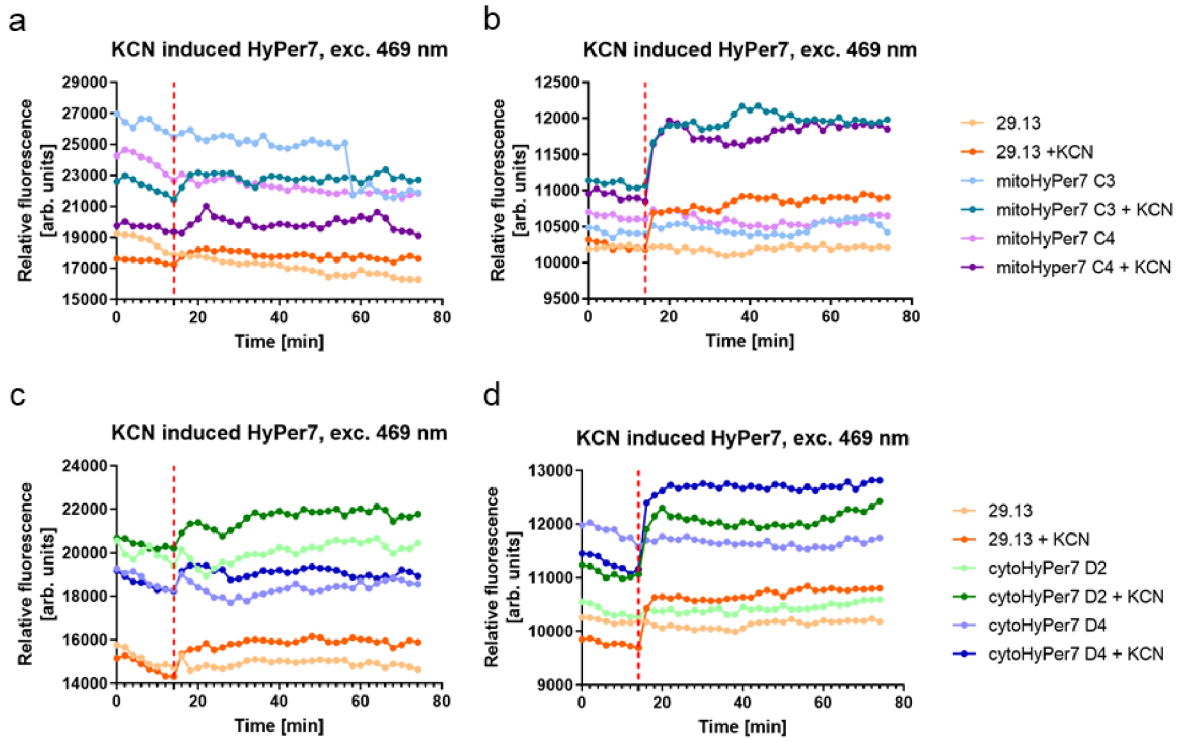

Figure 24: The fluorescence responses of HyPer7 cell lines induced by KCN and excited at 469 nm a) mitoHyPer7 cell lines seeded at $1x10^8$ cells/ml, **b)** mitoHyPer7 cell lines seeded at $1x10^7$ cells/ml **c)** cytoHyPer7 cell lines seeded at $1x10^8$ cells/ml and **d)** cytoHyPer7 cell lines seeded at $1x10^7$ cells/ml. All cell lines in cMM medium. KCN injected in 14 minutes (red line).

Unlike the cytoHyPer7 responses to externally added H_2O_2, the mitoHyPer7 and cytoHyper7 KCN data was a little more consistent in the experiments using $1x10^7$ cells /ml compared to the higher density $1x10^8$ cells/ml. However, even though the increase in fluorescence (exc. 469) for the Hyper7 cell lines was more obvious at this lower density, a very similar response was also recorded in the 29.13 parental cell lines that do not express Hyper7. Furthermore, the expected decrease in fluorescence (exc. 390 nm) was not observed. In fact, there was always a significant increase in fluorescence (exc. 390 nm) observed in the cell lines treated with KCN, regardless if they were expressing HyPer7 or not (Figure 25).

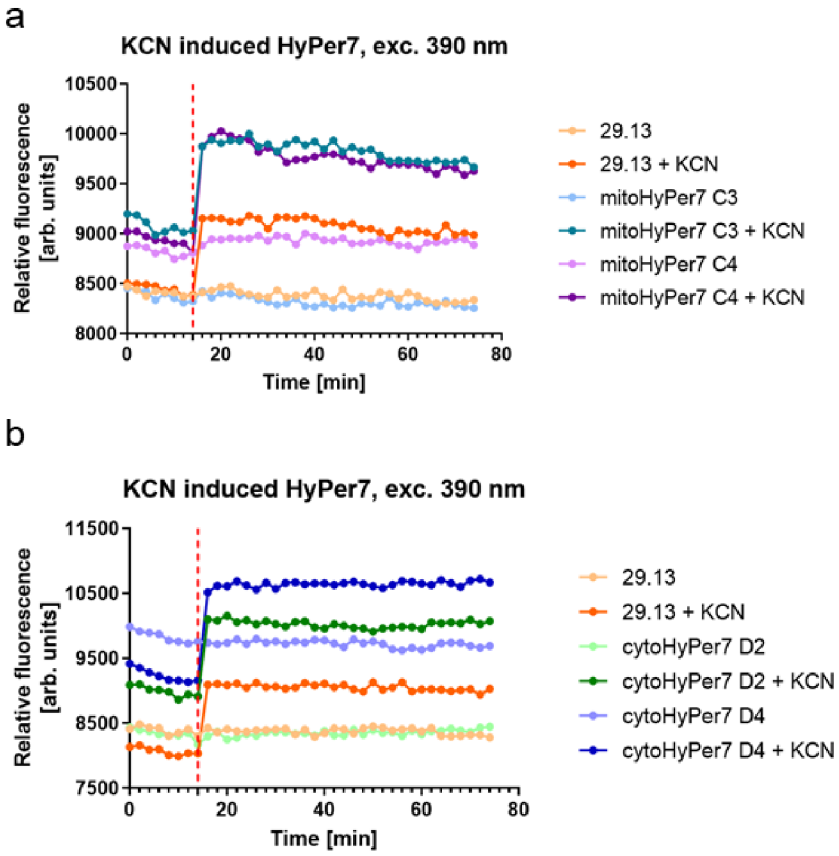

Figure 25: The fluorescence responses of HyPer7 cell lines induced by KCN and excited at 390 nm a) mitoHyPer7 cell lines seeded at $1x10^7$ cells/ml, **b)** cytoHyPer7 cell lines seeded at $1x10^7$ cells/ml. All samples in cMM media.

The second attempt to induce the parasites to generate mitochondrial ROS, involved treating the mitoHyPer7 and cytoHyPer7 cell lines with 10 µg/ml oligomycin (Figure 26).

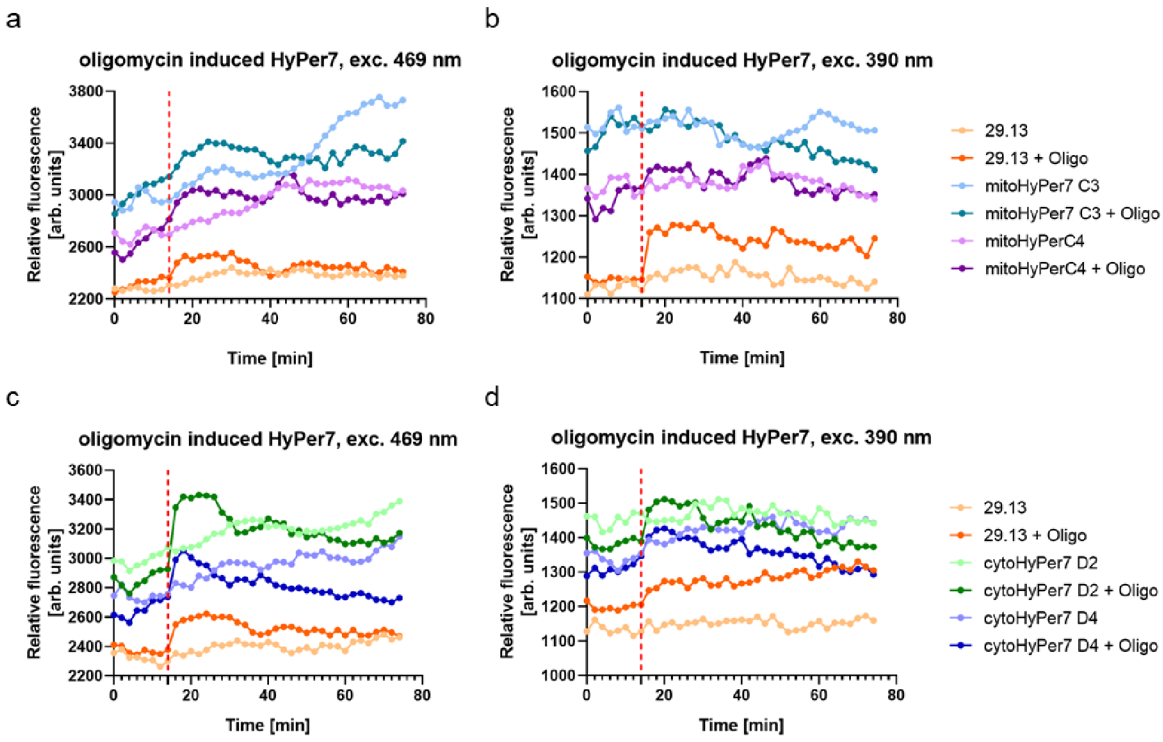

Figure 26: The fluorescence responses of HyPer7 cell lines when induced by oligomycin a) mitoHyPer7 cell lines seeded at $1x10^7$ cells/ml, excited at 469 nm **b)** mitoHyPer7 cell lines seeded at $1x10^7$ cells/ml, excited at 390 nm **c)** cytoHyPer7 cell lines seeded at $1x10^7$ cells/ml, excited at 469 nm and **d)** cytoHyPer7 seeded t $1x10^7$ cells/ml, excited at 390 nm. All samples in ANT medium.

While we tested all same variables that were used in the KCN experiments, the oligomycin data is very inconsistent and there is very little that we can interpret. The cleanest results occurred when cell lines were seeded at $1x10^7$ cells/ml and were resuspended in the ANT medium. We did detect some very modest increases in fluorescence (exc. 469 nm) in the mitoHyPer7 and cytoHyPer7 cell lines treated with oligomycin; however, there was no observed decrease in fluorescence (exc. 390).

4.4 HyPer7 spectrofluorometric analysis

After the difficulties we encountered with the experiments performed on the Tecan Spark, mainly concerning the low and inconsistent Hyper7 fluorescence measurements, we seeked consultation with RNDr. Radek Litvín, Ph.D. from Department of Chemistry at the University of South Bohemia who has extensive experience with fluorescence measurements. To determine if the biosensor was functioning properly, the HyPer7 signal was measured in Dr. Litvín's laboratory using the Fluorolog 3 machine.

In this experiment we measured the fluorescence response of 3 different samples – the 29.13 cytoHyPer7 D2, the 29.13 mitoHyPer7 C3 and the 29.13 parental cell line.

The $1x10^7$ cells were resuspended in 1 ml of the MiR05 medium and placed in a cuvette for fluorescence measurements.

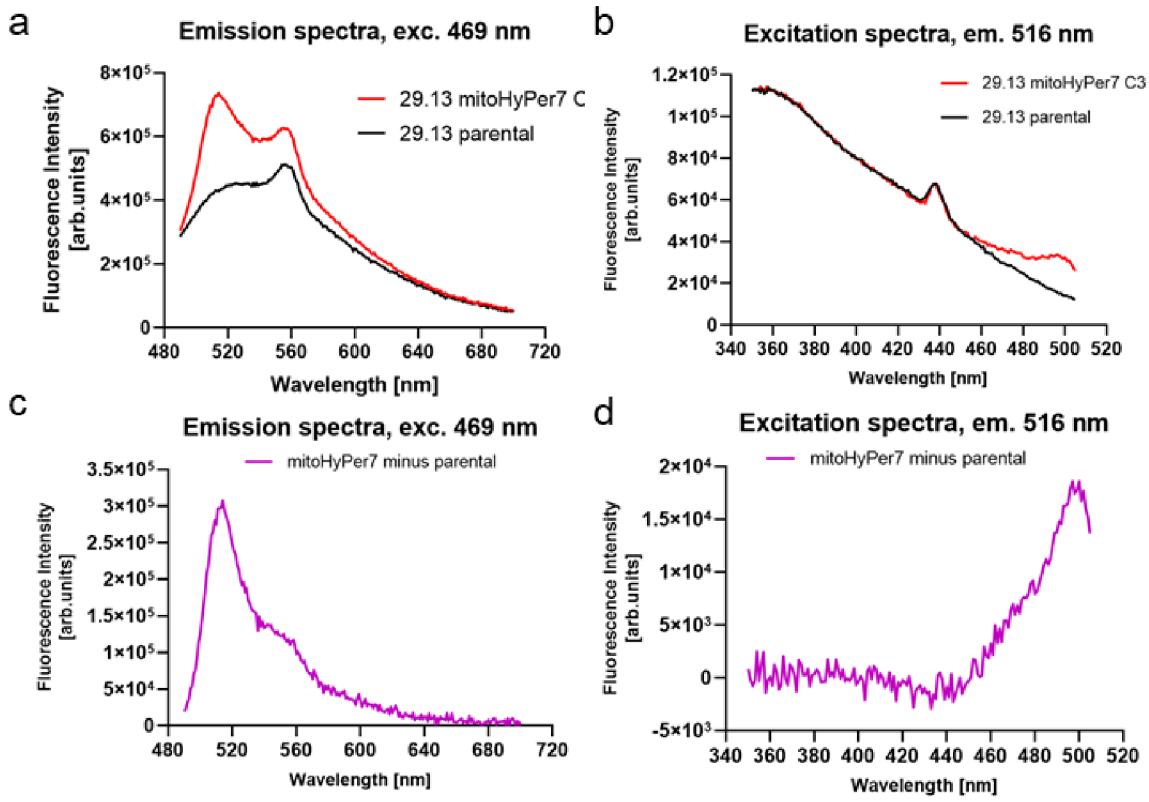

Figure 27: Fluorolog 3 measurements of HyPer7 fluorescence in the 29.13 mitoHyPer7 C3 and 29.13 parental cell lines a) the emission spectra obtained from the 469 nm excitation **b)** the excitation spectra detected at 516 nm **c)** the emission spectra of the 29.13 mitoHyPer7 cells after subtracting the parental 29.13 background **d)** the excitation spectra of the 29.13 mitoHyPer7 cells after subtracting the 29.13 parental background (data graphed based on Dr. Litvín's analysis).

When the 29.13 mitoHyPer7 C3 cell line was excited at 469 nm, the emission spectrum of the sample recorded a fluorescence maximum at ~ 520 nm (Figure 27a). Importantly, this peak was not detected in the emission spectrum of the 29.13 parental cell line. Interestingly, a second peak at ~ 560 nm was observed in both emission spectra. This peak coincides with the emission observed from the Raman scattering peak of water, which is usually a very minor peak detected in wavelength emission scans. The fact that it is almost the same intensity as the fluorescence response from HyPer7 indicates that we are detecting very low levels of fluorescence. After the values of the parental cell line fluorescence are subtracted from the HyPer7 emission spectrum, we identify a single peak (Figure 27c) that matches the value previously reported for Hyper7 (Pak *et al.*, 2020).

The excitation spectra at 516 nm indicate an absorption peak at ~ 440 nm detected in both the cells lines with and without HyPer7 (Figure 27b). This value again matches the excitation value observed with the Raman scattering peak of water. It was also clear that we could observe a difference in the absorption spectra between these two cell lines starting around 469 nm. However, this peak was less well defined compared to the Raman water absorption peak. Nevertheless, after subtracting the background values obtained from the parental 29.13 cell line, we identified a Hyper7 absorption peak with a maxima at ~ 495 nm (Figure 27d). The same experiments were also performed for the 29.13 cytoHyPer7 D2 clone, which showed very similar results as the mitoHyPer7 clone, just with an even lower fluorescence signal. Altogether, these data confirm that the HyPer7 in our procyclic *T. brucei* cell lines are emitting at 516 nm when the parasites are excited at 469 nm, just as described in other organisms. However, the detected fluorescence signal is very weak.

We also wanted to compare the amount of fluorescence detected in cell lines with HyPer7 targeted to the cytosol versus the mitochondrion. Therefore, when both cell lines were excited with light at 480 nm, we detected a peak fluorescence at 516 nm after the parental 29.13 background fluorescence values were subtracted (Figure 28a).

Interestingly, while the overall values were still very low, the mitoHyPer7 cell line gave approximately a 75% higher fluorescence signal than the cytoHyPer7 cells. This may indicate a more consistent HyPer7 expression throughout the cell population or higher fluorescence levels due to the concentration effect of restricting the HyPer7 biosensor to the mitochondrion. Alternatively, the mitoHyPer7 sample was measured approximately 1 hour later than the cytoHyPer7 cell line, therefore the cells might have been experiencing more stress in the limited medium that resulted in ROS production that might have influenced the Hyper7 fluorescence levels.

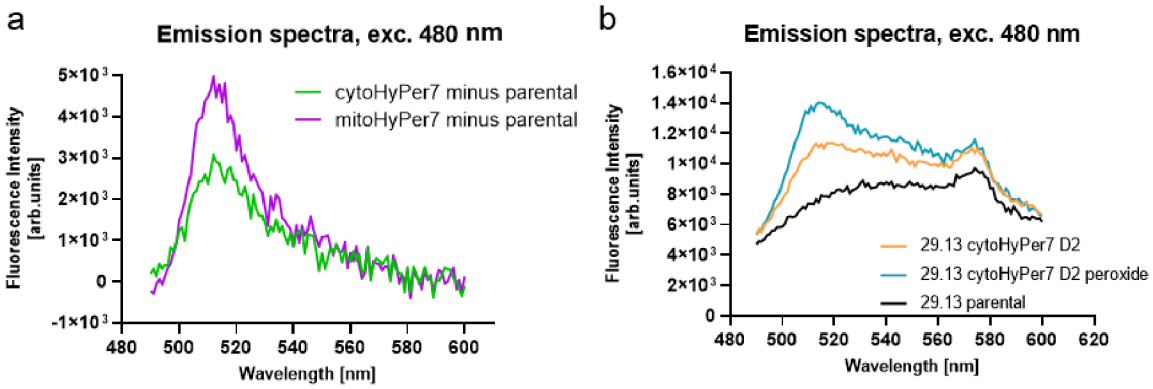

Figure 28: Fluorolog 3 emission spectra comparisons between HyPer7 a) from the 29.13 cytoHyPer7 D2 (green) and 29.13 mitoHyPer7 C3 (purple) cell lines after the 29.13 parental background fluorescence was subtracted **b)** from the 29.13 cytoHyPer7 D2 cell line treated with (blue) or without (orange) 294 mM H_2O_2. The fluorescence emission spectrum of the untreated 29.13 parental cells (black) was included as a reference.

We also examined how the cytoHyPer7 cell line reacts to the addition of 294 nM H_2O_2. When each of the cell lines were excited at 480 nm, the cytoHyper7 D2 cell line treated with H_2O_2 produced the greatest response at ~ 516 nm in the emission spectra (Figure 28b). Importantly, the parental cell line without Hyper7 did not have a peak at 516 nm. However, the increased H_2O_2 induced cytoHyper7 fluorescence response at this wavelength was only marginally larger than that observed in the untreated cytoHyper7 cell line (Figure 28b). While this experiment demonstrates that cytoHyper7 expressed in *T. brucei* can respond to increased H_2O_2, the overall fluorescence response is quite limited under these conditions.

4.5 Immunofluorescence reveals variability of HyPer7 expression levels

Since the Hyper7 probe seems capable of producing the expected fluorescence measurements upon treatment with high levels of H_2O_2, we wanted to reexamine HyPer7 expression levels. An immunofluorescence assay was performed to determine expression levels of the biosensor among all cells in a population of a HyPer7 cell lines. Compared to our previous western blot analyses on $1x10^7$ whole cell lysates, this method enabled us to monitor protein expression variability from cell to cell. Because we stained the mitochondria with Mitotracker in this method, we were also able to confirm the subcellular fractionation data of the targeted HyPer7.

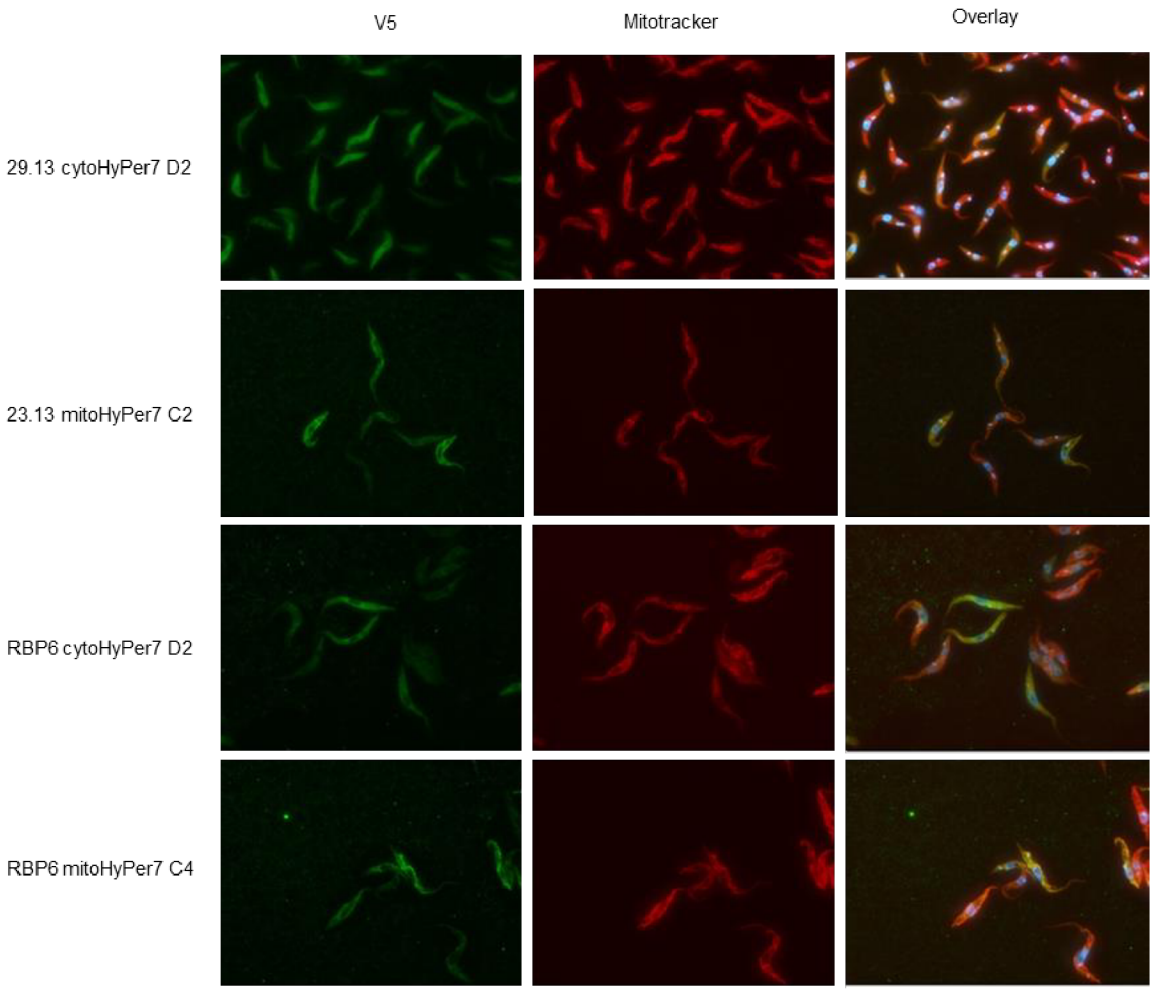

Figure 29: 29.13 and RBP6 cell lines constitutively expressing green fluorescent proteins (cytosolic or mitochondrial HyPer7). The V5 antibody labels the tagged HyPer7 in the green channel, while the Mitotracker red dye accumulates in charged mitochondria. Overlays show the merged images where the direct overlap of the green and red channels appear orange. The nucleus and kDNA are indicated in the blue channel due to the DAPI stain.

The immunofluorescence results verified the HyPer7 subcellular localizations (Figure 29). The cytoHyPer7 signal is diffused throughout the cell and does not overlay with the Mitotracker staining of the mitochondria. The mitoHyPer7 signal displays the typical procyclic phase branched mitochondrion and has a considerable overlap with the Mitotracker dye. However, the data also indicates that the probe's expression is not equal among the cell population. Some cells express HyPer7 a lot, while others have significantly less protein or almost not at all. This was true for each of the cell lines analyzed, irrespective of the Hyper7 subcellular localization. Since it is very difficult to generate true clones from transfected procyclic *T. brucei*, these results suggest that the cell lines were generated from a small number

of parasites with different genetic backgrounds, most likely due to the integration of the transfected plasmid occurring at one of several different β-tubulin alleles in the genome.

Upon closer inspection, the immunoflourescence images also revealed that some of the RBP6 Hyper7 cells were transitioning between various procyclic developmental stages. During differentiation, the kinetoplast DNA moves posteriorly towards the nucleus in the epimastigote stage before it returns back to the anterior in the metacyclic stage. Indeed, the kinetoplast DNA in some parasites was visualized not in the anterior, but near the nucleus. This would suggest that surprisingly some cells were differentiating even without the presence of tetracycline in the medium to induce RBP6 overexpression. To determine if this was just an abnormality, freshly thawed RBP6 Hyper7 cell lines were thawed and then stained with just DAPI before being visualized under the fluorescence microscope (Figure 30).

These new immunofluorescence images reveal that most cells have the kinetoplast DNA at the anterior end of the parasite, which corresponds to the expected promastigote life cycle stage of undifferentiated parasites. Perhaps, the mislocalized kinetoplast DNA in the RBP6 parasites from the previous experiment were the result of the cell lines being cultured for too long, which triggered RBP6 independent procyclic differentiation due to some stress response pathway.

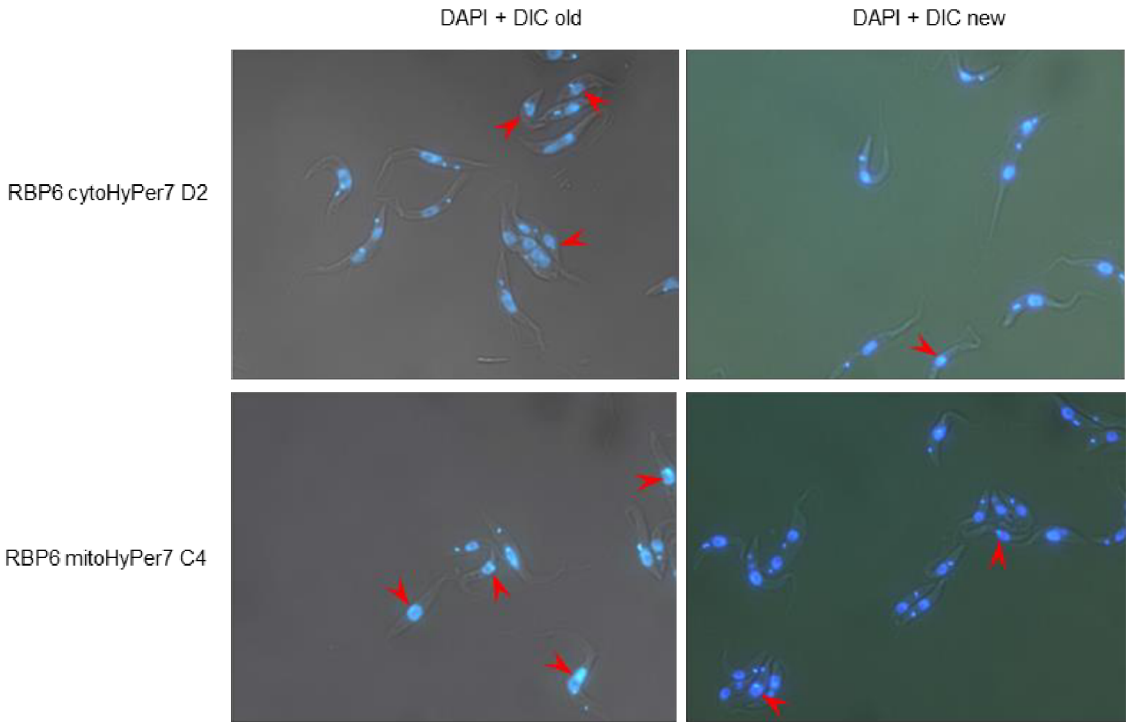

Figure 30: RBP6 cell line (cytosolic or mitochondrial HyPer7 clones) showing the amount of transforming cells via previous IFA (left) and control via next DAPI staining (right). DAPI detects the nucleus and the kinetoplast.

4.6 HyPer7 fluorescence responses detected by the flow cytometer

Due to the observed cell-to-cell variability in Hyper7 expression levels, we decided to analyze the procyclic *T. brucei* Hyper7 response using the Becton Dickinson FACSCantoII flow cytometer, where individual cells with presumably greater levels of Hyper7 could be selected from the larger population by gating the subset of cells with the largest change in fluorescence. This method allows us to analyze the Hyper7 fluorescence response using the FITC filter, while also monitoring the mitochondrial membrane potential using the PE filter when cells were stained with TMRE. The following cells lines were analyzed by the flow cytometer: 29.13 cytoHyPer D2, 29.13 mitoHyPer7 C3, RBP6 cytoHyPer D2 and RBP6 mitoHyPer7 C4.

4.6.1 29.13 HyPer7 cell lines treated with H_2O_2 and DTT

First, we wanted to determine if a gated subpopulation of *T. brucei* expressing HyPer7 had a greater fluorescence response when treated with 1 mM H_2O_2 and 30 mM DTT. As observed in the FACS dot plots (Figure 31a), 29.13 cytoHyPer7 cells incubated with H_2O_2 resulted in a significant subpopulation of cells that shifted along the FITC x-axis. Upon closer analysis, the histograms (Figure 31b) reveal that the 29.13 cytoHyper7 cells treated with H_2O_2

behaved as two largely distinct populations. While a smaller population (gated) had a much more significant increase in fluorescence, even the main population of 29.13 cytoHyPer7 cells treated with H_2O_2 displayed a slight increase in fluorescence compared to the untreated cells. This result indicates that the amount of cytoHyPer7 expression was not uniform throughout the cell culture.

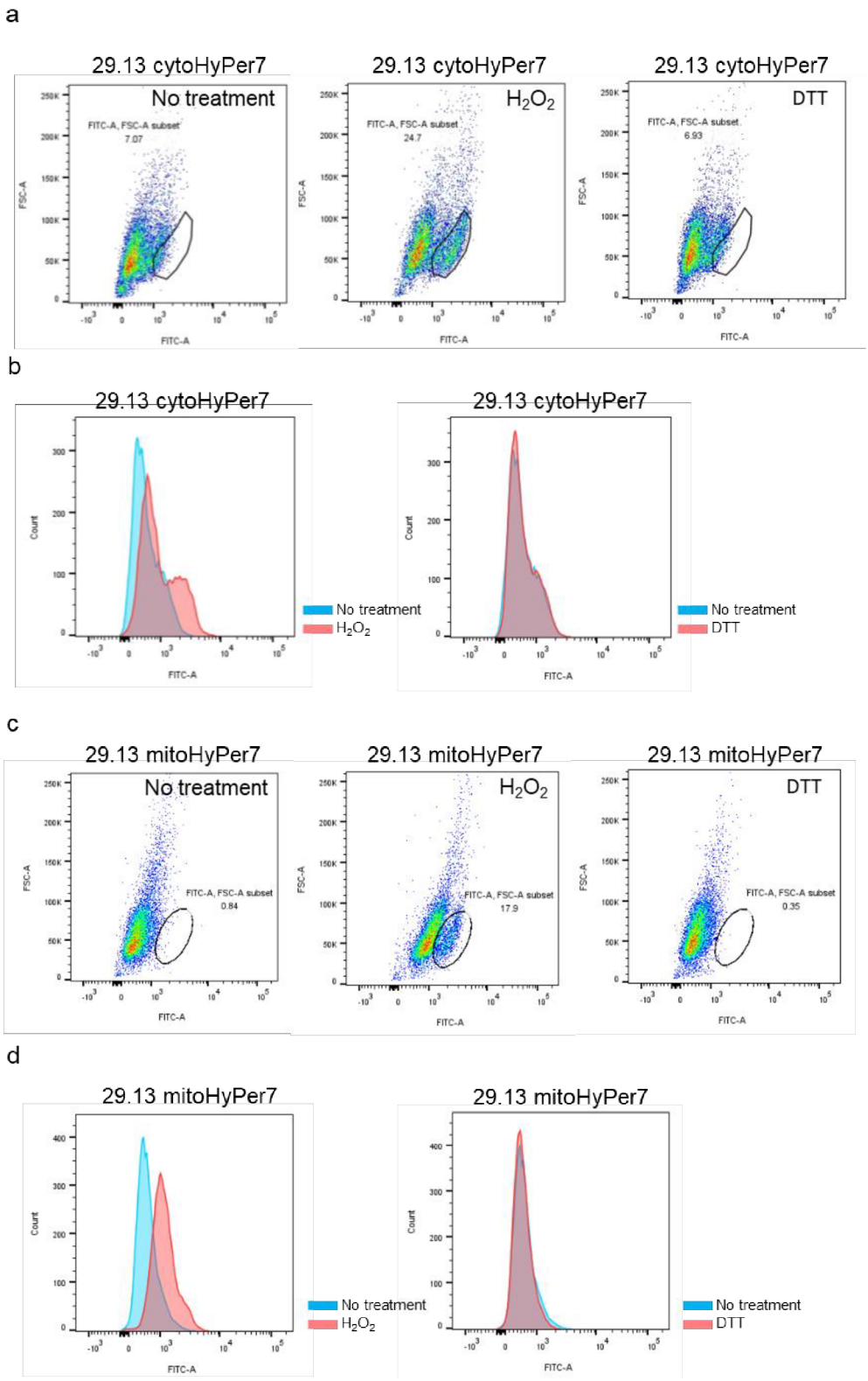

Figure 31: FACS analyses of 29.13 HyPer7 cell lines treated with H_2O_2 and DTT. a) plots with gated population of 29.13 cytoHyPer7 cell lines, FITC (x-axis) and FSC (y-axis) **b)** histograms of plots from a), **c)** plots with gated population of 29.13 mitoHyPer7 cell line, FITC (x-axis) and FSC (y-axis), **d)** histograms of plots from c).

Interestingly, the DTT treatment of 29.13 cytoHyPer7 cells did not result in any significant change in the fluorescence emitted compared to the untreated 29.13 cytoHyPer7 cells (Figure 31 a & b). This result indicates that throughout the sample preparations of the 29.13 cytoHyPer7 cells, the population of HyPer7 molecules remained almost all completely reduced. In other words, the manipulations of these parasites during the FACS analyses did not seem to lead to a stress response in the form of ROS production.

The same overall phenomenon was also observed with the 29.13 mitoHyPer7 cell line (Figure 31c), except this time the H_2O_2 histogram (Figure 31d) indicated that the vast majority of 29.13 mitoHyPer7 cells expressed uniform levels of HyPer7 as the increased fluorescence fell within a normal Gaussian distribution. A slight shoulder was visible on the right side of the curve, which represents the very minor population of 29.13 mitoHyPer7 cells gated in the dot plot that presumably had even greater levels of HyPer7 expression.

In an attempt to compare the overall fluorescence response between the treated and untreated cytoHyper7 and mitoHyper7 cell lines, the mean fluorescence values for each condition were normalized to the value measured for the untreated cytoHyper7 parasites (Figure 32).

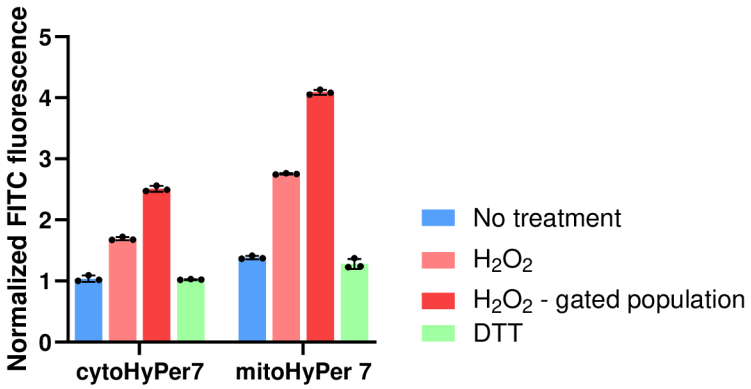

Figure 32: Comparison of the fluorescence intensity between the 29.13 cytoHyPer7 and 29.13 mitoHyPer7 cell lines treated with H_2O_2 or DTT. The mean fluorescence intensities of all the cell lines under various conditions were normalized to the mean fluorescence values obtained for the untreated cytoHyper7 cell line.

Graphed in this fashion, the data confirms a significant increase in the total mean fluorescence values of the gated 29.13 mitoHyper7 cell line compared to the 29.13 cytoHyPer7 cell line. Together with the fluorescence histograms (Figure 31 b&c), this data suggests that there is more uniform and higher expression levels of Hyper7 in the mitoHyper7 cell line. This correlates with the data retrieved from the Fluorolog 3 measurements comparing the two cell

lines. It is also a more robust way to quantify the cell-to-cell variability in Hyper7 expression observed in the immunofluorescence assays described previously. Furthermore, this FACS method seems to be a more reliable analysis to determine the uniformity of HyPer7 expression throughout a cell population compared to the scanning densitometry analysis performed on western blots where we did not consistently measure this difference.

4.6.2 Activation of 29.13 mitoHyPer7 through endogenous ROS production

In this experiment, we analyzed the ability of the mitoHyper7 to respond to the presumed endogenous mitochondrial ROS production stimulated by the cellular treatment of 10 µg/ml oligomycin for various lengths of time. Since oligomycin will inhibit the flow of protons localized in the intermembrane space through the F_oF_1-ATP synthase proton pore, we also incubated the cell lines with 60 nM TMRE to monitor changes in the mitochondrial potential.

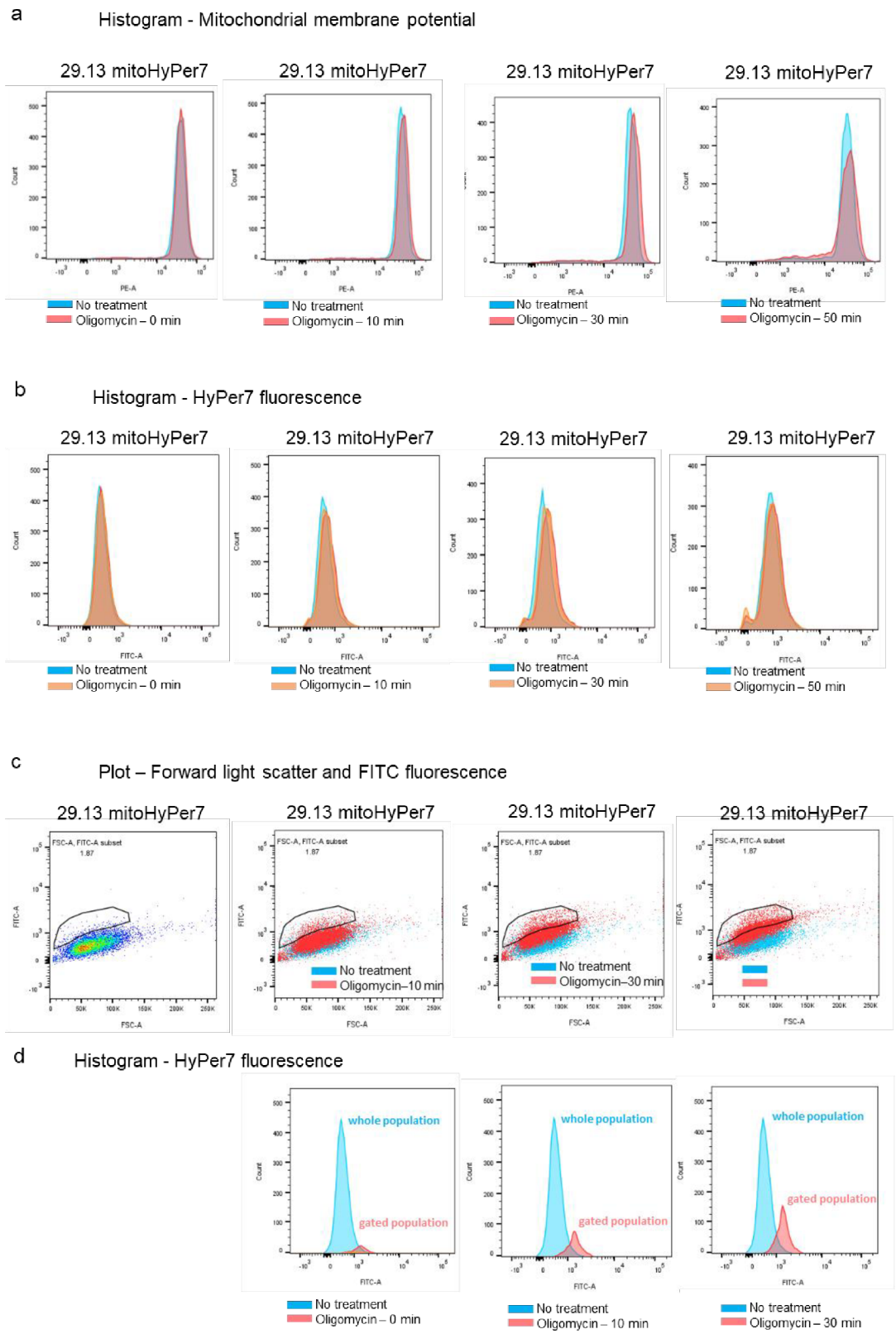

Figure 33: FACS analyses of the 29.13 mitoHyper7 cell line treated with TMRE and oligomycin. **a)** histograms of mitochondrial membrane potential, count (y-axis) and PE (x-axis); **b)** histograms of HyPer7 fluorescence, count (y-axis) and FITC (x-axis); **c)** plots with gated population, FITC (y-axis) and FSC (x-axis); **d)** histograms of plots from c).

Surprisingly, the FACS fluorescence histogram of TMRE did not indicate that the oligomycin treatment resulted in any significant increase in the mitochondrial membrane potential (Figure 33a). Without an increased mitochondrial membrane potential, it was no surprise that we did not detect any significant increase in H_2O_2 induced HyPer7 fluorescence of the entire cell population based on their histogram analyses (Figure 33b).

However, upon closer inspection of the FACS dot blots (Figure 33c), we observed a very minor population of cells with increased fluorescence along the FITC y-axis. The number of cells in this gated population increased as the exposure to oligomycin lengthened. The increased fluorescence of these gated cells is clearly reflected in the Hyper7 fluorescence histogram that plots the median fluorescence values for the untreated 29.13 mitoHyper7 population and the gated oligomycin treated 29.13 mitoHyPer7 cells (Figure 33d). This minor subpopulation with increased fluorescence might represent the same minor gated population we observed during H_2O_2 treatment of the 29.13 mitoHyPer7 cells. This would again indicate that only a very small portion of the population expressed high enough mitoHyper7 levels to elicit a response. A more likely scenario due to the lack of an observed increased mitochondrial membrane potential is that these few cells were the only ones that produced mitochondrial ROS in response to the oligomycin treatment.

To further illustrate the changes observed in the mean fluorescence values of the TMRE mitochondrial staining (Figure 34a) and the H_2O_2 induced mitoHyper7 fluorescence (Figure 34b), each of the measured FACS values were normalized against the untreated mitHyper7 cell line. This demonstrates that there was a very minor increase in the mitochondrial membrane potential in the oligomycin treated cells compared to untreated cells. Moreover, the increased H_2O_2 induced HyPer7 fluorescence observed in just the small gated population does not correlate with the lack of an increased mitochondrial membrane potential observed between the gated and larger ungated population of the mitoHyper7 cell line treated with oligomycin.

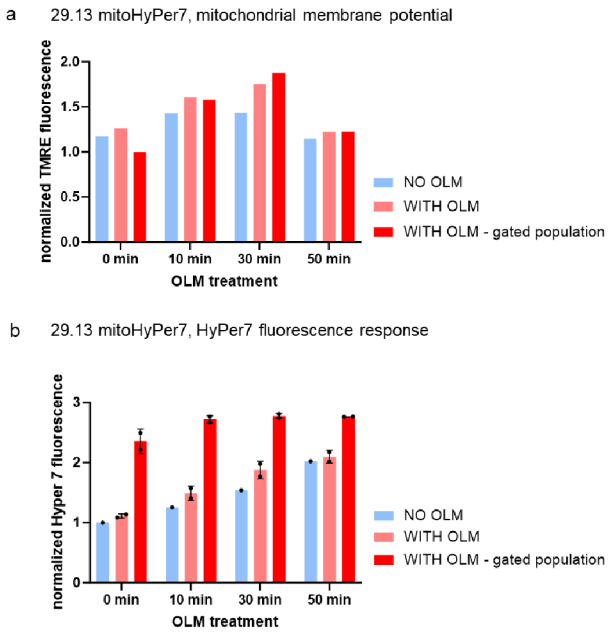

Figure 34: Graphs showing the changes in a) mitochondrial membrane potential and **b)** fluorescence coming from HyPer7. The mean fluorescence intensities of either the TMRE fluorescence or the H_2O_2 induced mitoHyper7 fluorescence as measured on the FACS were normalized to the mean fluorescence values obtained for the untreated mitoHyper7 cell line.

4.6.3 FACS measurements of H_2O_2 production during procyclic *T. brucei* differentiation

Finally, we implemented the Hyper7 FACS analyses during the RBP6 induced differentiation of procyclic *T. brucei* cell lines. The goal was to use this data from the RBP6 cytoHyPer7 or RBP6 mitoHyPer7 cell lines to determine where and when we can detect increased levels of H_2O_2 that could be used as an intracellular differentiation signal.

It has been well-characterized in our laboratory (Doleželová *et al.*, 2020) that during differentiation we observe an increased mitochondrial membrane potential in a subpopulation of the culture, specifically from day 4 of the RBP6 induced differentiation (Figure 35a, left panel). Unfortunately, in our experiment the mitochondrial membrane potential was steadily decreasing in both the RBP6 cytoHyPer7 and RBP6 mitoHyPer7 cell lines (Figure 35a right panel and b). Therefore, it was not surprising that we did not detect an increase in fluorescence originating from the cytoHyPer7 or mitoHyPer7 during differentiation (Figure 35c). Since there was time to only perform this experiment once, the results probably indicate that we were unlucky and failed to induce sufficient differentiation of our RBP6 HyPer7 cell lines.

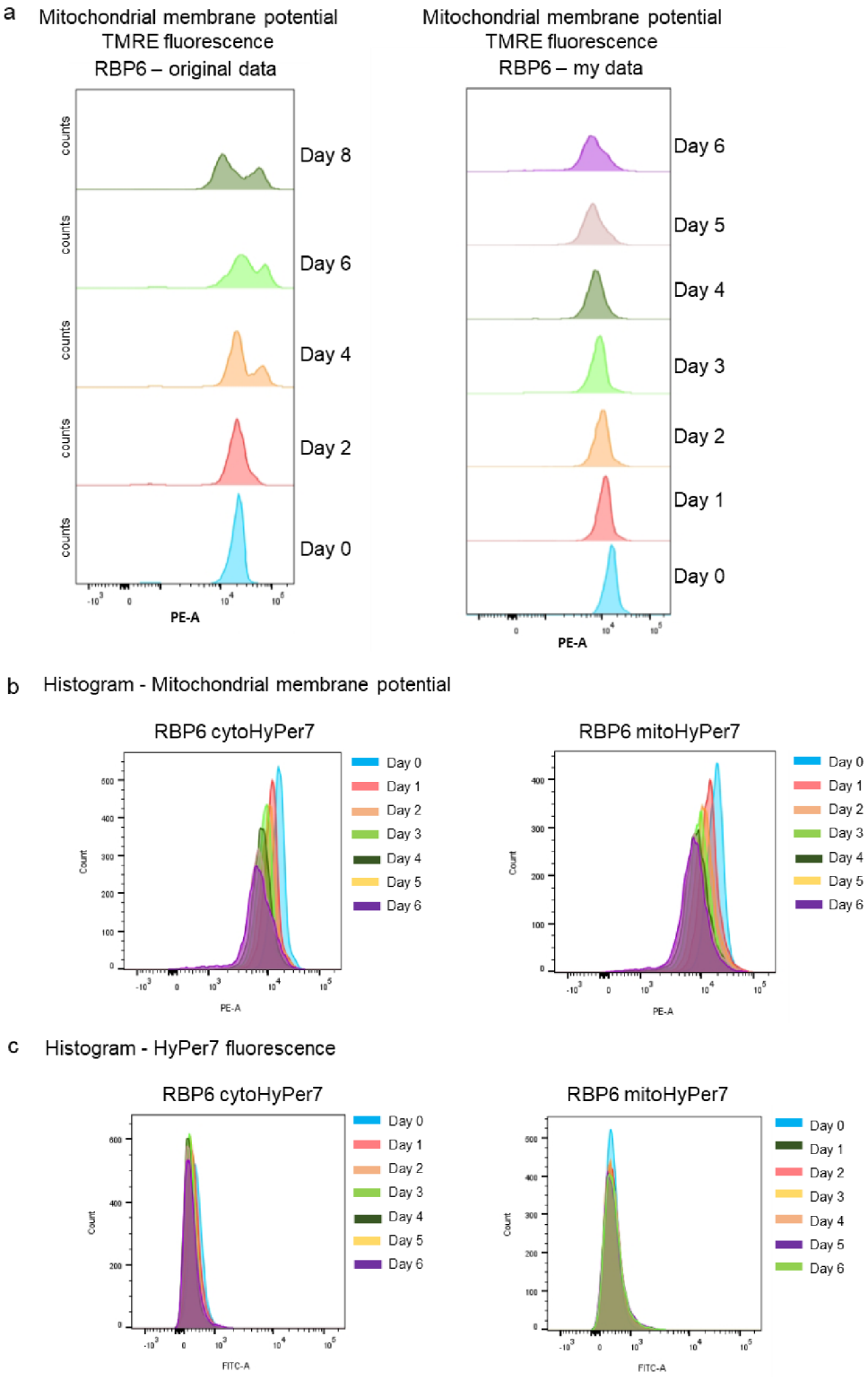

Figure 35: FACS analyses of RBP6 differentiation experiment a) mitochondrial membrane potential measured during RBP6 differentiation in our lab previously (unpublished data) (left) and mitochondrial membrane potential in this experiment (right), count (y-axis) and PE (x-axis); **b)** histograms of mitochondrial membrane potential in RBP6 cytoHyPer7 cell line (left) and RBP6 mitoHyPer7 (right), count (y-axis) and PE (x-axis); **c)** histograms of HyPer7 fluorescence response in RBP6 cytoHyPer7 (left) and RBP6 mitoHyPer7 (right), count (y-axis) and FITC (x-axis).

4.7 Generation of pT7 3V5 PAC plasmid with HyPer7 gene

In an attempt to increase the expression levels of the fluorescent probe HyPer7, we subcloned it into the pT7 3V5 PAC plasmid. While the pHD1344-t plasmid gives robust HyPer7 expression from the endogenous tubulin transcription, maybe the expression could be increased by using a plasmid that utilizes the T7 promotor from the T7 bacteriophage.

The cytosolic and mitochondrial HyPer7 coding sequences were excised from the previously created Hyper7 pHD1344-t plasmids with the restriction enzymes HindIII and BamHI. The destination vector pT7 3V5 PAC was also digested with the same restriction enzymes. The resulting DNA fragments were resolved on an agarose gel (Figure 36) and the expected sized bands for cytoHyPer7 (1457 bp), mitoHyPer7 (1529 bp) and the pT7 3V5 PAC plasmid backbone (5909 bp) were gel purified.

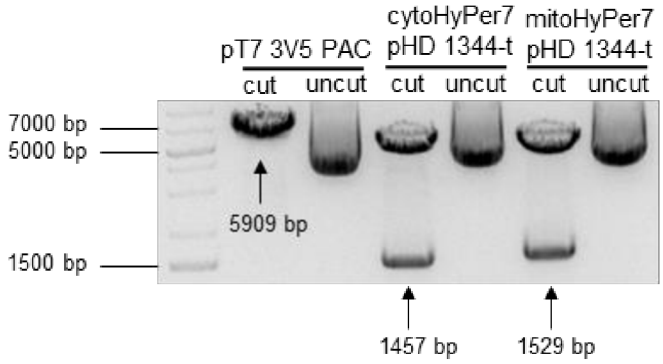

Figure 36: DNA fragments isolated by BamHI and HindIII restriction digests of plasmids pT7 3V5 PAC, pHD1344-t with cytosolic or mitochondrial HyPer7. Uncut plasmids were loaded as controls. Ladder: GeneRuler 1kb Plus DNA ladder (Thermo Fisher Scientific).

The cytoHyper7 and mitoHyper7 coding sequences were ligated into the digested pT7 3V5 PAC plasmid and then transformed into *E. coli* XL-1 blue competent cells. To verify the successful subcloning of the targeted HyPer7, the isolated plasmid DNA from five positively selected bacterial clones were digested again with the restriction enzymes HindIII and BamHI and resolved on an agarose gel stained with ethidium bromide (Figure 37).

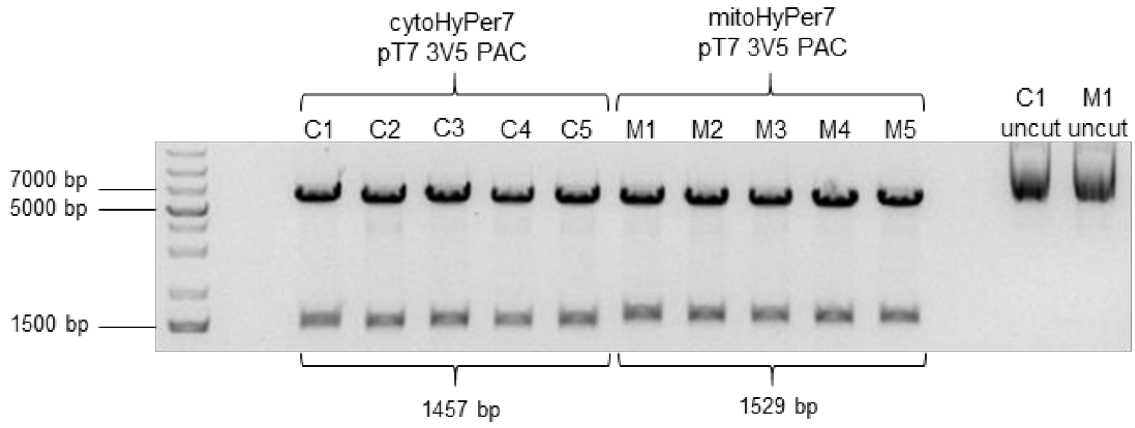

Figure 37: Representative digest analysis of plasmids pT7 3V5 PAC with cytosolic or mitochondrial HyPer7 all by restriction enzymes BamHI and HindIII. Two uncut plasmids as controls. Ladder: GeneRuler 1kb Plus DNA ladder (Thermo Fisher Scientific).

All of the tested clones contained the expected size DNA fragment of cytoHyPer7 or mitoHyPer7, indicating a successful subcloning into the destination vector. Cyto clone C1 and mito clone M5 were sent for sequencing at the SEQme company to confirm that the HyPer7 genes were not accidentally mutated in the cloning process. Finally, both pT7 3V5 PAC plasmids with the cytoHyPer7 or mitoHyPer7 were linearized by the restriction enzyme NotI and ethanol precipitated. These concentrated plasmids resuspended in sterile water were now prepared for *T. brucei* transfections in the near future.

4.8 Thioredoxin 5780 double knock out cell lines

4.8.1 Creating KO1 and KO2 amplicons

To determine if the thioredoxin that was identified to have significantly increased levels of protein expression throughout procyclic *T. brucei* differentiation is essential or plays a role in differentiation, we needed to create double knock outs in the background of the RBP6 cell line and the parental 29.13 cell line. Usually we transfect *T. brucei* with linearized plasmids containing the coding sequence of a selectable marker flanked by ends that are complementary to the intergenic regions of the alleles that are to be knocked out. Since this requires multiple cloning steps, we attempted to accelerate the cloning process by transfecting *T. brucei* with PCR products. To accomplish this, we needed to perform a fusion PCR that would stitch together the coding sequence of the selectable marker with the 5' and 3' intergenic regions flanking thioredoxin 5780. The thioredoxin intergenic regions for the PCR amplicon to replace the second allele (PCR KO2) were nested inside the intergenic regions selected for PCR KO1 in order to direct the genomic integration of PCR KO2 into the second

thioredoxin 5780 allele. This meant that two different 5'and 3'intergenic regions needed to be amplified from genomic DNA isolated from the 427 Lister cell line (Figure 38). The antibiotic resistance markers for puromycin and blasticidin were amplified from the pT7 3V5 PAC and pHD1334- t plasmids, respectively (Figure 38).

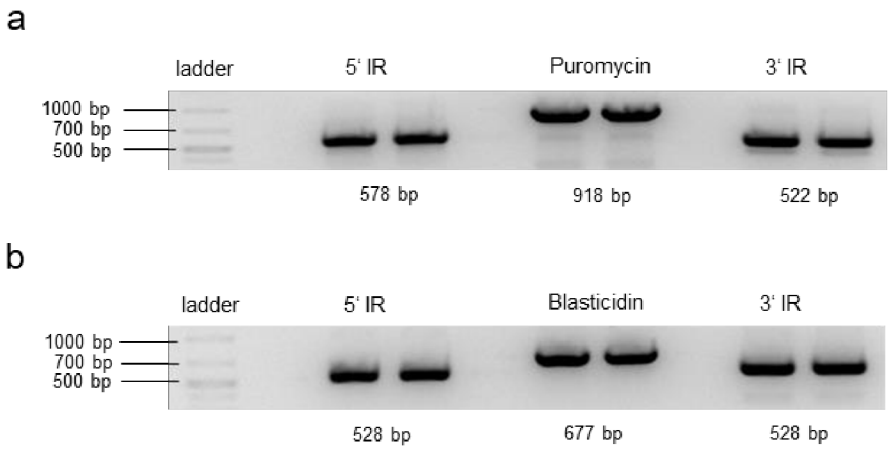

Figure 38: a) Individual PCR amplicons created for fusion PCR KO1. **b)** Individual PCR fragments for fusion PCR KO2. Ladder: GeneRuler 1kb Plus DNA ladder (Thermo Fisher Scientific).

The complete PCR KO1 amplicon was then created by fusing together all three gel extracted PCR fragments via a two run PCR protocol where the individual DNA fragments first served as the primers to join the DNA into the longer desired product before nested primers were added to amplify enough DNA for two transfections (Figure 39a). The PCR KO2 amplicon was generated in a similar format, but this time a gradient PCR was utilized because our first attempt at optimizing the annealing temperature generated sufficient amounts of the desired PCR amplicons (Figure 39b). The final PCR KO1 and KO1 amplicons were gel extracted and ethanol precipitated to concentrate enough DNA to transfect both the 29.13 parental and the RPB6 cell lines.

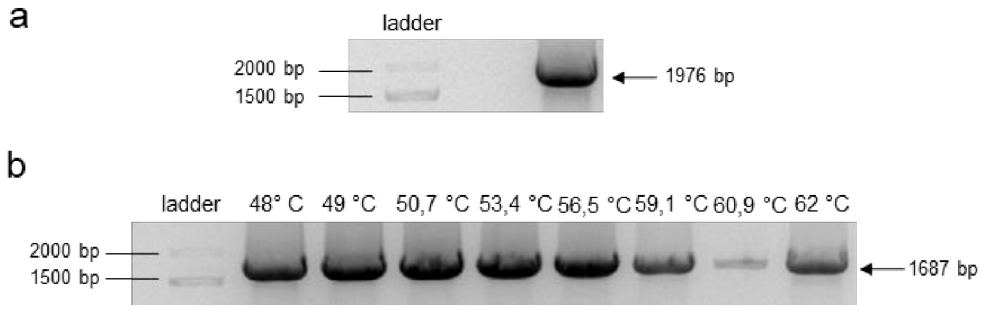

Figure 39: a) Representative fusion PCR fragment of the complete KO1 amplicon. b) Gradient fusion PCR amplification of complete PCR KO2 amplicon. Annealing temperatures for each sample of the gradient PCR are indicated above the samples. Expected sizes of the final PCR KO1 and KO2 amplicons are indicated on the right. Ladder: GeneRuler 1kb Plus DNA ladder (Thermo Fisher Scientific).

4.9 PCR verification of the Thioredoxin 5780 sKO and dKO cell lines

To verify the correct integration of the first selectable marker into the thioredoxin 5780 allele, we analyzed the PCR products amplified with specific forward and reverse primers that were designed that one annealed within the newly integrated plasmid DNA and the other outside of this integration site within the *T. brucei* genome. PCR products of the expected sizes would indicate that the selectable marker was correctly integrated into the genome at both the 5'and 3'genomic integration sites. Negative controls for the 5'and 3' integration sites utilized genomic DNA isolated from wildtype 427 *T. brucei*. An additional PCR would amplify any thioredoxin coding sequence that remained in the *T. brucei* genome.

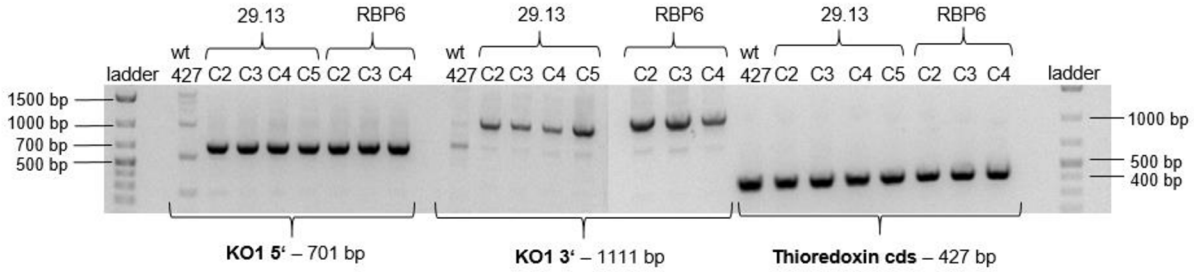

Figure 40: PCR verification of Thioredoxin 5780 sKO cell lines. wt – wild type. Ladder: GeneRuler 1kb Plus DNA ladder (Thermo Fisher Scientific).

The PCR products of the expected sizes were observed for both the 5'and 3' integration sites of PCR KO1 (Figure 40). As expected, the thioredoxin 5780 coding sequence was still detected in the genome as the second allele should remain intact. These results indicate

the PCR KO1 was integrated into the *T. brucei* gemone and successfully replaced the thioredoxin 5780 allele to create the sKO cell line.

Next, the selected 29.13 Thx sKO C5 and RBP6 Thx sKO C3 cell lines were transfected with the PCR KO2 amplicon. PCR products of the expected sizes were observed for each of the 5'and 3' integrations sites for both PCR KO1 and KO2 (Figure 41a). However, we wanted to investigate the strange double band observed for the PCR product analyzing the 3' integration site for PCR KO2. To verify that this second band was a nonspecific PCR amplification product, a gradient PCR was performed. Indeed, at the highest annealing temperature the lower band was almost completely absent, leaving just the upper band of the expected size (Figure 41b).

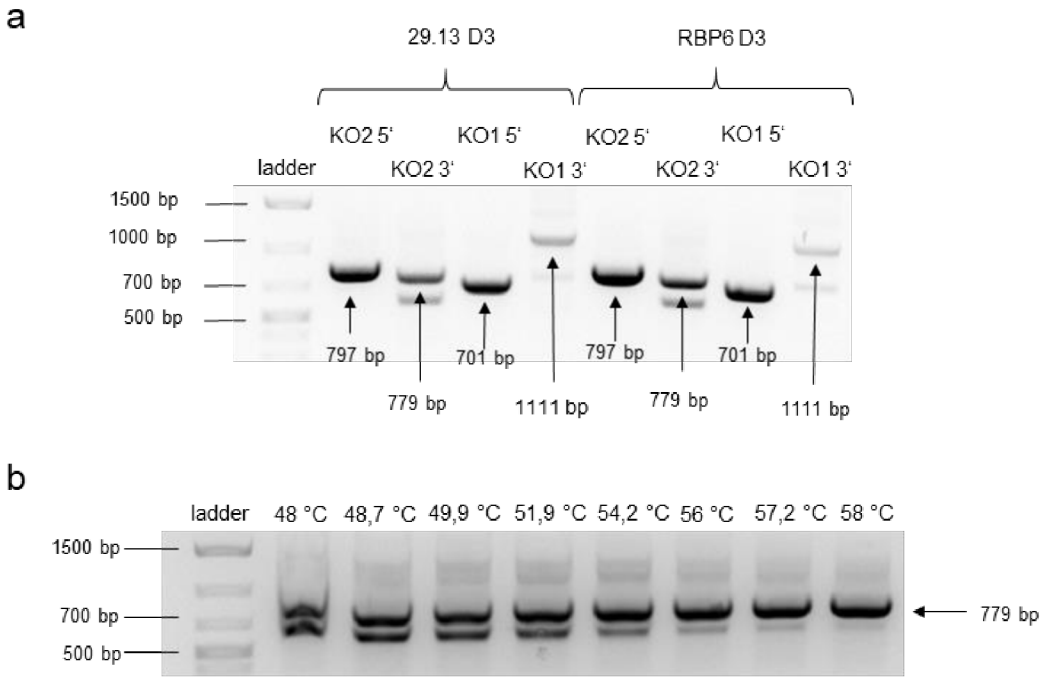

Figure 41: a) Representative PCR illustrating the presence of fusion PCRs amplicons in unsucessful dKO 29.13 and RBP6 cell lines. b) Representative gradient PCR of 29.13 KO2 3' double band. KO1 – knock out 1, KO2 – knock out 2, Ladder: GeneRuler 1kb Plus DNA ladder (Thermo Fisher Scientific).

However, these promising results were quickly quelled by the presence of the thioredoxin 5780 coding sequence still present somewhere in the genome of all clones tested (Figure 42a). Since 29.13 Thx dKO D3 and RBP6 Thx dKO D3 cell lines contained the weakest signal for the thioredoxin 5780 coding sequence, these two cell lines we analyzed again with proper negative control to verify that there was no contamination in the original PCR. Unfortunately, sharp bands of the expected size were observed again, while the negative

control lacked any signal at this size (Figure 42b). This analysis would indicate that the only Thx dKO cell lines selected after the transfection were clones that mutated and kept the Thx coding sequence somewhere in the genome. This strongly suggests that Thx will prove to be an essential *T. brucei* redox scavenger under even normal conditions.

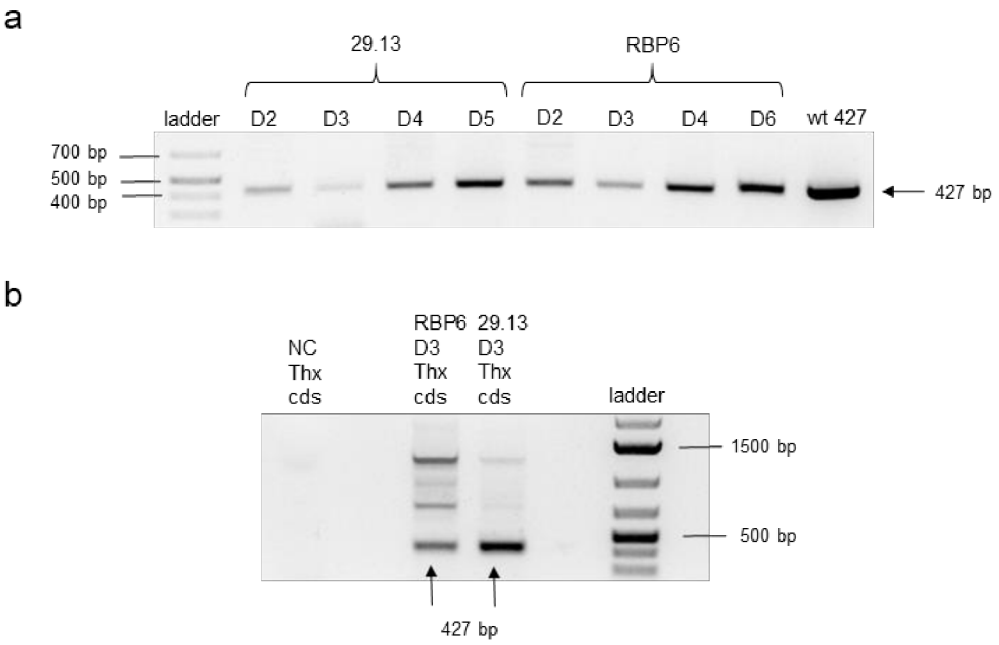

Figure 42: a) PCR verifying the presence of the thioredoxin 5780 coding sequence in both the 29.13 and RBP6 Thx dKO cell lines. b) Representative PCR showing present thioredoxin 5780 cds in RBP6 Thx dKO D3 and 29.13 Thx dKO C3. Expected PCR amplicon sizes are indicated on the right. wt – wild type, Thx – thioredoxin, NC – negative control, cds – coding sequence (water instead of DNA template). Ladder: GeneRuler 1kb Plus DNA ladder (Thermo Fisher Scientific)

5 Discussion

The goal of this thesis was to implement Hyper7 into the procyclic *T. brucei in vitro* differentiation model (RBP6) to characterize when and where ROS production plays a role as an intracellular signaling molecule. Hyper7 is the most recent reiteration of the state- of- the- art biosensor that has previously been reported to be capable of measuring physiological levels of H_2O_2 in yeast and mammalian cell lines. As a pilot project in an evolutionary divergent organism, we first generated procyclic *T. brucei* cell lines that targeted Hyper7 to either the cytosol (29.13 cytoHyper7) or the mitochondrial matrix (29.13 mitoHyper7). The correct subcellular targeting of Hyper7 was verified and we began to characterize the functionality of the biosensor in *T. brucei*. While the cytoHyper7 responded rapidly and largely as expected when the parasite was treated with excessive amounts of external H_2O_2, the biosensor did not seem capable of being recycled in the unique cytosolic redox environment of *T. brucei*. Furthermore, we had much less success analyzing the mitoHyper7 attributes. Through our repeated attempts to optimize the Hyper7 measurements, we have identified several important aspects that need to be pursued in more depth before we can reliably use this tool to explain the role of ROS during procyclic *T. brucei* differentiation.

One attribute of Hyper7 is the ability of the enzyme to be recycled by the components of the cell's antioxidant system (de Cubas *et al.*, 2021). However, when we treated the 29.13 cytoHyper7 cell line with 1 mM H_2O_2, we did not observe any significant recycling of the Hyper7 more than 60 minutes after the addition of H_2O_2. Previously, it was shown in fission yeast that the loss of either the main cytosolic thioredoxin or the thioredoxin reductase had significant impacts on the ability of a cytosolic Hyper7 biosensor to be recycled after stressing the cells with H_2O_2 (de Cubas *et al.*, 2021). Here it is important to note, that while *T. brucei* has a cytosolic thioredoxin, it does not encode a thioredoxin reductase (Jackson *et al.*, 2006). However, it has been demonstrated that the cytosolic *T. brucei* thioredoxin can be reduced by physiological concentrations of trypanothione (Schmidt & Krauth-Siegel, 2003). Therefore, the absence of the Hyper7 recycling effect in our pilot experiments is more likely the result of overwhelming the *T. brucei* cytosolic antioxidant system with excessive amounts of H_2O_2. Indeed, the reduction of Hyper7 in yeast was only noticeable when the cells were incubated with lower concentrations (25-200 mM) of H_2O_2 (de Cubas *et al.*, 2021). Future experiments will include treating the 29.13 cytoHyper7 cell line will an array of lower H_2O_2

concentrations to more closely examine the capability of Hyper7 to be recycled using the *T. brucei* redox metabolism.

A more troubling aspect of our Hyper7 assays emerged when we attempted to stimulate a response from our 29.13 mitoHyper7 cell lines. Specifically, when these cell lines were treated with OXPHOS inhibitors that should increase the mitochondrial membrane potential and lead to increase ROS production, the mitochondrial HyPer7 responses were very muted. We chose to treat our *T. brucei* cell lines with KCN or oligomycin because of our familiarity with their effects on the bioenergetics of the parasites. For example, we have established a KCN IC_{50} for procyclic *T. brucei* grown in a glucose rich medium as > 20 mM. Thus, when grown in medium promoting ATP production through glycolysis over OXPHOS, the cells can tolerate large amounts of KCN before it becomes lethal for them. Furthermore, we have demonstrated that the portion of the mitochondrial membrane potential generated by cytochrome c oxidase is significantly reduced when *T. brucei* cell lines overexpressing RBP6 were treated with 0.5 mM KCN (Doleželová *et al*., 2020). These data indicate that our Hyper7 assays performed with 1 mM KCN should not be lethal for the parasite, but it should be enough to inhibit cytochrome c oxidase activity. Alternatively, instead of using KCN, the literature is full of assays using antimycin A to inhibit the activity of cytochrome bc_1 to create mitochondrial superoxide (Quinlan *et al*., 2011), (Hoehne *et al*., 2022). Since the quinone binding sites of cytochrome bc_1 have one of the highest maximum rates of superoxide production in the cell (Brand, 2010), targeting this site with antimycin A may be a more efficient way of stimulating mitochondrial ROS.

The oligomycin IC_{50} concentration for procyclic *T. brucei* was established to be ~ 20 µM in our laboratory. We also previously determined that there is a significant increase in the mitochondrial membrane potential when procyclic *T. brucei* cell lines expressing RBP6 are treated with just 3.15 µM oligomycin (Doleželová *et al*., 2020). Our Hyper7 experiments utilized ~ 13 µM oligomycin, which is approaching the IC_{50} values. Perhaps this amount was too high and became cytotoxic to the parasites. Follow-up experiments should implement a reduced 3 µM oligomycin treatment to better stimulate an H_2O_2 induced mitochondrial Hyper7 response.

While we have demonstrated that the oligomycin treatment of procylic parasites will trigger an increased mitochondrial membrane potential that should theoretically generate mitochondrial ROS, we have not specifically measured the amount of ROS under these

conditions. Compounding this situation in *T. brucei* is the presence of an alternative oxidase (AOX) that does not contribute to the mitochondrial membrane potential (Chaudhuri *et al.*, 2002). Therefore, it is possible that when OXPHOS is inhibited, the parasite can alleviate the production of ROS by allowing electrons to redirect from the canonical ETC complexes to AOX (Fang & Beattie, 2003). While this scenario of AOX indirectly contributing to the *T. brucei* redox homeostasis is intriguing, we would still like to implement a tool to stimulate mitochondrial ROS that can be used to define the sensitivity of Hyper7 in our system. One option is to transfect our 29.13 mitoHyper7 cell line with a genetically encoded mitochondrial D-amino acid oxidase (DAAO) (Krebs, 1935). This FAD-containing flavoenzyme catalyzes the oxidative deamination of D-amino acids with absolute stereoselectivity. This reaction results in a reduced FAD that is reoxidized by oxygen, generating H_2O_2 and a recycled enzyme. DAAO is a tunable enzyme that can generate various amounts of H_2O_2 depending on the concentration of the D-amino acid added to cell medium (Stegman *et al.*, 1998). By co- expressing the mitochondrial targeted DAAO and Hyper7, we should be able to more accurately determine the sensitivity of the Hyper7 fluorescence assays.

Ultimately, we would like to utilize HyPer7 to measure physiological H_2O_2 changes that appear in nM concentrations (Pak *et al.*, 2020). To achieve this goal, we must consider maximizing Hyper7 expression, not only within a cell, but throughout the entire population of a cell line. This latter concern was revealed to be problematic when Hyper7 fluorescence assays performed by microscopy on a transfected mammalian cell line revealed substantial heterogeneity of HyPer7 dynamics between individual cells (Hoehne *et al.*, 2022). Since we cloned the HyPer7 gene into the pHD1344-t plasmid that integrates into the tubulin locus, the biosensor is constitutively expressed from this active transcription site by the endogeneous RNA polymerase II. In *T. brucei*, there is an array of alternating alpha and beta tubulin genes on chromosome 1 (Berriman *et al.*, 2005), (Jackson *et al.*, 2006), presumably to increase gene expression of these abundant gene products in an organism with polycistronic transcription. However, it is possible that differences in the intergenic regions between the tandem repeats might allow for differential expression of a specific tandem repeat (Bringaud & Baltz, 1994). Then, depending on the specific site of Hyper7 integration, there can be differences in heterologous expression (Biebinger *et al.*, 1996). Since procyclic *T. brucei* parasites do not tolerate low densities when grown in flasks, it is very difficult to create true clones originating from a single cell after a transfection. This genetic heterogeneity within a procyclic cell line was evident when we analyzed our Hyper7 cell lines by immunofluorescence microscopy and

discovered cells within the population that had poor Hyper7 expression. Fortunately, it has been demonstrated recently that a true procyclic clone can be obtained by limiting dilution of a transfected culture that is aliquoted into 96-well plates seeded with wild type procyclic *T. brucei*. After allowing for some doubling times to elapse, it is possible to treat the *T. brucei* populations with a selectable antibiotic to eliminate the wild type cells and select the desired transfected clone.

Alternatively, we could utilize a *T. brucei* 2T1 cell line that has been generated with a unique landing pad sequence located at a single rDNA spacer locus that was demonstrated to generate high levels of inducible heterologous gene expression (Alsford *et al.* 2005) from endogenous RNA polymerase I. This cell line was originally developed in bloodstream *T. brucei* to overcome the variable position effect experienced at the different rDNA loci found throughout the genome. If adapted for procyclic *T. brucei*, this methodology could be used to essentially create a clone with robust HyPer7 expression throughout the cell line. This would require subcloning HyPer7 into a pRPa plasmid that is compatible with the integration at the landing pad site within the 2T1 cell line (Alsford & Horn, 2008). If we wanted to generate a Hyper7 system in differentiating procyclic parasites using this approach, it would be best to coexpress the Hyper7 and RBP6 within a single pRPa plasmid to ensure high levels of expression for both proteins.

Another aspect to consider for increasing the sensitivity of the Hyper7 biosensor is the optimization of its subcellular localization so that it is in close proximity of the enzymatic source of ROS This is important because recent Hyper7 studies have indicated that there are steep gradients of H_2O_2 due to the robust activity of the cell's antioxidant system (de Cubas *et al.*, 2021), (Hoehne *et al.*, 2022), (Koren *et al.*, 2023). Due to time constraints, we initially targeted HyPer7 to the cytosol and the mitochondrial matrix. In retrospect, it may have been more advantageous to target Hyper7 to the mitochondrial inner membrane where the biggest producers of ROS are localized. These enzymatic complexes of the electron transport chain can release reactive oxidative species either into the matrix or the intermembrane space where superoxide is rapidly converted to H_2O_2 by superoxide dismutases (SODs). In *T. brucei*, it has been suggested that there is an SOD in the matrix and another isoform in the intermembrane space (Dufernez *et al.*, 2006). Therefore, the ideal future experimental design would include generating additional *T. brucei* cell lines in which the Hyper7 is fused with carefully selected inner membrane proteins with different topologies so that in one version the membrane

tethered Hyper7 faces the matrix and the other faces the intermembrane space. If this still proves to not be sensitive enough to detect localized H_2O_2 generated during procyclic *T. brucei* differentiation, the Hyper7 could be fused with various mitochondrial enzymes known for their propensity to generate ROS (Kritsiligkou *et al.* 2023).

As a final resort, we could implement another class of H_2O_2 probes called roGFP (Gutscher *et al*., 2009), (Morgan *et al*., 2016). These redox active fluorescent proteins are fused to redox enzymes that can directly interact with H_2O_2 and relay the electrons to the GFP, which results in a spectral shift. Some of these fusion probes are pH insensitive and display H_2O_2 sensitivity about five times greater than Hyper7, even if they demonstrate a slower rate of responsiveness.

The attempt to generate a double knock out of the thioredoxin 5780 identified in our proteomics analysis of differentiating procyclic parasites was not successful. While the PCR products designed to replace each thioredoxin allele were confirmed to be integrated properly, all of the selected cell lines retained the thioredoxin coding sequence somewhere in the genome. While this could be a technical limitation of generating knock outs with long PCR products compared to linearized plasmids, it could also indicate that the thioredoxin 5780 is essential for the parasite under normal growth conditions. In an attempt to eliminate multiple cloning steps to generate the usual two knockout constructs, we successfully optimized the complex conditions for both the fusion PCR and subsequent transfections. Furthermore, the knockout of a single thioredoxin 5780 allele results in an RBP6 cell line with a significant growth phenotype. While the cells are still able to replicate, the doubling time is almost twice as long. Ongoing experiments will monitor the progression through the various procyclic life cycle stages observed during RBP6 induced differentiation to determine if the depleted thioredoxin plays a role in the redox relay signaling pathway.

6 Conclusion

In this research, two variants of the H_2O_2 detecting fluorescent probe HyPer7 were cloned into pHD 1344-t plasmids, one of them with cytosolic localization and the other with localization into the mitochondrial matrix. The plasmids were amplified, linearized and transfected into 29.13 and RBP6 *T. brucei* cell lines. Therefore, four new cell lines were created: 29.13 cytoHyPer7, 29.13 mitoHyPer7, RBP6 cytoHyPer7 and RBP6 mitoHyPer7. The 29.13 is a parental cell line to RBP6 and was meant to be the reference, whereas in the RBP6 cell line it is possible to perform *in vitro* differentiation during which monitor H_2O_2 changes by these targeted HyPer7 probes. The presence of the HyPer7 probe in all these newly created cell lines was verified by western blot and immunofluorescence assay. Immunofluorescence assays also confirmed the proper localization of targeted probes, which were also supported by subcellular fractionation analyses.

The fluorescence responses of the HyPer7 variants were measured by two devices – a microplate reader and a flow cytometer. The function of the HyPer7 probes was tested by externally added H_2O_2 and DTT as well as by OXPHOS inhibitors KCN and oligomycin, which internally increased the levels of H_2O_2. While the probe responses to externally added solutions were significant, the responses after treatment by OXPHOS inhibitors were muted. The induced RBP6 differentiating cell lines also did not produce any significant Hyper7 responses. These results were indicative of low HyPer7 expression levels within the cell populations. Therefore, as one of the possible solutions, the HyPer7 variants were subcloned into the pT7 PAC 3V5 plasmid, which might generate a more robust gene expression through the inducible T7 RNA polymerase expression system.

As a side project, a double knock out of one of the H_2O_2 scavengers, thioredoxin 5780, was performed. Through fusion PCR, two amplicons with selective antibiotics were prepared and sequentially transfected into 29.13 and RBP6 cell lines in order to remove thioredoxin 5780 from both alleles in the *T. brucei* genome. Even though the PCR amplicons were successfully targeted to both thioredoxin alleles, the thioredoxin 5780 coding sequence was still present in both the 29.13 and RBP6 transfected cell lines. Most likely the enzyme incorporated into a different place within the genome, which indicates it probably performs an essential function for the parasite.

7 References

Alphey, Leonard, G. A., Gourley, D. G., Tétaud, E., Fairlamb, A. H., & Hunter, W. N. (1999). The High Resolution Crystal Structure of Recombinant Crithidia fasciculata Tryparedoxin-I. the Journal of Biological Chemistry (Print), 274(36), 25613–25622. https://doi.org/10.1074/jbc.274.36.25613

Alsford, S., Kawahara, T., Glover, L., & Horn, D. (2005). Tagging a T. brucei RRNA locus improves stable transfection efficiency and circumvents inducible expression position effects. Molecular and Biochemical Parasitology, 144(2), 142–148. https://doi.org/10.1016/j.molbiopara.2005.08.009

Alsford, S., & Horn, D. (2008). Single-locus targeting constructs for reliable regulated RNAi and transgene expression in Trypanosoma brucei. Molecular and Biochemical Parasitology, 161(1), 76–79. https://doi.org/10.1016/j.molbiopara.2008.05.006

BD FACSCanto II Instructions For Use. (2019). BD Biosciences. https://www.bdbiosciences.com/content/dam/bdb/marketing-documents/23-20269-00%20BD%20FACSCanto%20II%20IFU%20EN.pdf

Belousov, V. V., Fradkov, A. F., Lukyanov, K. A., Staroverov, D. B., Shakhbazov, K. S., Terskikh, A. V., & Lukyanov, S. (2006). Genetically encoded fluorescent indicator for intracellular hydrogen peroxide. Nature Methods, 3(4), 281–286. https://doi.org/10.1038/nmeth866

Berriman, M., Ghedin, E., Hertz-Fowler, C., Blandin, G., Renauld, H., Bartholomeu, D. C., Lennard, N., Caler, E., Hamlin, N., Haas, B. J., Böhme, U., Hannick, L. I., Aslett, M., Shallom, J. M., Marcello, L., Hou, L., Wickstead, B., Alsmark, U. C. M., Arrowsmith, C., . . . El-Sayed, N. M. (2005). The Genome of the African Trypanosome Trypanosoma brucei. Science, 309(5733), 416–422. https://doi.org/10.1126/science.1112642

Biebinger, S., Rettenmaier, S., Flaspohler, J. A., Hartmann, C., Peña-DíAz, J., Wirtz, L., Hotz, H., Barry, J. D., & Clayton, C. (1996). The PARP promoter of trypanosoma brucei is developmentally regulated in a chromosomal context. Nucleic Acids Research, 24(7), 1202–1211. https://doi.org/10.1093/nar/24.7.1202

Brand, M. D. (2010). The sites and topology of mitochondrial superoxide production. Experimental Gerontology, 45(7–8), 466–472. https://doi.org/10.1016/j.exger.2010.01.003

Brand, M. D. (2016). Mitochondrial generation of superoxide and hydrogen peroxide as the source of mitochondrial redox signaling. Free Radical Biology & Medicine, 100, 14–31. https://doi.org/10.1016/j.freeradbiomed.2016.04.001

Bringaud, F., & Baltz, T. (1994). African trypanosome glucose transporter genes: organization and evolution of a multigene family. Molecular Biology and Evolution. https://doi.org/10.1093/oxfordjournals.molbev.a040104

Chaudhuri, M., Sharan, R., & Hill, G. C. (2002). Trypanosome Alternative Oxidase is Regulated Post-transcriptionally at the Level of RNA Stability. the Journal of Eukaryotic Microbiology/□the □Journal of Eukaryotic Microbiology, 49(4), 263–269. https://doi.org/10.1111/j.1550-7408.2002.tb00367.x

Chaudhuri, M., Ott, R., & Hill, G. C. (2006). Trypanosome alternative oxidase: from molecule to function. Trends in Parasitology, 22(10), 484–491. https://doi.org/10.1016/j.pt.2006.08.007

Chinopoulos, C., Vajda, S., Csanády, L., Mándi, M., Mathe, K., & Ádám-Vizi, V. (2009). A novel kinetic assay of mitochondrial ATP-ADP exchange rate mediated by the ANT. Biophysical Journal (Print), 96(6), 2490–2504. https://doi.org/10.1016/j.bpj.2008.12.3915

Clayton, C. (2013). The regulation of trypanosome gene expression by RNA-Binding proteins. PLOS Pathogens, 9(11), e1003680. https://doi.org/10.1371/journal.ppat.1003680

De Cubas, L., Pak, V. V., Belousov, V. V., Ayté, J., & Hidalgo, E. (2021). The Mitochondria-to-Cytosol H2O2 gradient is caused by Peroxiredoxin-Dependent cytosolic scavenging. Antioxidants, 10(5), 731. https://doi.org/10.3390/antiox10050731

Doleželová, E., Kunzová, M., Dejung, M., Levin, M., Panicucci, B., Regnault, C., Janzen, C. J., Barrett, M. P., Butter, F., & Zíková, A. (2020). Cell-based and multi-omics profiling reveals dynamic metabolic repurposing of mitochondria to drive developmental progression of Trypanosoma brucei. PLOS Biology, 18(6), e3000741. https://doi.org/10.1371/journal.pbio.3000741

Dufernez, F., Yernaux, C., Gerbod, D., Noël, C., Chauvenet, M., Wintjens, R., Edgcomb, V. P., Capron, M., Opperdoes, F., & Viscogliosi, É. (2006). The presence of four iron-containing superoxide dismutase isozymes in Trypanosomatidae: Characterization, subcellular localization, and phylogenetic origin in Trypanosoma brucei. Free Radical Biology & Medicine, 40(2), 210–225. https://doi.org/10.1016/j.freeradbiomed.2005.06.021

Dyer, N., Rose, C., Ejeh, N., & Acosta-Serrano, Á. (2013). Flying tryps: survival and maturation of trypanosomes in tsetse flies. Trends in Parasitology, 29(4), 188–196. https://doi.org/10.1016/j.pt.2013.02.003

Fang, J., & Beattie, D. S. (2003). Alternative oxidase present in procyclic Trypanosoma brucei may act to lower the mitochondrial production of superoxide. Archives of Biochemistry and Biophysics, 414(2), 294–302. https://doi.org/10.1016/s0003-9861(03)00196-6

Gnaiger, E., Kuznetsov, A. V., Schneeberger, S., Seiler, R., Brandacher, G., Steurer, W., & Margreiter, R. (2000). Mitochondria in the cold. In Springer eBooks (pp. 431–442). https://doi.org/10.1007/978-3-662-04162-8_45

Gutscher, M., Pauleau, A., Marty, L., Brach, T., Wabnitz, G. H., Samstag, Y., Meyer, A., & Dick, T. P. (2008). Real-time imaging of the intracellular glutathione redox potential. Nature Methods, 5(6), 553–559. https://doi.org/10.1038/nmeth.1212

Gutscher, M., Sobotta, M. C., Wabnitz, G. H., Ballikaya, S., Meyer, A., Samstag, Y., & Dick, T. P. (2009). Proximity-based protein thiol oxidation by H2O2-scavenging peroxidases. Journal of Biological Chemistry/˜the œJournal of Biological Chemistry, 284(46), 31532–31540. https://doi.org/10.1074/jbc.m109.059246

Hanson, G. T., Aggeler, R., Oglesbee, D., Cannon, M. B., Capaldi, R. A., Tsien, R. Y., & Remington, S. (2004). Investigating Mitochondrial Redox Potential with Redox-sensitive Green Fluorescent Protein Indicators. Journal of Biological Chemistry, 279(13), 13044–13053. https://doi.org/10.1074/jbc.m312846200

Hoehne, M., Jacobs, L., Lapacz, K. J., Calabrese, G., Murschall, L. M., Marker, T., Kaul, H., Trifunović, A., Morgan, B., Fricker, M. D., Belousov, V. V., & Riemer, J. (2022). Spatial and temporal control of mitochondrial H 2 O 2 release in intact human cells. The EMBO Journal, 41(7). https://doi.org/10.15252/embj.2021109169

Jackson, A. P., Vaughan, S., & Gull, K. (2006). Evolution of Tubulin Gene Arrays in Trypanosomatid parasites: genomic restructuring in Leishmania. BMC Genomics, 7(1). https://doi.org/10.1186/1471-2164-7-261

Jacobs, L., Hoehne, M., & Riemer, J. (2022). Measuring intracellular H2O2 in intact human cells using the genetically encoded fluorescent sensor HYPER7. Bio-protocol, 12(20). https://doi.org/10.21769/bioprotoc.4538

Kolev, N. G., Ramey-Butler, K., Cross, G. A., Ullu, E., & Tschudi, C. (2012). Developmental Progression to Infectivity in Trypanosoma brucei Triggered by an RNA-Binding Protein. Science, 338(6112), 1352–1353. https://doi.org/10.1126/science.1229641

Kolev, N. G., Ullu, E., & Tschudi, C. (2014). The emerging role of RNA-binding proteins in the life cycle of Trypanosoma brucei. Cellular Microbiology, 16(4), 482–489. https://doi.org/10.1111/cmi.12268

Koren, S., Selim, N. A., De La Rosa, L., Horn, J., Farooqi, M. A., Wei, A. Y., Müller-Eigner, A., Emerson, J., Johnson, G. V., & Wojtovich, A. P. (2023). All-optical spatiotemporal mapping of ROS dynamics across mitochondrial microdomains in situ. Nature Communications, 14(1). https://doi.org/10.1038/s41467-023-41682-z

Krebs, H. A. (1935). Metabolism of amino-acids. Biochemical Journal. Cellular Aspects, 29(7), 1620–1644. https://doi.org/10.1042/bj0291620

Kritsiligkou, P., Shen, T. K., & Dick, T. P. (2021). A comparison of Prx- and OxyR-based H2O2 probes expressed in S. cerevisiae. Journal of Biological Chemistry, 297(1), 100866. https://doi.org/10.1016/j.jbc.2021.100866

Kritsiligkou, P., Bosch, K., Shen, T. K., Meurer, M., Knop, M., & Dick, T. P. (2023). Proteome-wide tagging with an H 2 O 2 biosensor reveals highly localized and dynamic redox microenvironments. Proceedings of the National Academy of Sciences of the United States of America, 120(48). https://doi.org/10.1073/pnas.2314043120

Mach, J., Poliak, P., Matušková, A., Žárský, V., Janata, J., Lukeš, J., & Tachezy, J. (2013). An Advanced System of the Mitochondrial Processing Peptidase and Core Protein Family in Trypanosoma brucei and Multiple Origins of the Core I Subunit in Eukaryotes. Genome Biology and Evolution, 5(5), 860–875. https://doi.org/10.1093/gbe/evt056

Manta, B., Comini, M. A., Medeiros, A., Hugo, M., Trujillo, M., & Radí, R. (2013). Trypanothione: A unique bis-glutathionyl derivative in trypanosomatids. Biochimica Et Biophysica Acta. G, General Subjects (Print), 1830(5), 3199–3216. https://doi.org/10.1016/j.bbagen.2013.01.013

Matthews, K. R. (2005). The developmental cell biology of Trypanosoma brucei. Journal of Cell Science, 118(2), 283–290. https://doi.org/10.1242/jcs.01649

Morgan, B., Van Laer, K., Owusu, T. N. E., Ezeriņa, D., Pastor-Flores, D., Amponsah, P. S., Tursch, A., & Dick, T. P. (2016). Real-time monitoring of basal H2O2 levels with peroxiredoxin-based probes. Nature Chemical Biology, 12(6), 437–443. https://doi.org/10.1038/nchembio.2067

Muller, F. L. (2000). The nature and mechanism of superoxide production by the electron transport chain: Its relevance to aging. Age (Omaha), 23(4), 227–253. https://doi.org/10.1007/s11357-000-0022-9

Muller, F. L., Liu, Y., & Van Remmen, H. (2004). Complex III releases superoxide to both sides of the inner mitochondrial membrane. Journal of Biological Chemistry, 279(47), 49064–49073. https://doi.org/10.1074/jbc.m407715200

Mugo, E., & Clayton, C. (2017). Expression of the RNA-binding protein RBP10 promotes the bloodstream-form differentiation state in Trypanosoma brucei. PLOS Pathogens, 13(8), e1006560. https://doi.org/10.1371/journal.ppat.1006560

Ooi, C., & Bastin, P. (2013). More than meets the eye: understanding Trypanosoma brucei morphology in the tsetse. Frontiers in Cellular and Infection Microbiology, 3. https://doi.org/10.3389/fcimb.2013.00071

Pak, V. V., Ezeriņa, D., Lyublinskaya, O. G., Pedre, B., Tyurin-Kuzmin, P. A., Mishina, N. M., Thauvin, M., Young, D., Wahni, K., Gache, S. a. M., Demidovich, A. D., Ermakova, Y. G., Maslova, Y. D., Shokhina, A. G., Eroğlu, E., Bilan, D. S., Bogeski, I., Michel, T., Vriz, S., . . . Belousov, V. V. (2020). Ultrasensitive genetically encoded indicator for hydrogen peroxide identifies roles for the oxidant in cell migration and mitochondrial function. Cell Metabolism, 31(3), 642-653.e6. https://doi.org/10.1016/j.cmet.2020.02.003

Penketh, P. G., & Klein, R. A. (1986). Hydrogen peroxide metabolism in Trypanosoma brucei. Molecular and Biochemical Parasitology, 20(2), 111–121. https://doi.org/10.1016/0166-6851(86)90023-x

Poburko, D., Santo-Domingo, J., & Demaurex, N. (2011). Dynamic Regulation of the Mitochondrial Proton Gradient during Cytosolic Calcium Elevations. Journal of Biological Chemistry/the Journal of Biological Chemistry, 286(13), 11672–11684. https://doi.org/10.1074/jbc.m110.159962

Quinlan, C. L., Gerencser, A. A., Treberg, J. R., & Brand, M. D. (2011). The mechanism of superoxide production by the antimycin-inhibited mitochondrial Q-cycle. Journal of Biological Chemistry, 286(36), 31361–31372. https://doi.org/10.1074/jbc.m111.267898

Rotureau, B., Subota, I., Buisson, J., & Bastin, P. (2012). A new asymmetric division contributes to the continuous production of infective trypanosomes in the tsetse fly. Development (Cambridge), 139(10), 1842–1850. https://doi.org/10.1242/dev.072611

Rotureau, B., & Van Den Abbeele, J. (2013). Through the dark continent: African trypanosome development in the tsetse fly. Frontiers in Cellular and Infection Microbiology, 3. https://doi.org/10.3389/fcimb.2013.00053

Schmidt, H., & Krauth-Siegel, R. L. (2003). Functional and Physicochemical Characterization of the Thioredoxin System in Trypanosoma brucei. Journal of Biological Chemistry, 278(47), 46329–46336. https://doi.org/10.1074/jbc.m305338200

Sena, L. A., & Chandel, N. S. (2012). Physiological roles of mitochondrial reactive oxygen species. Molecular Cell, 48(2), 158–167. https://doi.org/10.1016/j.molcel.2012.09.025

Sharma, R. S. K., Gluenz, E., Peacock, L., Gibson, W., Gull, K., & Carrington, M. (2009). The heart of darkness: growth and form of Trypanosoma brucei in the tsetse fly. Trends in Parasitology, 25(11), 517–524. https://doi.org/10.1016/j.pt.2009.08.001

Smith, T., Bringaud, F., Nolan, D. P., & Figueiredo, L. M. (2017). Metabolic reprogramming during the Trypanosoma brucei life cycle. F1000Research, 6, 683. https://doi.org/10.12688/f1000research.10342.2

Stegman, L. D., Zheng, H., Neal, E. R., Ben-Yoseph, O., Pollegioni, L., Pilone, M. S., & Ross, B. D. (1998). Induction of cytotoxic Oxidative stress BYD-Alanine in brain tumor cells ExpressingRhodotorula gracilisd-Amino Acid Oxidase: A Cancer Gene Therapy Strategy. Human Gene Therapy, 9(2), 185–193. https://doi.org/10.1089/hum.1998.9.2-185

Sullivan, L. B., & Chandel, N. S. (2014). Mitochondrial reactive oxygen species and cancer. Cancer and Metabolism, 2(1). https://doi.org/10.1186/2049-3002-2-17

Taleva, G., Husová, M., Panicucci, B., Hierro-Yap, C., Pineda, E., Biran, M., Moos, M., Šimek, P., Butter, F., Bringaud, F., & ZíKová, A. (2023). Mitochondrion of the Trypanosoma brucei long slender bloodstream form is capable of ATP production by substrate-level

phosphorylation. PLOS Pathogens, 19(10), e1011699. https://doi.org/10.1371/journal.ppat.1011699

Tecan SPARK Instructions for Use-Reference Guide. (2022). Tecan. https://www.tecan.com/hubfs/Knowledgebase/Manuals/Spark%20series/30124664_IFU_SPARK_REF_ENGLISH_V2_1.pdf

Urwyler, S., Studer, E., Renggli, C. K., & Roditi, I. (2006). A family of stage-specific alanine-rich proteins on the surface of epimastigote forms of Trypanosoma brucei. Molecular Microbiology, 63(1), 218–228. https://doi.org/10.1111/j.1365-2958.2006.05492.x

Vickerman, K. (1985). DEVELOPMENTAL CYCLES AND BIOLOGY OF PATHOGENIC TRYPANOSOMES. British Medical Bulletin, 41(2), 105–114. https://doi.org/10.1093/oxfordjournals.bmb.a072036

Vickerman, K., Tetley, L., Hendry, K. a. K., & Turner, C. M. R. (1988). Biology of African trypanosomes in the tsetse fly. Biology of the Cell, 64(2), 109–119. https://doi.org/10.1016/0248-4900(88)90070-6

Wirtz, E., Leal, S., Ochatt, C. M., & Cross, G. A. (1999). A tightly regulated inducible expression system for conditional gene knock-outs and dominant-negative genetics in Trypanosoma brucei. Molecular and Biochemical Parasitology, 99(1), 89–101. https://doi.org/10.1016/s0166-6851(99)00002-x

World Health Organization: WHO. (2023, May 2). Trypanosomiasis, human African (sleeping sickness) (cited 2024, March 31). https://www.who.int/news-room/fact-sheets/detail/trypanosomiasis-human-african-(sleeping-sickness)